NONLINEAR, QUASI-STATIC BEHAVIOR OF SOME PHOTOELASTIC AND MECHANICAL MODEL MATERIALS

Thesis for the Degree of Ph. D.

MICHIGAN STATE UNIVERSITY

Ernst W. Kiesling

1966

TI

ABSTRACT

NONLINEAR, QUASI-STATIC BEHAVIOR OF SOME PHOTOELASTIC AND MECHANICAL MODEL MATERIALS

by Ernst W. Kiesling

A study was made of the effects of time upon the birefringent and mechanical properties of four plastics: Polyester Resin CR-39 (Cast Optics Co., Inc.); Polyester Resin PS-1 and Epoxy Resin PS-2 (Photolastic, Inc.); and Polyester Resin Palatal P6-K (Badische Anilin und Soda-Fabrik, Germany). The isothermal, quasi-static behavior under constant, uniaxial stress conditions was examined exhaustively--for approximately five decades of logarithmic time, and for a range of stress sufficiently broad to cover the linear and much of the nonlinear range (where non-linearities appeared).

The stresses limiting the linear range of behavior--called linear limit stresses--were determined approximately for both one percent and five percent deviations from linearity. The variation with time after loading of these linear limit stresses was also examined.

Data is presented graphically for all materials. Certain characteristic functions defined by viscoelastic and photoviscoelastic theories are given for Polyester

Resin CR-39 in both the linear and nonlinear regions. Both these theories are discussed in some detail.

Several wave lengths of radiation, covering the visible range, were employed in the investigations of birefringence. Two phenomena--dispersion of birefringence and the possible variation with wave length of linear limit stresses--could thus be studied.

Tapered models were used to obtain birefringence and mechanical data essential to this study. The moire method, used in conjunction with tapered models, provided a convenient means of obtaining continuous strain-stress data from a single model and loading.

NONLINEAR, QUASI-STATIC BEHAVIOR OF SOME PHOTOELASTIC AND MECHANICAL MODEL MATERIALS

By

Ernst W. Kiesling

A THESIS

Submitted to
Michigan State University
in partial fulfillment of the requirements
for the degree of

DOCTOR OF PHILOSOPHY

Department of Metallurgy, Mechanics and Materials Science

1966

ACKNOWLEDGMENTS

The advice and encouragement given by the members of the Guidance Committee--Drs. W. A. Bradley (Chairman), G. L. Cloud, J. L. Lubkin, and C. P. Wells--are gratefully acknowledged. Dr. J. T. Pindera gave valuable guidance during the early stages of this research effort.

Funds and laboratory facilities for the experimental program were provided by the Department of Metallurgy, Mechanics and Materials Science, and by the Division of Engineering Research. The first year of advanced graduate study was made possible by a National Science Foundation Science Faculty Award.

TABLE OF CONTENTS

CONTENTS--Continued

CONTENTS--Continued

LIST OF ILLUSTRATIONS

ILLUSTRATIONS--Continued

ILLUSTRATIONS--Continued

ILLUSTRATIONS--Continued

ILLUSTRATIONS--Continued

LIST OF SYMBOLS

σ	= uniaxial stress
σ_{xx}, σ_{yy}	= normal stresses along axes of coordinates
σ_1, σ_2	= principal stresses
σ_{ij}	= stress tensor or typical component of stress tensor
σ_{ii}	= $\sigma_{11} + \sigma_{22} + \sigma_{33}$
s_{ij}	= $\sigma_{ij} - \frac{1}{3} \delta_{ij}\sigma_{kk}$, the stress deviator
ε	= uniaxial strain
ε_1, ε_2	= principal strains
ε_{ii}	= $\varepsilon_{11} + \varepsilon_{22} + \varepsilon_{33}$
ε_{ij}	= strain tensor or typical component of strain tensor
e_{ij}	= $\varepsilon_{ij} - \frac{1}{3} \delta_{ij}\varepsilon_{kk}$, the strain deviator
n	= isochromatic fringe order or order of isochromatic or order of interference
n_{xx}, n_{yy}	= indices of refraction along coordinate directions
m	= moire fringe order
t	= time
$\sigma_{\ell\ell}$	= linear limit stress

SYMBOLS--Continued

$n(\sigma_{\ell\ell})_{1.0}$, $n(\sigma_{\ell\ell})_{5.0}$	= linear limit stresses for birefringence at 1.0% and 5.0% deviations from linearity, respectively
$\varepsilon(\sigma_{\ell\ell})_{1.0}$, $\varepsilon(\sigma_{\ell\ell})_{5.0}$	= linear limit stresses for strain at 1.0% and 5.0% deviations from linearity, respectively
nm	= abbreviation for nanometer, one nanometer = 10^{-6} mm or 10^{-3} microns
f_σ, f	= a material "fringe constant"
d	= thickness of model
λ	= wave length of radiation
C_σ, C_ε	= stress-optic and strain-optic coefficients, respectively
P, P', Q, Q'	= linear differential operators with respect to time
G	= shear modulus
K	= bulk modulus
D(t)	= extension compliance
E(t)	= relaxation modulus
J(t)	= creep compliance in shear
B(t)	= bulk compliance
μ	= Poisson's ratio
$\beta(t)$	= difference in secondary principal stresses for unit sustained birefringence
$\alpha(t)$	= birefringence for a unit sustained difference in secondary principal stresses

SYMBOLS--Continued

n_σ = $(n_1 - n_2)$, the difference in secondary principal values of index of refraction

φ_n = angle between secondary principal optical directions and coordinate axes

φ_σ = angle between secondary principal stress directions and coordinate axes

φ_ε = angle between secondary principal strain directions and coordinate axes

$D_1, D_2, \ldots, D_n$ = kernels of integrals, for representing viscoelastic behavior

D = dispersion of birefringence

R = $n\lambda$, relative retardation

r = $\frac{R(\lambda)}{R(\lambda_0)}$, normalized retardation

D_λ = $\frac{dr}{d\lambda}$, normalized dispersion of birefringence

k = stress concentration factor

CHAPTER I

INTRODUCTION

Objective and Scope

The demands for more efficient use of materials in today's technology, particularly in areas of air and space travel, have elevated the importance of accurate stress analysis to unprecedented heights. These demands have fostered, or forced, rapid developments in the methods of stress analysis, both analytical and experimental. Though the theory of elasticity offers mathematically exact solutions to some problems, difficulties multiply sharply when boundaries or loads are complicated. Comparable or even greater difficulties may arise in viscoelasticity and plasticity. Development of the vast capability in data processing has broadened the range of problems which can be satisfactorily solved analytically but has not enabled the analytical approach to encompass all problems.

Some problems which defy analytical solution yield to experimental methods. One such method is photoelasticity, which has been used successfully in a number of cases. Although the photoelastic effect has been known since 1816, when Sir David Brewster published his account, it became a useful tool to the engineer much more recently.

The Treatise on Photoelasticity, first published in 1931 by E. G. Coker and L. N. G. Filon, opened the eyes of many to the potential of the method and established a firm foundation for its further development. The invention of "Polaroid" provided a relatively inexpensive means of producing large beams of polarized light. In recent years, and continuing at present, the development of new materials (plastics) possessing desirable optical characteristics has expanded the application of the method to a wider variety of problems, including those in the realm of viscoelasticity and plasticity.

The moire method has emerged as another important tool to the experimental stress analyst, despite its late introduction--less than twenty years ago. Present intensive research on the method promises to make it more useful in the near future.

Upgrading in techniques and equipment has made its impact. The addition of courses in experimental stress analysis in engineering curricula, coupled with more participation in professional organizations devoted to the advancement of experimental stress analysis, should further enhance the capability and broaden the applications of both the methods mentioned.

The distinct advantage of these experimental methods over most others, that of yielding quantitative representations of stress or strain over an entire field, not only

excites the imagination of this writer but also partially explains his optimism regarding their future.

Despite progress in all areas of experimental stress analysis, many difficulties and sources of error in their application remain. Among them is model similarity, particularly as it pertains to properties of model materials. This study aims at elucidating some aspects of this problem and giving data and recommendations to help resolve the problem.

The mechanical and optical properties of several materials commonly used in photoelastic analyses were studied and are herein reported. Any impact that the results of this study may have, therefore, will be most pronounced for the analyst solving problems in the elastic domain. The method of determining the material properties, however, is felt to be unique and applicable to a much broader class of materials, including low-modulus ones such as might be useful to model studies of viscoelasticity. One chapter of the thesis is devoted to discussing the experimental approach to solving viscoelastic stress analysis problems.

The moire method is employed in studying mechanical properties. Existing literature on the theory and interpretation of moire patterns is extensive. Relatively little has been reported, however, regarding the production of suitable grids and the techniques of their application.

A discussion of various methods tried in the course of this study, therefore, is included.

This study investigates the phenomenological behavior only. The optical and mechanical properties are investigated without consideration of causes or effects at the molecular level. Furthermore, only the relatively long-time--i.e., quasi-static--behavior at constant temperature is considered.

Problem of Model Similarity

Certain laws of similarity must be observed in structural-model analysis, model photoelasticity, photo-viscoelasticity, photoelastic coatings, or in any model analysis. That complete physical similarity requires geometric similarity between model and prototype presents no real problem in photoelasticity, since plastics used for models can be cast and/or machined to practically any desired shape. In the usual application of photoelastic coatings, a layer of plastic is bonded to the surface of the prototype so that geometric similarity is automatic.

But complete physical similarity imposes other requirements upon the model material. The theory of elasticity generally assumes a Hookean material--i.e., one for which stress-strain relations are linear, single-valued, and independent of time. Despite such a sweeping idealization, valuable solutions for a broad class of problems can be obtained by this theory. Apparently such an

idealization is satisfactory for a number of materials and conditions.

With such an assumption and those of homogeneity and isotropy the stress distribution in a restricted class of elasticity problems is found to be independent of the elastic constants of the material. This is true for "plane strain" or "generalized plane stress" problems in which the resultant force over each boundary vanishes separately and the boundary conditions involve only stresses. Many practical problems, such as those in plates with singly-connected boundaries, fall into this class. The independence of stress distribution from elastic constants "opens the door" to model studies, such as photoelasticity.

The elastic constants of the material cannot be eliminated from the equations formulating three-dimensional or general two-dimensional elasticity problems. The stress distribution is found to depend upon one elastic constant, such as Poisson's ratio. But in investigating several problems of this more general type Clutterbuck [5][1] found that the differences in stress distributions due to the effects of Poisson's ratio are quite small--so small that the effects can seemingly be regarded as secondary ones. Photoelasticity thus provides a potential for obtaining approximate solutions to a wide variety of problems.

---

[1]Numbers in brackets refer to the List of References at the end of the thesis.

If model materials were available for which the constitutive equations were linear, single-valued, and independent of time, then the problem of physical similarity would be quite trivial. But the plastics usually used for structural or photoelastic models are viscoelastic or photoviscoelastic so that stress-strain relations or stress-birefringence relations are not independent of time. These relations may be rather complicated functional relations, such as $\varepsilon = \varepsilon(\sigma,t)$ or $n = n(\varepsilon,t)$, where n denotes the fringe order of the birefringence.

Fortunately, some model materials are momentarily linear for a broad range of stress--i.e., at any given time after a constant load is applied the stress-strain and birefringence-stress relations are linear. This linearity, at a given time, makes such materials more useful for models and fulfills another important requirement of complete physical similarity. But this "broad range of stress," for which momentarily linear behavior is manifested, is limited and is time dependent in most plastics. The range and the time dependence vary greatly with materials, but in the case of almost all plastics which exhibit momentarily linear behavior the stress which limits the linear range is considerably below the ultimate or fracture strength at a given time after loading. This makes an analysis based on linearity vulnerable to serious error: if the initial stress is too high and/or if a given stress

is sustained too long before desired information is collected, gross anomalies can result. The latter of these possibilities becomes particularly relevant when a viscoelastic prototype is being studied by means of models, since extended time periods are sometimes necessary.

Primary Objectives of Thesis

Determination of linear limit stresses.--Determining the value of stress which limits the momentarily linear range of behavior for a number of plastics subjected to constant axial load is one of the primary objectives of this study. This value of stress, called the "linear limit stress" and denoted by $\sigma_{\ell\ell}$, is, of course, a function of time. That such a limit exists and that it is time-dependent is well-known, but few published results can be found regarding it, none showing explicit values for it at a given time after loading or for its variation with time.

The linearity and its limiting values pertain to both birefringence-stress and strain-stress relations. In an earlier publication by the author [50] the opinion was expressed that the linear limit stress for birefringence, as a function of time, might be accepted also for strain. At least one published result [18], in which time effects were considered negligible, contradicted this opinion. In this study both mechanical and optical properties are considered and the linear limit stresses for the two compared.

A discussion of the experimental data obtained, a description of the models and testing procedures, and a list of the materials chosen for the study are presented in Chapter II. This is followed by the presentation of principal results in Chapter III.

Laws of viscoelasticity, experimental results.--The mathematical theory of viscoelasticity has provided a fruitful field of investigation in recent years. High temperature applications of conventional structural materials, the increasing use of plastics in industry (e.g., tubing in refineries), increased interest in soil and rock mechanics, and other factors have all kindled interest in the subject. Linear viscoelasticity may now be considered well-established, with many elegant theoretical developments and with considerable experimental evidence to support its applicability to a large group of problems. Nonlinear viscoelasticity, on the other hand, has not yet achieved this status.

Because of the viscoelastic nature of plastics used in structural and photoelastic models and because of the increased importance of the experimental approach to viscoelastic stress analysis, some understanding of the theory and applications of viscoelasticity is important, if not imperative, to successful work in this area of experimental stress analysis. A brief review of some of the theories is presented in Chapter IV, along with plotted results

correlating the experimental data gathered in this study with some of the theories.

Collateral Objectives

Variation of $\sigma_{\ell\ell}$ with wave length of radiation.-- Though a number of attempts have been made to explain the cause and the nature of birefringence (or double refraction or retardation) and its relation to stress, strain, wave length of radiation, and other variables, none has been completely successful. The order n of the isochromatic fringes in a uniaxial stress state is often assumed to be inversely proportional to the predominant wave length of radiation. Several investigators have observed and reported deviations from such a relationship. Pindera and Cloud [49] and Cloud [4] very recently reported their findings on the dependence of the order of isochromatic and consequently of the photoelastic coefficients upon wave length of radiation. This dependence is known as dispersion of birefringence.

Since the order of isochromatic depends upon the wave length of radiation, even when the birefringence-stress relationship is linear for a certain range of stress, it seems reasonable to ask whether the linear limit stress for birefringence $\sigma_{\ell\ell}$ might also vary with wave length. To pursue this question, approximately ten different wave lengths ranging from 0.410 microns to 0.800 microns were used at various times throughout the tests.

The results indicating the dependence of $\sigma_{\ell\ell}$ on wave length are given in Chapter V.

Dispersion of birefringence.--Data obtained from the investigations above readily yield information on the dispersion of birefringence. Some of the materials tested are the same as those tested by Cloud [4], and hence these results are merely a supplement to or a continuation of his work. However, this study includes other materials, as well as a different (but narrower) range of wave lengths. Chapter V also reports on these findings.

Organization of Thesis

In the ensuing, Chapter II discusses the plots desired for data presentation, the models and testing procedures employed to obtain the data, and a list of materials tested. This is followed by the presentation of principal results in Chapter III.

The theory of viscoelasticity, both linear and nonlinear, is discussed in Chapter IV. Some plots of "characteristic functions" describing viscoelastic behavior in the linear range are given, together with mathematical expressions intended to describe both linear and nonlinear behavior.

Chapter V discusses the collateral objectives just mentioned: dispersion of birefringence and variation of linear limit stress with wave length.

This work closes with a summary, conclusions, and some recommendations for future research in Chapter VI. Appendix I gives the theoretical and experimental analysis of the stress distribution in the tapered model used throughout this work. Appendix II reviews briefly the prior developments of the moire method, as well as the efforts of this study.

The results presented graphically in Chapters III through V are for Polyester Resin CR-39 supplied by Cast Optics Co., Inc. Similar results for other materials tested are presented in Appendix III.

CHAPTER II

CALIBRATION TESTS

Part A. Description of Material Properties

Introduction

The materials tested in this study are inherently viscoelastic or photoviscoelastic--i.e., the response to stress, whether strain or birefringence, is a function of time. The viscoelastic properties of such materials may be defined in various ways; for an incompressible, isotropic, linear viscoelastic material, Alfrey [1] listed seven distinct methods. He then showed that they are all mathematically equivalent. For a real material some measure of compressibility, such as Poisson's ratio, must also be known. At least as many ways are available for specifying the photoviscoelastic properties.

The choice of specification depends upon the intended use of the information. For visualization of material response the graphical representation seems most useful. Such representation suffices for experimental stress analysis, whereas analytical work usually favors a representation in mathematical form--e.g., a constitutive equation.

Suitable mathematical forms are discussed in Chapter IV. Part A of the present chapter describes various graphical forms of representation and how one form is deduced from another. Part B describes the testing procedure followed in this investigation.

All calibration models employed in this study were formed from plates of uniform thickness. The stress state applied was basically one-dimensional, constant throughout the thickness of the model. Although the results obtained from such one-dimensional tests cannot be guaranteed to be general, particularly in the nonlinear range, they give valuable insight into the general behavior. In the linear range one-dimensional tests furnish results which are sufficient for the complete characterization of the material, whether it be elastic or viscoelastic.[1] These results can be used to predict with confidence the behavior of the material under more general states of stress.

In addition to yielding data of value to the stress analyst, one-dimensional tests yield valuable data for the comparison of different materials and compositions. All of these features, coupled with the relative ease of conducting such tests, seem to be sufficient to justify their use. The present studies are confined to one-dimensional loading, partly because the additional

---

[1] This is further discussed in the next section and again in Chapter IV where the uniaxial stress state is resolved into deviatoric and dilatational parts.

complication of time-dependence has been investigated exhaustively.

The question of how long constant load should be maintained in a creep test also has several aspects. Photoelastic stress analysis usually requires knowledge of material properties for no more than a few hours. This may be much too short a time interval for a structural model test of a viscoelastic material.

According to Leaderman [32] the behavior of polymers, as described by the creep compliance, changes significantly over six to ten decades of logarithmic time, depending upon the type of polymer. Supposing the first measurement possible at 0.001 hours (3.6 sec) after loading, six decades of logarithmic time would dictate the duration of test to be 1,000 hours and ten decades over 1,140 years! Hence, to cover the entire range of time other tests must be devised. These may be dynamic tests, wherein short-term effects are determined, or tests at different temperatures, providing information sufficient for the application of the time-temperature correspondence principle.[1]

In this study the time range covered by the isothermal creep tests is from a few seconds to ten days (240 hr)--i.e., approximately five decades of logarithmic time.

---

[1]See Eirich [16], vol. II, pp. 67ff.

In the majority of solid mechanics problems which have been successfully analyzed by model techniques (analogs) the prototype material may reasonably be assumed linear (elastic or viscoelastic), homogeneous, and isotropic. If data from a model test is to be interpreted conveniently and accurately, the model material must exhibit linearity, homogeneity, and isotropy. The last two are quite easy to attain--at least to an acceptable degree of approximation--in most potential model materials. If the response to stress of a given material is linear at any instant of time after loading and if this linearity extends over a sufficiently broad range of stress to allow accurate measurement of the response, then the material may be useful for models.

Results of a model test can be no more accurate than the investigator's knowledge of the model material's behavior. Such knowledge can be gained only through carefully conducted calibration tests.

Calibration of Mechanical Model Materials

Two aspects of the calibration of model materials deserve careful attention. First, the range of stress for which the constitutive (stress-strain) equation is linear is limited and time-dependent. Second, the material properties may significantly change with time. Then the ordinary material constants, such as the modulus of

elasticity E and Poisson's ratio μ, may have to be redefined or even abandoned. In such cases a suitable viscoelastic description of the material behavior might be enlisted.

When time effects are significant, the equations describing material behavior become functional ones which include time--for example:

$$\varepsilon = \varepsilon(\sigma,t) \tag{2.1}$$

or

$$\sigma = \sigma(\varepsilon,t). \tag{2.2}$$

The problem of defining such relations[1] is not, in general, simple. If, however, the strain is proportional to stress at a given time after loading--i.e., the behavior is "momentarily linear"--then the well-developed theories of linear viscoelasticity can be employed to determine specific forms of relations (2.1) and (2.2).

A graphical approach is employed in this study to portray both the mechanical and optical (birefringent) behavior of the materials tested. This behavior is determined as the response to a one-dimensional stress state, suddenly applied and constantly maintained. The usefulness of the data given is not limited, however, to one-dimensional applications. As Theocaris [64,65] has

---

[1]Some possible forms of such relations are given in Chapter IV.

explained, "a simultaneous measurement of the mechanical and optical quantities of a linear viscoelastic material in a simple tension test supplemented with one initial value of another characteristic function . . . suffices for the complete characterization of the material." For the other characteristic function mentioned, Theocaris used a "lateral contraction ratio," defined as the ratio of lateral strain (negative) to axial strain in a creep test with constant axial stress. This ratio might be thought of as a "time-dependent Poisson's ratio"; indeed, it is so called by Daniel [10].

As explained in Chapter IV, this ratio might accurately be assumed constant for the materials and tests herein reported. Its value can be easily determined for each material tested. With this value and the one-dimensional mechanical and optical properties determined by the creep tests of this study, other functions, such as the bulk and shear compliances, relaxation moduli, and optical coefficients, may be evaluated [65]. All of these functions and coefficients are defined in Chapter IV.

The strain response to a constant stress is expressed in a form suitable for graphical representation by:

$$\varepsilon = \varepsilon(\sigma),\ t = \text{const}\ (t_1, t_2, t_3, \ldots). \qquad (2.3)$$

If the stress-strain relation is linear at any given time--say t_i--after loading, then a relation of the form

$$\varepsilon(t_i) = D(t_i)\sigma \tag{2.4}$$

may be written, where $D(t_i)$ is the momentary value of the "extension compliance." But $D(t)$ is related[1] to a "relaxation modulus" $E(t)$ by:

$$D(t) = \frac{1}{E(t)}. \tag{2.5}$$

Thus Equation (2.4) may be written:

$$\varepsilon(t_i) = \frac{\sigma}{E(t_i)}. \tag{2.6}$$

The striking resemblance of Equation (2.6) to the familiar Hooke's law for one-dimensional stress should be noted. It seems that the entire discussion and development thus far presented might be recast within the framework of a "modified, time-dependent" Hooke's law. Although this point is not pursued in depth, it is further discussed in Chapter VI.

Both the extent of the linear range and momentary values of $E(t)$ can conveniently be obtained from a plot of the relations expressed by Equation (2.3). Figure 2.1 shows schematically such a plot for a uniaxial stress state.

---

[1]The reader is again referred to Chapter IV for further definitions and discussion.

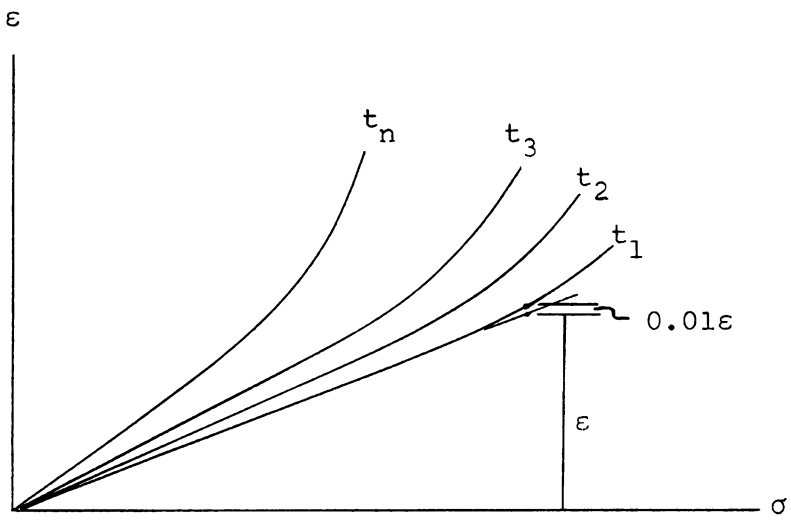

Fig. 2.1--Representative plot of $\varepsilon = \varepsilon(\sigma)$, $t = \text{const}$ ($t_1, t_2, t_3, \ldots$) for uniaxial stress, constant load.

If a sufficient number of curves are shown in a plot, such as Figure 2.1, then a curve of E(t) as a function of time can be drawn (see Figure 2.2). Equation (2.6) may then be replaced by:

$$\varepsilon(t) = \frac{\sigma}{E(t)}; \tag{2.7}$$

and the response to stress can be found at any specific time within the range of the calibration test.

Since the stress-strain curve gradually deviates from linearity, the exact limit of linearity cannot be defined, much less determined. However, the limit can be defined and quite accurately determined for an arbitrarily

chosen deviation from linearity. This deviation is illustrated as a percentage of strain (1.0%) in Figure 2.1. The stress at this deviation is called the linear limit stress and is denoted by ${}_{\varepsilon}(\sigma_{\ell\ell})_{1.0}$, where the subscript on the left indicates that the linear limit stress is based on strain and the subscript on the right denotes the percentage deviation from linearity.

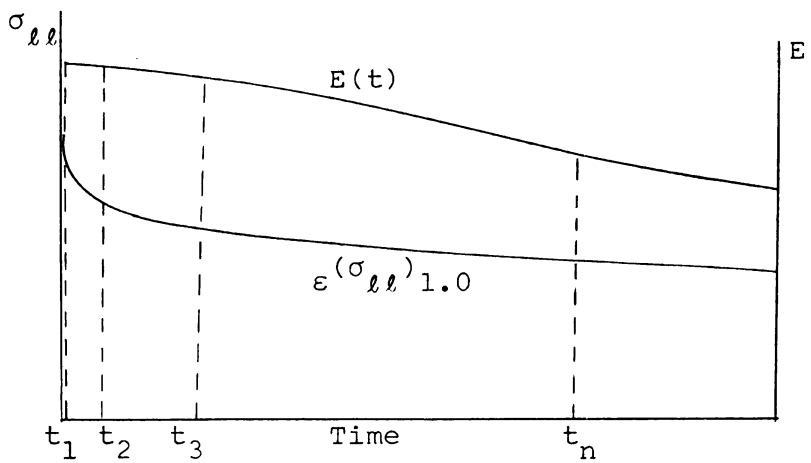

Fig. 2.2--Linear limit stress and relaxation modulus as functions of time for uniaxial stress, constant load.

Again, if a sufficient number of curves are drawn in a plot, such as Figure 2.1, then a curve of linear limit stress (for strain) as a function time can be drawn, as in Figure 2.2.

A plot of the strain as a function of time for a given (constant) stress aids visualization of the nature of

mechanical creep. Figure 2.3 represents such a plot. It can be deduced from Figure 2.1, or it may be required for the construction of Figure 2.1, depending upon how the data is obtained. This is discussed later in the chapter.

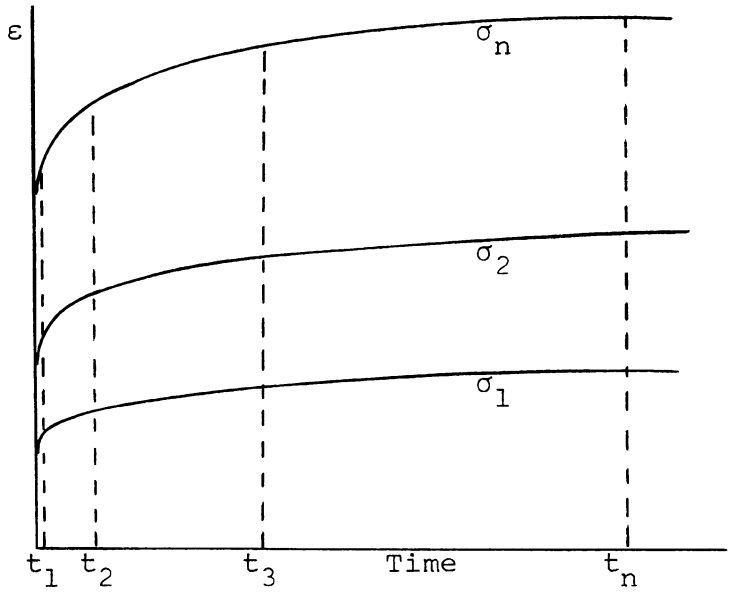

Fig. 2.3--Representative plot of $\varepsilon = \varepsilon(t)$, $\sigma = \text{const}$ ($\sigma_1, \sigma_2, \sigma_3, \ldots$) for uniaxial stress, constant load.

The Photoelastic Effect

Some materials possess the property of resolving incident light rays into two orthogonal components and transmitting them on orthogonal planes (see [4], p. 16). This phenomenon is known as "double refraction" or "birefringence." The optical properties on the two planes, in general, will be different so that the two components will

be transmitted with different velocities. When they emerge from a plate of the material, there is a difference in phase--i.e., a relative retardation--between the two component waves that is proportional to the thickness of the plate and to the difference in velocities of the two components.

In many synthetic resins this double refraction depends upon the nature and intensity of stress. For normal incidence on flat plates of such materials, subjected to plane stress, the transmission of light obeys two laws which form the basis of photoelastic stress determination [13]:

1. The planes of transmission coincide with the principal-stress axes.[1] Only on the principal planes of stress is light transmitted.
2. The velocity of transmission in each principal plane depends upon the intensities of the principal stresses in these two planes.

If the principal-stress intensities differ, so will the velocities of transmission in the principal planes, resulting in a phase difference in the two components proportional to the difference between the principal stresses. Any method that can be employed to determine this phase difference can be used to measure the difference between

---

[1]This is generally true for certain high-modulus materials but may not be true in some low-modulus ones. See Chapter IV for further discussion.

the principal stresses. A device called a "polariscope" serves such a purpose. The function of each of its components, possible variations in arrangement of components, and interpretations of the patterns it produces are explained in many books on photoelasticity, such as [6,13, 18,28].

Basically two types of photoelastic patterns (fringes) are produced. Both of these are sufficient, and generally necessary, for the complete determination of plane stresses (or the corresponding strains) in an elastic body. One type of fringe, called the "isoclinic," is the locus of points having constant stress direction. The other, called the "isochromatic," is the locus of points having constant difference between principal stresses. In uniaxial stress fields, such as are usually employed in calibration tests, only the isochromatics are needed.

Daylight, or white light, is made up of a number of constituent vibrations possessing different wave lengths which can be distinguished from one another through the sense of color. The wave lengths of visible light run from about 390 nm (nm is abbreviation for nanometer; one nanometer = 10^{-6} mm or 10^{-3} microns) to 770 nm. When light enters the polariscope, the double refraction of the model produces a phase difference which depends upon the wave length. Hence if white light is used, each constituent wave length is affected differently at a given point in the

model. As a result, every color in the visible spectrum appears between integral orders of isochromatics, where an integral order is represented by a particular color and fractional orders by bands of other colors.

If monochromatic light is used--i.e., light consisting of one wave length or color--the isochromatic fringes appear simply as dark or light bands. Here integral orders are represented by either the dark or the light bands, depending upon the setup of the polariscope, while fractional orders are represented by various levels of intensity between the light and dark. Since the phase difference produced by the relative retardation of the model depends upon wave length, so also does the order of isochromatic at a given point. As previously stated, it also depends upon the stresses in the model and upon its thickness.

Monochromatic light is generally preferred for photoelastic analysis. Though it can be produced in a number of ways, the method most commonly employed is that of "filtering" a chosen wave length from the continuous emission of a light source. Filtering consists of blocking out all but a certain wave length, or rather, a limited range of wave lengths. Information on types of filters, their specification, and instructions for their use may be found in a number of sources, a very concise one being available from Eastman Kodak [29].

Usually only one wave length is used in a photoelastic investigation; the choice is governed by available light sources and filters, sensitivity and transmission characteristics of photoelastic material, and other factors such as personal preference.

In some plastics the birefringence, or the order of isochromatic, is found to be directly proportional to the difference in principal stresses for a range of stress. This may be expressed in one standard form as [18]:

$$n = \frac{d}{2f_\sigma}(\sigma_1 - \sigma_2), \tag{2.8}$$

where (typically)

$f_\sigma = f$ = a "fringe constant" for the material, $\left(\frac{\text{lb}}{\text{in x order}}\right)$,

d = thickness of the photoelastic model (in),

n = order of interference, or fringe order,

σ_1, σ_2 = principal stresses;

or alternatively as:

$$n = \frac{C_\sigma d}{\lambda}(\sigma_1 - \sigma_2), \tag{2.9}$$

where

C_σ = stress-optic coefficient for the material,

λ = wave length of radiation.

A similar equation can be written in terms of strain as:

$$n = \frac{C_\varepsilon d}{\lambda}(\varepsilon_1 - \varepsilon_2), \tag{2.10}$$

where

C_ε = strain-optic coefficient for the material,

$\varepsilon_1, \varepsilon_2$ = principal strains.

The linearity between birefringence and stress (or strain) manifested by some plastics makes them useful as model materials for photoelastic analysis. The evaluation of the difference between the principal stresses at some point in the prototype depends upon determining the order of interference n [Equation (2.8)] at the corresponding point in the model of known thickness d and on knowing the fringe constant f for the model material. Knowledge of the difference between principal stresses at various points in the model can then be combined with information gained from the isoclinics to "separate" the stresses and to determine the stress field. Several techniques, such as shear difference or oblique incidence, have been employed to achieve this [18].

Calibration of Photoelastic Model Materials

Evaluation of the fringe "constant" f of Equation (2.8) for a given wave length of radiation, or of C_σ in Equation (2.9), or of C_ε in Equation (2.10) is a calibration of the stress-optic or strain-optic properties of the material. These values are sometimes assumed to be independent of time, temperature, and other variables. Indeed, some manufacturers and suppliers go so far as to provide

values of the constants without stipulating the conditions under which tests are to be performed. Indiscriminate use of such constants can lead to gross errors. Only if careful calibration tests are carried out under conditions of temperature, time, and humidity very similar to those of the model test can a high degree of accuracy be expected.

As implied above, creep phenomena are manifested in the birefringent properties of most model materials, as well as in the mechanical properties. The results of this study indicate that birefringence is, in fact, more closely related to strains than to stresses. The effect of time upon f or C_σ, in general, cannot be neglected. If constant load is maintained, then Equation (2.8) should perhaps be written:

$$n(t_i) = \frac{d}{2f(t_i)} (\sigma_1 - \sigma_2), \qquad (2.11)$$

where the subscript on t again indicates that reliable values can be stated only at specific times after a constant load is applied. The sequel to Equation (2.1) is thus a functional relation, such as:

$$n = n(\sigma,t). \qquad (2.12)$$

The complications of trying to express mathematically such a relation can again be avoided by expressing the order of isochromatic n as a function of stress at

given times after loading--i.e.:

$$n = n(\sigma),\ t = \text{const}\ (t_1, t_2, t_3, \ldots). \qquad (2.13)$$

For many photoelastic model materials the n-σ relation, at a given time, is linear. The extent of the linear range is again limited and time-dependent.

If the stress state is uniaxial, then the quantity $(\sigma_1 - \sigma_2)$ becomes simply σ. In many photoelastic analyses a one-dimensional calibration test is conducted to determine momentary values of the photoelastic coefficients. These momentary values are then used in an equation, such as Equation (2.11), to determine the more general states of stress in photoelastic models of the same materials.

For materials exhibiting significant time effects, such applications should seemingly be made within the framework of a photoviscoelastic theory instead of a "momentary-elastic" one. However, in an overwhelming number of cases, close agreement with theoretical results has been obtained using the momentary-elastic "theory." This not only attests to the validity of such a theory for the optical (birefringent) behavior but also implies that a similar theory might be valid for the mechanical behavior--e.g., a "time-dependent Hooke's law." Such a theory could be expected to apply only to the behavior of relatively "high-modulus" or "stiff" materials.

Both the extent of the linear range and the fringe constant f for a given wave length of radiation can be deduced from a plot of the relation expressed by Equation (2.13). Such a plot is shown in Figure 2.4.

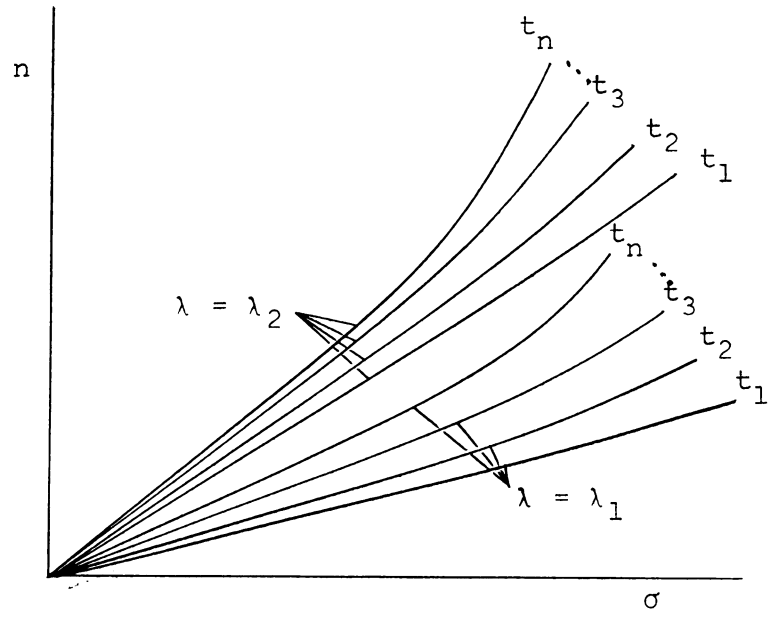

Fig. 2.4--Isochromatic fringe order n vs. stress for two wave lengths, λ_1 and λ_2.

If enough such curves for each wave length are drawn and enough wave lengths are considered, then sufficient data can be deduced to determine:

1. ${}_n(\sigma_{\ell\ell})_{1.0}$, the linear limit stress (1.0% deviation from linearity) based on birefringence for a given wave length, and its variation with time.
2. The variation of ${}_n(\sigma_{\ell\ell})_{1.0}$ with wave length for a given time.

3. The fringe constant f as a function of time for a known thickness and given wave length.
4. The stress-optic coefficient C_σ as a function of time for a given wave length.
5. The variation of C_σ with wave length for a given time--i.e., information on dispersion of birefringence.
6. The relation $n = n(t)$, $\sigma = \text{const}$ $(\sigma_1, \sigma_2, \ldots)$.

All six of the above relations can be plotted; however, most photoelastic analyses employ only one wave length of radiation for both the calibration of the material and the model study. Dispersion of birefringence then becomes irrelevant. Typical sample curves of 1, of 3 and 4, and of 6 may prove very useful and are illustrated in Figures 2.5, 2.6, and 2.7, respectively.

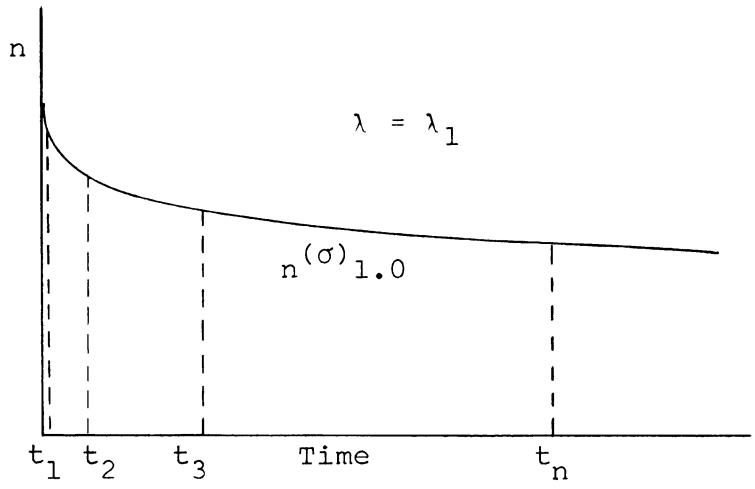

Fig. 2.5--Variation of linear limit stress with time, based on birefringence.

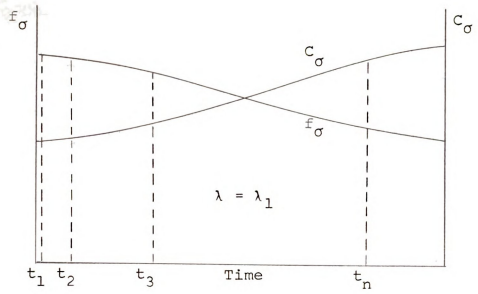

Fig. 2.6--Fringe constant f and stress-optic coefficient C_σ as functions of time for given wave length.

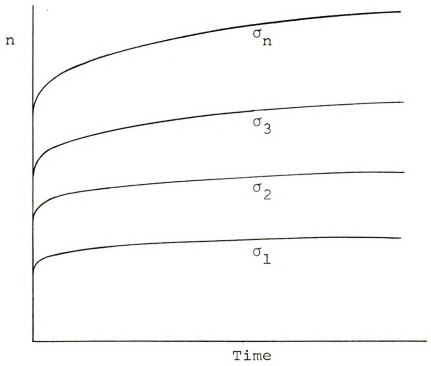

Fig. 2.7.--Order of interference n vs. time for various stress levels, uniaxial stress.

Curves showing mechanical properties can be combined with those of photoelastic ones for other useful relations. If common times are used in determining the relations [see Equations (2.3) and (2.13)]

$\varepsilon = \varepsilon(\sigma)$, $t = \text{const } (t_1, t_2, t_3, \ldots)$, see Figure 2.1,

and

$n = n(\sigma)$, $t = \text{const } (t_1, t_2, t_3, \ldots)$, see Figure 2.4;

then they may be combined to yield

$$n = n(\varepsilon),\ t = \text{const } (t_1, t_2, t_3, \ldots) \qquad (2.14)$$

for a given wave length λ. If the times are not common in the above relations, Equation (2.14) may still be deduced from

$\varepsilon = \varepsilon(t)$, $\sigma = \text{const } (\sigma_1, \sigma_2, \sigma_3, \ldots)$, see Figure 2.3,

and

$n = n(t)$, $\sigma = \text{const } (\sigma_1, \sigma_2, \sigma_3, \ldots)$, see Figure 2.7,

if common stress values are chosen in plotting Figures 2.3 and 2.7. Figure 2.8 shows a representative plot of Equation (2.14).

One further extension of the data can be executed. From Figure 2.8 the relation

$$n = n(t),\ \varepsilon = \text{const } (\varepsilon_1, \varepsilon_2, \varepsilon_3, \ldots) \qquad (2.15)$$

may be obtained. A plot of Equation (2.15) might appear as in Figure 2.9.

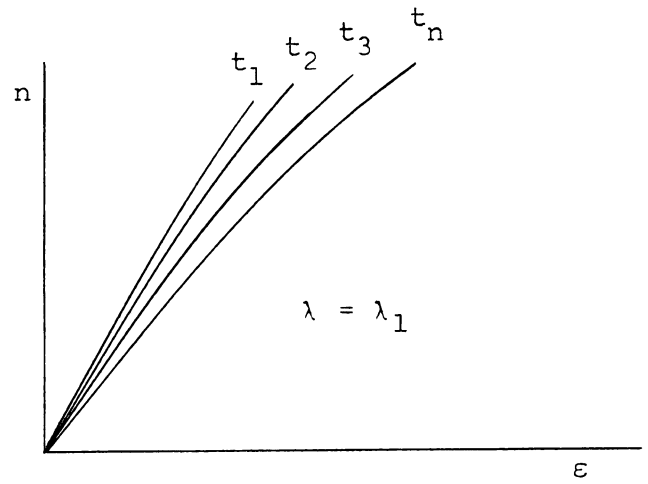

Fig. 2.8--Order of interference n vs. strain for t = const and $\lambda = \lambda_1$.

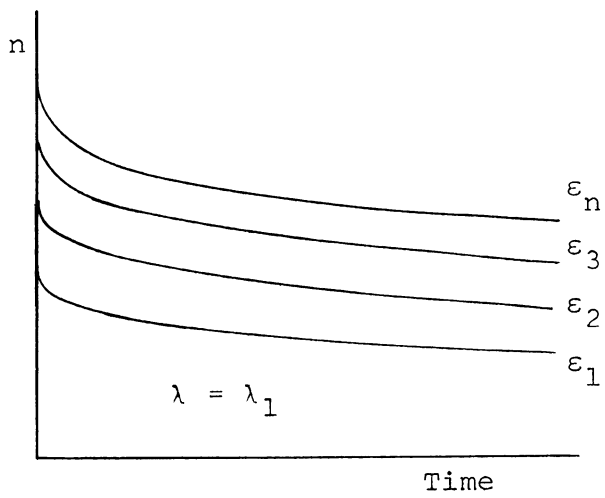

Fig. 2.9--Order of interference n vs. time for ε = const and $\lambda = \lambda_1$.

Complete Description of Material Properties

All of the material properties necessary for mechanical or photoelastic model studies may be deduced from plots of the following relations:

$$\varepsilon = \varepsilon(\sigma),\ t = \text{const}\ (t_1, t_2, t_3, \ldots)$$

$$\varepsilon = \varepsilon(t),\ \sigma = \text{const}\ (\sigma_1, \sigma_2, \sigma_3, \ldots)$$

$$n = n(\sigma),\ t = \text{const}\ (t_1, t_2, t_3, \ldots)$$

$$n = n(t),\ \sigma = \text{const}\ (\sigma_1, \sigma_2, \sigma_3, \ldots) \qquad (2.16)$$

$$n = n(\varepsilon),\ t = \text{const}\ (t_1, t_2, t_3, \ldots)$$

$$n = n(t),\ \varepsilon = \text{const}\ (\varepsilon_1, \varepsilon_2, \varepsilon_3, \ldots).$$

The relations involving n--i.e., those expressing the birefringent properties of photoelastic materials--are assumed to be determined for one wave length of radiation. As previously stated, this requires only that the same wave length be used in the model study as in the calibration. Furthermore, relations (2.16) take no account of the effect of temperature upon the material properties; this effect is very pronounced. Constant (and identical) temperature is, of course, desirable for calibration of the material and the model study, either mechanical or photoelastic. If

constant temperature cannot be maintained, then it is essential that the temperature cycle be the same for both.

The times expressed in relations (2.16) are measured from the "instant" a constant load is applied. Since the load cannot be instantaneously applied, some error is introduced by the loading procedure. The smallest meaningful times in relations (2.16), as well as earliest times at which readings should be taken in the model test, depend upon the manner and speed of the loading. This point is further discussed in Part B of this chapter.

Part B. Calibration Procedure

Possible Calibration Models

Theoretically, any model for which there is a known analytical solution for the stress distribution can be used for calibration. In practice, limitations of experimental technique, available equipment, and the accuracy required may govern the selection. Possible models include prismatic tension bars or "stepped" tension bars with prismatic sections, circular disks in diametral compression, beams in pure bending, and concentrated loads on "semi-infinite" plates.

Each of these has distinct advantages as well as disadvantages. Since none of the models mentioned were used successfully for obtaining the data essential to this study, only their disadvantages will be stressed.

For a given load, only one level of stress prevails in a prismatic tension bar. Hence only one value of strain or one value of the isochromatic fringe order can be obtained for a given load at a given time. Determination of the properties for a range of stress and time requires either a number of models or repeated or step loading on a single model. When a number of models are used, they must be machined and handled identically. If repeated loading is used, the specimen must be allowed to recover completely between loads and the repeatability of response must be checked. For complete recovery annealing is sometimes required. If step loadings are employed, creep effects are more difficult to account for, especially if response is nonlinear. Should "crazing" of the material occur, as it did at high stresses in some of the materials tested, then neither repeated nor step loadings would seem satisfactory.

The stresses in a circular disk in diametral compression are biaxial [68] and somewhat difficult to relate to strain or isochromatic order at any given point on the disk. If this difficulty is avoided by considering only one point in the disk, such as the center, then repeated or step loads are necessary.

Beams in pure bending, though not presenting the same problems as the prismatic bar or the disk, are somewhat more difficult to load than the other models mentioned. In addition, if large deflections occur, as

they often do in plastics, the elementary beam theory must be abandoned in favor of a more complex theory. Then problems similar to the ones mentioned for the disk appear.

Although the stress distribution for a concentrated load on a semi-infinite plate is quite easily related to strain or order of isochromatic [13], the loading is somewhat difficult, especially for thin plates. The "semi-infinite" condition also imposes restrictions on the smallest permissible size of plate.

Another possible model, which better meets the requirements for this study, is a tapered model or "wedge." Coker and Filon [6] suggested the use of a wedge, loaded symmetrically in compression, for use as a compensator. The frozen stress method was applied to a modified wedge model by Frocht [18] to produce a permanent compensator. The wedge was further modified and used by Pindera [47] in studying rheological photoelastic properties of various materials. The first known attempt to use the moire method on a tapered model for studying rheological mechanical properties is made in this study. It also includes a slightly modified technique in machining to ensure the desired symmetry.

Model Used in This Study

The obvious advantage of the wedge over the models mentioned above lies in the fact that a range of stress is produced by a single load, this stress being distributed

radially and varying continuously. Hence a single model produces data for a chosen range of stress at any given time after a load is applied. That the stress distribution in a wedge is purely "radial" was shown by Frocht [18] and is given in Appendix I of this thesis, along with the procedure used for determining the stress at any point on the centerline of the modified wedge used in this study. A sketch showing the approximate shape of the model is also presented in Appendix I.

For the photoelastic calibration test a scale was scribed along the centerline (previously scribed) of a tapered model and the smallest division of the scale chosen as either 0.10 inch or 0.20 cm. A vernier height gage moving on a surface plate, shown in Figure 2.10, allowed a high degree of accuracy in the scribed scale. The width of the model at specified points along the centerline was then measured with either a micrometer caliper or a measuring microscope. The radial (or actual) stress at these specified points was computed from the nominal stresses and the stress concentration

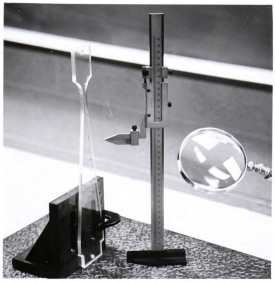

Fig. 2.10--Equipment used to scribe scale on models.

factors given in Appendix I. Plotting of stress vs. distance along the centerline followed.

The model was loaded in tension by means of dead weight on the lever of a stationary load frame within the field of a circular polariscope. Photographs were taken of the model showing isochromatic fringes, as well as the scale on the model, at chosen times after application of the load. From these photographs data was obtained for a plot of isochromatic fringe order n vs. distance along the centerline. Then the relation between stress and fringe order could be obtained for every time at which a photograph was taken--i.e., the relation

$$n = n(\sigma),\ t = \text{const}\ (t_1, t_2, t_3, \ldots)$$

was obtained.

With the aid of the moire method, data for mechanical properties was obtained from the same type of tapered model. Since the stress in the wedge portion of the model is radial, it follows that the strain is also radial. A grid of density 500 lines per inch was applied (see Appendix II) along the centerline, with the grid lines perpendicular to the centerline of the model. A matching grid on a "dummy" model placed in front of the active one produced moire fringes whose spacing depends upon relative displacement between the two grids. Following the same procedure (from scratching the scale to photographing

fringes) as explained above for the photoelastic calibration, a plot of the moire fringe order m vs. distance along the centerline was obtained. As explained in Appendix II, the slope of such a curve at any point yields the strain at that point. After these slopes were obtained, at chosen points corresponding to chosen values of stress, the relation

$$\varepsilon = \varepsilon(\sigma),\ t = \text{const}\ (t_1, t_2, t_3, \ldots)$$

was obtained.

Other details of the test procedure are outlined in the following sections.

Model Preparation and Clamping

The tapered models were cut to coarse dimensions with a band saw and finished with a high-speed routing tool integrated into a Ratiobar Pantograph. Symmetry could not be achieved with a single mounting of the model on the table of the pantograph. The problem was circumvented by drilling, on the centerline of the model near each end, a small hole which fit tightly over a stationary pin on the machining table. After one side of the model was machined, it was turned over and aligned by means of the pins for machining of the other side.

When brittle materials were used, the edges of the model were hand polished with three grades (1,2,0) of

metallurgical emery polishing paper followed by two grades (1.0 and 0.3 micron) of powdered alumina abrasive to partially eliminate stress concentrations arising from minute machining notches or scratches.

The jaws of the mounting clamps were padded with thin sheets of nearly pure aluminum to prevent surface damage to the model. As one further means of reducing stress concentration, the effects of bending of the clamp jaws were minimized. This was shown to be necessary by fracture at the clamps of several specimens. Both the problem and the solution are illustrated in Figure 2.11.

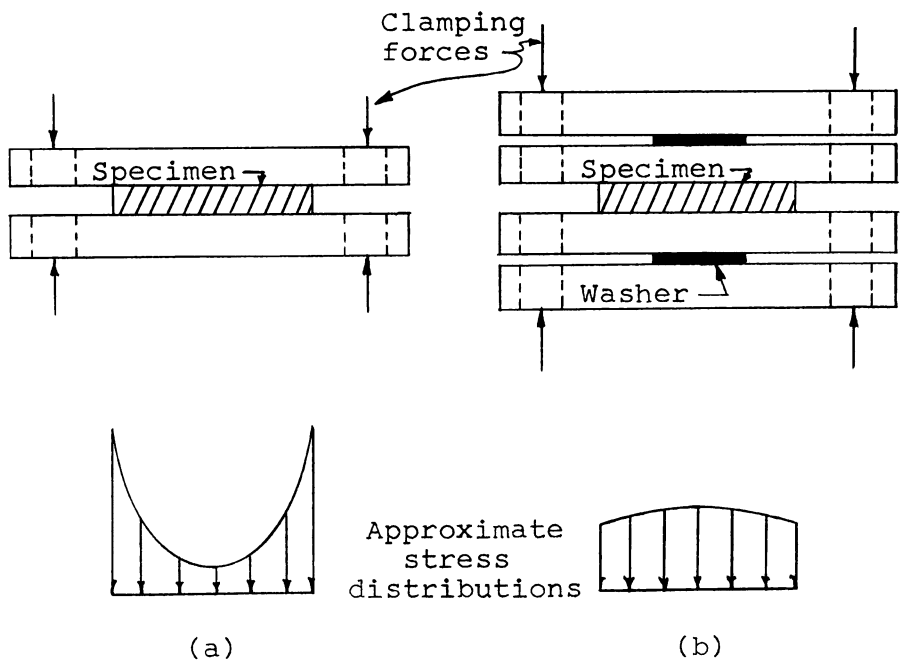

Fig. 2.11--Sketches illustrating (a) the effect of bending of the clamp jaws, and (b) improvement by modification.

Test Procedure--Photoelastic Calibration

After the model was completely prepared and measured, it was mounted in the upper clamp of the load frame. The lever, on a knife-edge fulcrum, was then balanced with the load hanger in place. Hence no correction for the weight of the lower clamp was required. After the model was secured in the lower clamp, dead-weight load was applied to the hanger.

Usually the load was applied within about two seconds, in a single step. When relatively large loads demanded a two-step loading process, five to six seconds were consumed. Time measurement began when the full load was reached. Because of the loading time, measurements within the first few seconds seemed meaningless. Hence first measurements were usually taken after four to six seconds in case of single-step loads and ten to twelve seconds for two-step loads.

Duration of the constant load was intended to be 240 hours in all tests; however, in several tests fracture of the model occurred in less time. When it occurred in less than about 100 hours, the test was repeated; otherwise the results were used. Though creep tests ideally maintain constant stress on the specimen, rather than constant load, the difference is small for high-modulus materials where changes in cross-section are small.

Recovery data was collected when the model carried the load for the full 240 hours. Though not essential to this study, such data might be useful for checking superposition theories of viscoelastic materials, to name only one possibility.

The load frame was within the field of a standard type of circular polariscope consisting of a light source, condensing lens, dispersing screen, polarizer, quarter wave plate, model, quarter wave plate, analyzer, filters, and camera. Figure 2.12 shows the polariscope. The light source, as well as the camera and filter wheel, was repositioned for the photograph. Space limitations prevented taking a composite photograph with all elements in normal position.

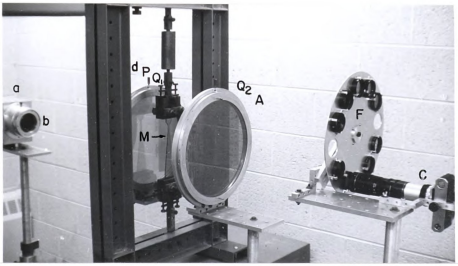

Fig. 2.12--Polariscope used in photoelastic studies: (a) light source, (b) condensing lens, (d) dispersing screen, (P) polarizer, (Q_1) quarter wave plate, (M) model, (Q_2) quarter wave plate, (A) analyzer, (F) filters, and (C) camera.

The function of each of these elements has been explained by a number of authors. Frocht's [18] presentation was concise and appealing; Jessop and Harris [28] also included a thorough explanation of possible errors arising from the improper use of some arrangements.

A "mixed setup" of the circular polariscope was employed for producing the isochromatic fringes pertinent to this study. The quarter wave plates were kept crossed and 45° from the plane of polarization. Generally a "light field," produced by crossing the planes of the polarizer and analyzer, was used because it offered the advantage of making visible the boundaries of the model.

As stated, the circular polariscope causes only the isochromatic fringes to appear, each fringe being the locus of points having a constant difference between principal stresses. Since the model is symmetrical about its centerline, the isochromatic fringe pattern is symmetrical. Furthermore, in the wedge portion of the model the isochromatic fringes are radial, as a consequence of the radial stress distribution there. Isoclinics, representing constant stress direction, are not required.

Because a range of wave lengths was used with the same polariscope, the performance of the quarter wave plates was checked. Their performance must be questioned, because a plate can give a relative retardation of exactly one-quarter wave length for only the one particular wave

length for which it is designed. Mindlin [40] showed, however, that if crossed plates are not quarter wave plates for the wave length used, but are nevertheless identical, then the isochromatic fringe pattern is unaffected. The only effect is the incomplete removal of the isoclinics. Jessop and Harris [28] showed further that if the plates are identical and each produces a relative phase retardation of one-fourth wave length plus some error, then the maximum error introduced into the fringe pattern will be the algebraic difference of their individual errors when they are crossed but will be the algebraic sum when the plates are used parallel. Since they were crossed in this investigation, the accuracy of their over-all performance depended only upon their being identical.

The check for possible error consisted simply of comparing the location of isochromatic fringes produced by two "setups" of the polariscope for a wave length other than the one for which the quarter wave plates were intended. One setup was the mixed circular one used throughout. The other consisted of putting the quarter wave plates' axes in the plane of vibration of the polarizer, 45° from the model axis;[1] hence these plates produced no effect upon fringe formation.

---

[1]Both isoclinics and isochromatics were produced in the second setup. To eliminate the objectionable effect of having a zero-order isoclinic along the centerline of the model, the plane of polarization was shifted 45° from the centerline. The zero-order, 45° isoclinic does not appear on the centerline.

This comparison revealed no difference in the isochromatic fringe location for any wave length used in the investigation; the quarter wave plates apparently qualify as "identical."

Nine filters, all manufactured by Zeiss Jena, were used to isolate wave lengths of 410, 436, 500, 546, 578, 600, 650, 750, and 800 nm, emitted by a 200 watt high pressure mercury lamp by Osram. Within this range of wave lengths the mercury lamp emits high intensity "peaks" at 405-408, 436, 546, and 577-79 nm. However, the highest intensity is produced at 365-66 with a rather broad band. Coupled with the relatively broad transmission band of a Zeiss Jena 405 nm interference filter, this led to difficulty in attempting to isolate the 405 nm wave length, which seemed a natural one to use. Fortunately, a 410 nm filter transmitted very little of the 365 nm emission band but enough of the 405 nm band so that the 410 nm wave length could be isolated.

At frequent intervals throughout the tests, pictures were taken of the isochromatic fringes with at least three wave lengths, usually 410, 578, and 800 nm. Analyses of the effects of time--i.e., the creep characteristics--were deduced from these. At one or two selected times during the test, pictures were taken using all nine wave lengths. These provided information on the possible variation of linear limit stress with wave length, as well as data on

the dispersion of birefringence. Taking a series of nine pictures required approximately six minutes; only after the load had been on the model for a long period of time--say 100 hours--was such a series taken. The effect of creep during the six-minute interval could then be neglected.

All pictures were taken with a Nikon F camera (35 mm) fitted with a Coligon Zoom lens, f = 95 mm to f = 205 mm. The long focal-length lens allowed sufficient separation of the camera from the model so that the maximum deviation from normal incidence was less than 3°.

Kodak High Speed Infrared film was used throughout the photoelastic studies. Exposures varied from one second at f-16 for wave lengths of high intensity (peak outputs of the mercury light source) to sixty seconds at f-6.3 for wave lengths filtered from the "background" or continuous radiation of the source.

Film negatives were projected and magnified (15X) for observation. Possible distortion by camera or projector lenses or of the film was not important, since the reference scale was scribed on the model. Slight distortion by the projector lens was detectible.

Test Procedure--Mechanical Calibration

The load frame used and the loading procedure for the mechanical model tests were identical to those described for the photoelastic ones. Figure 2.13 shows

the essential parts of the apparatus. The light source and camera were repositioned to permit a composite photograph.

The optical system is illustrated in Figure 2.14. To approximate a point light source a small hole (0.039-in diameter) was drilled through an opaque diaphragm and introduced into the optical system.

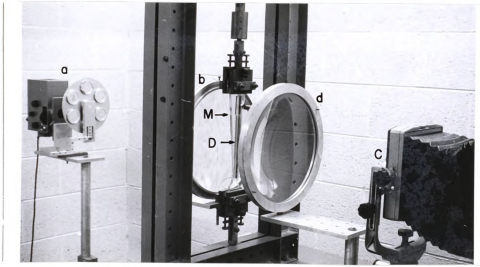

Fig. 2.13--Apparatus used in mechanical model tests: (a) light source, (b) collimating lens, (M) model, (D) "dummy" model or analyzer, (d) condenser lens, and (C) camera.

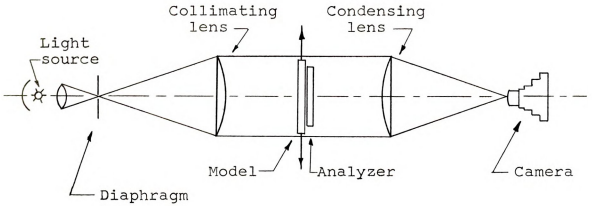

Fig. 2.14--Optical system used in mechanical model tests.

A 200 watt high pressure mercury lamp, a double convex condenser lens, and a blue filter were contained in a Leitz Model 250 lamp housing. The collimator and condenser consisted of a matched pair of plano-convex lenses of 13-inch diameter and 39-inch focal length. A Linhof Technika camera with a Schneider-Kreuznach Xenar 1:4.5/300 lens was used to photograph the moire fringe pattern. Kodak Panatomic-X (4 in x 5 in) sheet film was used.

Since model and analyzer were placed in a parallel-light field, spacing between them was not critical, although fringe quality improved with smaller spacing. The dummy model, made of the same material as the active one, was attached to the active model near one end by means of a small C-clamp. A thin shim between the models, spanning a small length on each side of the clamp, provided the necessary complete separation between the active and dummy models outside the clamped region. Location of the shim and clamp are illustrated in Figure 2.15.

Since the load lever was balanced after the analyzer was attached but before the model was secured in the lower loading clamp, no corrections for the weight of analyzer or clamp were necessary.

Loading procedure and duration, as well as the timing of pictures, were the same as for the photoelastic models described earlier. A check for symmetry of loading

was accomplished with the aid of a small circular polariscope held by hand.

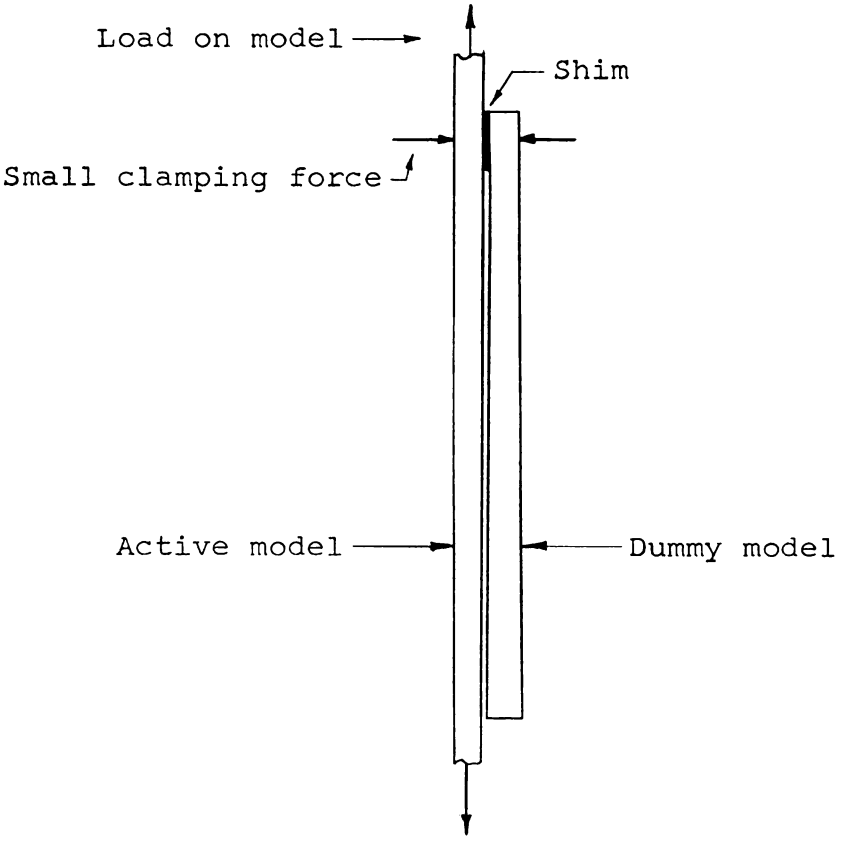

Fig. 2.15--Illustration of method of attaching moire analyzer to model.

All tests, both mechanical and optical, were conducted at 68°F $\pm$ 1°F. With the humidistat existing in the laboratory precise control of the relative humidity could not be maintained. It was observed on a recording hygrometer to vary between 55% and 70%.

Materials Tested

Because the primary aims of this study are to investigate certain possible sources of error and to suggest ways of improving the accuracy of photoelastic stress analysis, those materials commonly used in photoelasticity were selected for testing. Polyester Resin CR-39 was the first choice, because of its extensive use in photoelasticity; it is probably the most commonly used of all birefringent materials in this country. This material was supplied by Cast Optics Co., Inc.

Also selected for examination were two materials commonly used for photoelastic coatings but believed to be potentially useful also for models. These were supplied by Photolastic, Inc.: Epoxy Resin PS-2 and Polyester Resin PS-1. These, as well as CR-39, are available in sheets of various sizes and thicknesses.

Polyester Resin Palatal P6-K, manufactured by Badische Anilin und Soda-Fabrik (Germany), was also tested. The material in liquid form was donated by the manufacturer. Plates were cast in 1/4-inch and 3/8-inch thicknesses and then cured.

In summary, the materials tested were:

Polyester Resin CR-39.

Epoxy Resin PS-2.

Polyester Resin PS-1.

Polyester Resin Palatal P6-K.

CHAPTER III

BIREFRINGENT AND MECHANICAL PROPERTIES OF CR-39

Birefringence vs. Stress, Time Constant

Details of the testing procedure and of the graphical presentation of results were given in the preceding chapter. Discussion in this chapter is therefore limited mostly to the results obtained.

The birefringence data presented in this chapter is based on the shortest wave length used in the study--namely, 410 nm. Since the isochromatic fringe order is inversely related to wave length, the highest possible number of fringes was thus obtained.

Figure 3.1 shows the fringe order n as a function of length along the centerline of the specimen. The extensive use of the 410 nm wave length was not anticipated when the test was conducted. Consequently, two pictures with another wave length were taken before the first one with 410 nm at one minute after the load was applied. The accuracy and fineness of the scribed scale (smallest division 0.20 cm) allowed accurate location of both integral and half-order fringes. The data furnished very smooth curves with no observable irregularities.

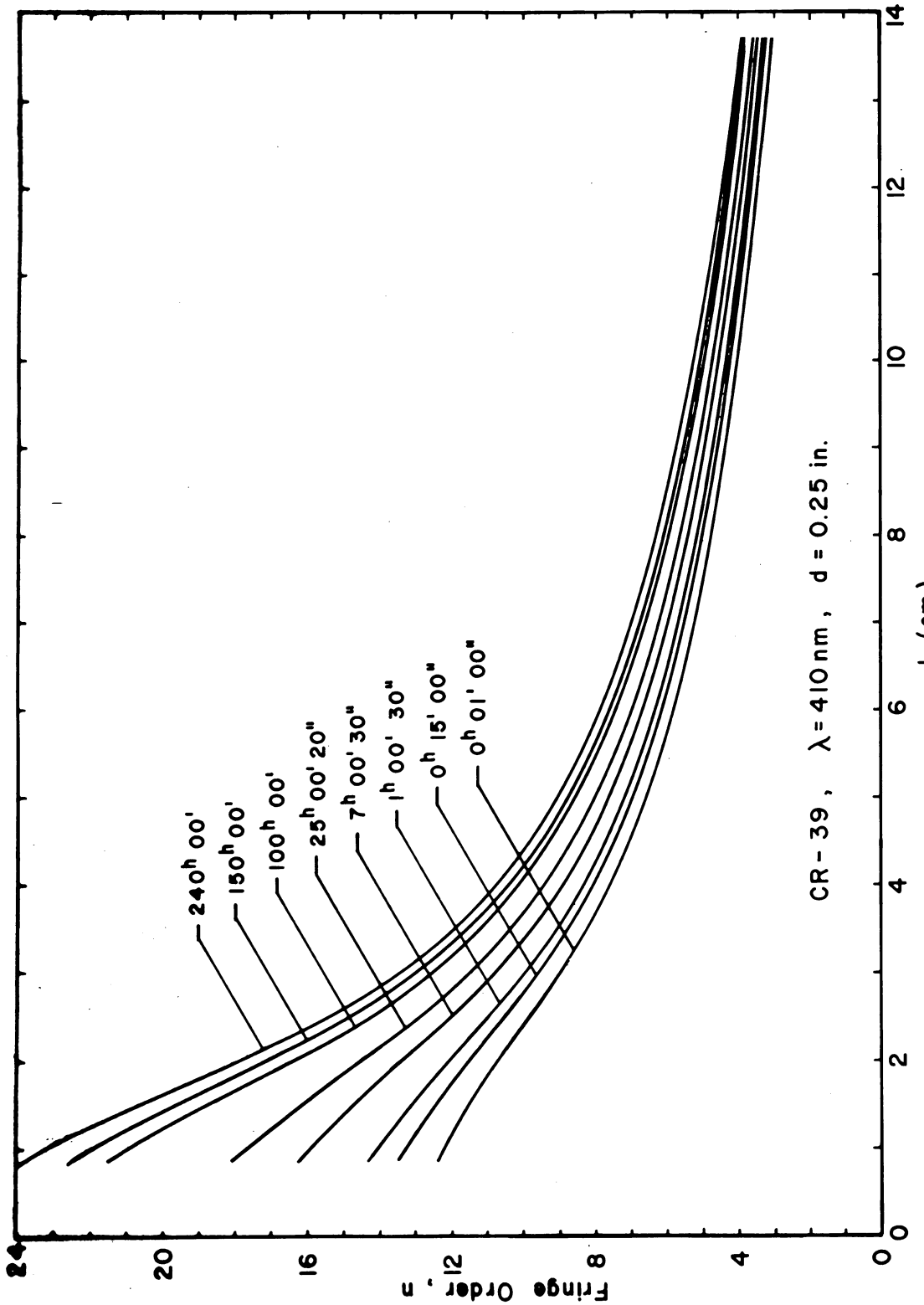

Fig. 3.1--Isochromatic fringe order n vs. distance along centerline, $t = t_1, t_2, \ldots, t_n$ for CR-39.

A measuring microscope permitted corresponding accuracy in measuring the width of the specimen at a number of locations. The thickness was measured at several points with a micrometer caliper. The nominal stress was computed from the area and the load of 320.85 pounds (64.17 magnified 5.00 times by the load lever). By using the values of the "stress concentration factor" described in Appendix I, the actual stress was computed at each of the points where the area was known. A plot of stress vs. length along the centerline (not shown) yielded no detectible scatter.[1]

The fringe order for each of the times represented in Figure 3.1 was then read at about fifteen values of stress, ranging from 800 psi to 2,900 psi. One additional set of points corresponding to fringe order and stress in the shank is also available. Data was thereby obtained for a plot of fringe order as a function of stress for each time represented. This plot is shown in Figure 3.2.

The nonlinearity of the stress-optic behavior is clearly evident in this plot. The linear limit stress at one percent deviation from linearity, denoted by $_n(\sigma_{\ell\ell})_{1.0}$, is marked by an "x" on each curve. For the assumption of linearity to be accurate within one percent, it appears necessary that the fringe order remain below seven fringes

---

[1]The term "scatter" usually implies the testing of more than one specimen and some sort of data averaging for each point plotted. Tapered models were used in this study to avoid such scatter. Herein, scatter denotes observable irregularities or lack of smoothness.

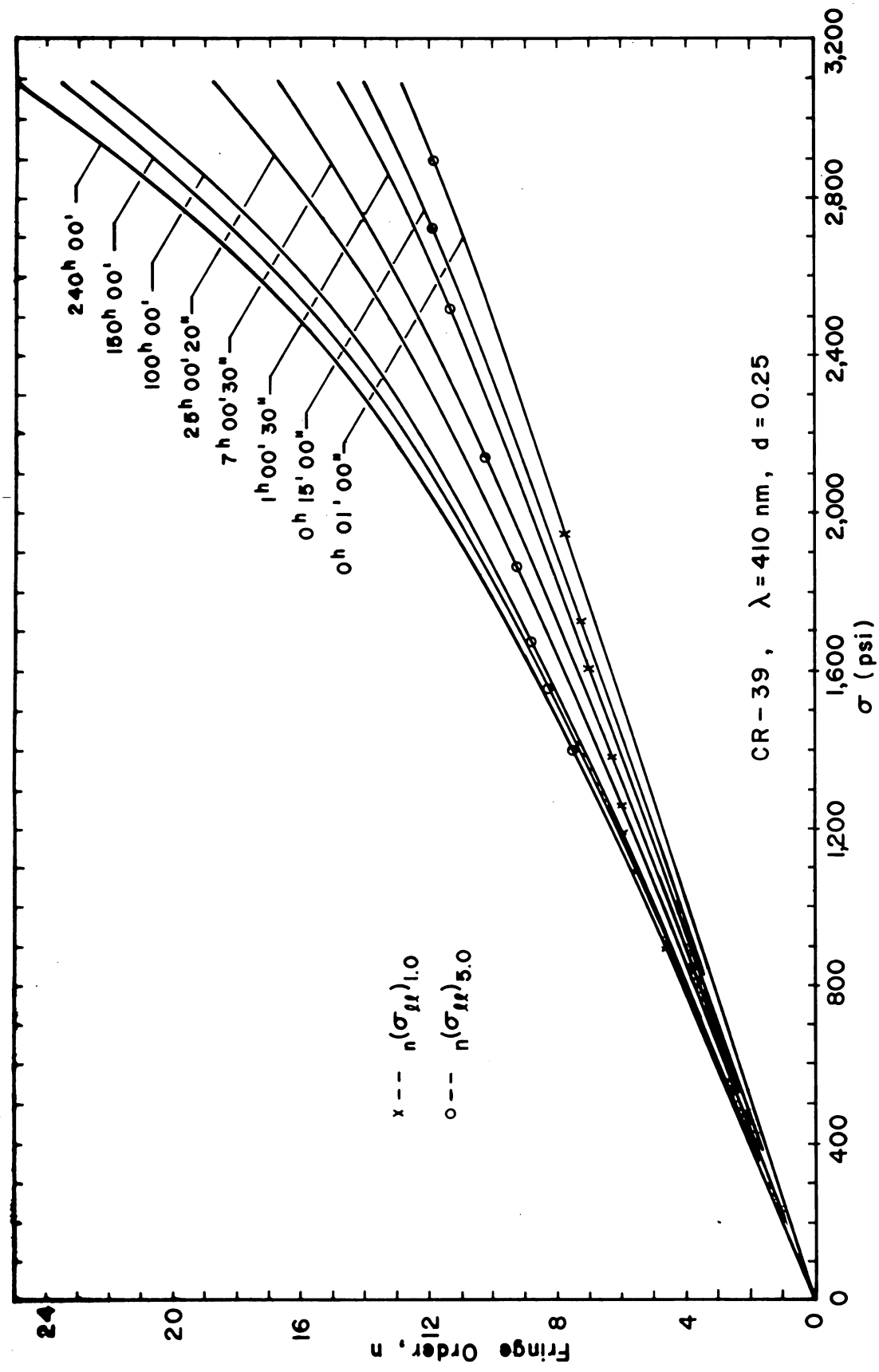

Fig. 3.2--Isochromatic fringe order n vs. stress, $t = t_1, t_2, \ldots, t_n$ for CR-39.

within the first hour after loading. This number depends, of course, upon the wave length of radiation and the thickness of the model.

It should also be observed that within the first hour after loading a much higher fringe value (or stress) is permissible if a deviation from linearity of, say, five percent is allowed. The linear limit stress at five percent deviation from linearity is marked by an "O" in Figure 3.2. The difference between $_{n}(\sigma_{\ell\ell})_{1.0}$ and $_{n}(\sigma_{\ell\ell})_{5.0}$ is seen to decrease with increasing time.

The error in assuming the linearity at small stresses to extend to higher stresses may be considerable. At 3,000 psi, for example, this error is approximately 7% at one minute, 11% at one hour, 28% at 25 hours, and 56% at 240 hours.

Birefringence vs. Time, Stress Constant

At the eight times represented in Figure 3.2 the fringe order at any stress within the prescribed range may be obtained, thus providing data for plotting fringe order as a function of time with σ = constant. Figure 3.3 shows such a plot. Nonlinearity at a given time may again be observed as increasing distance between consecutive curves as the stress level increases.

Any irregularities (or "scatter") of raw data would have shown in Figure 3.1 and have been "smoothed" by

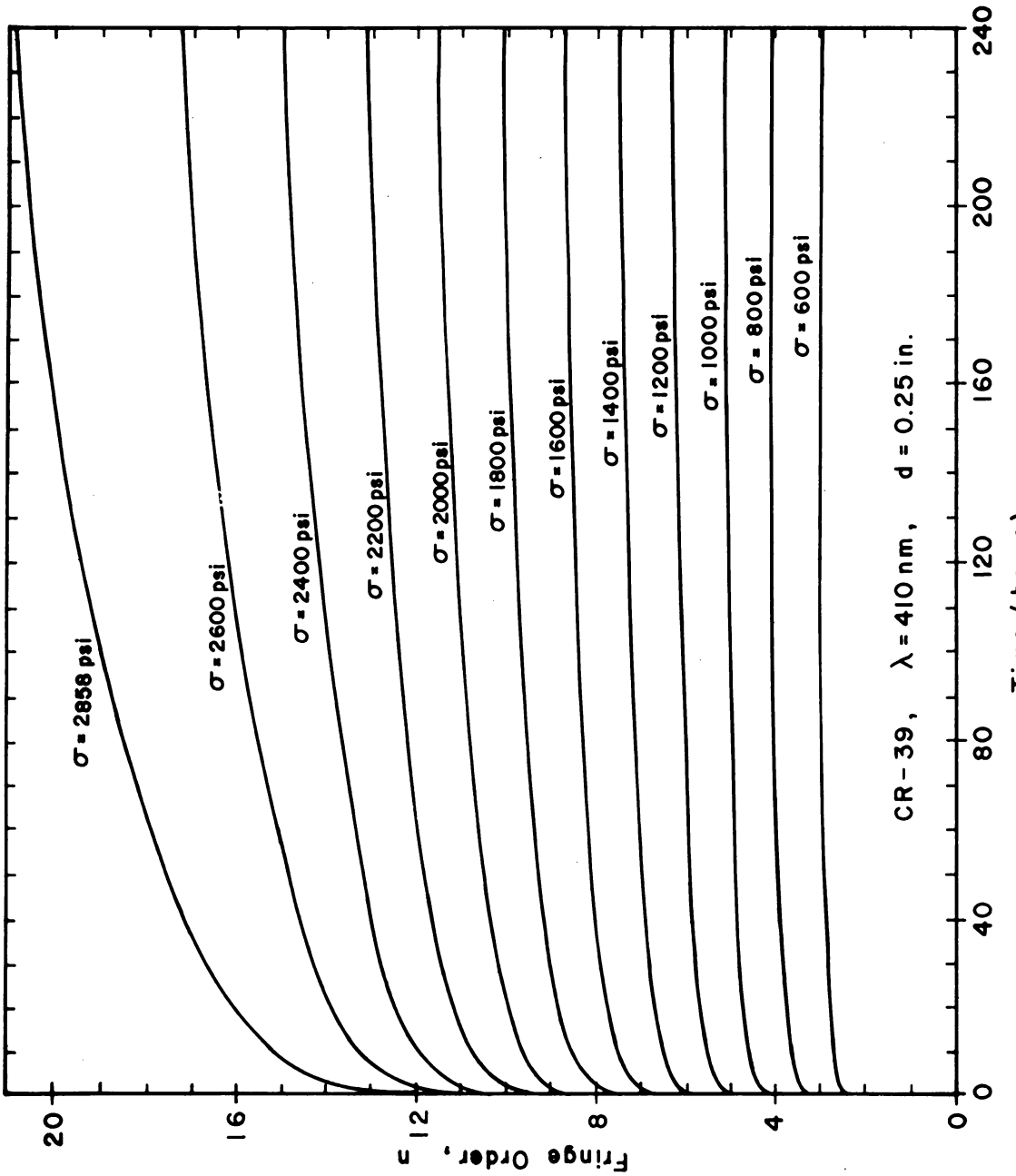

Fig. 3.3--Isochromatic fringe order n vs. time, $\sigma = \sigma_1, \sigma_2, \ldots, \sigma_n$ for CR-39.

careful plotting to a large scale (21 in x 33 in). The last two figures were deduced from Figure 3.1; thus no irregularities were apparent in these plots.

Strain vs. Stress, Time Constant

With the aid of the moire method of strain analysis, evaluation of mechanical properties followed a procedure very similar to that used in evaluating birefringence properties. In Figure 3.4 the moire fringe order is shown as a function of distance along the centerline of the specimen for eight values of time after the load was applied. The grids were apparently distorted in the course of applying them to the specimen and analyzer. This gave rise to an initial moire pattern represented by the lowest curve shown.

The first picture of the moire pattern was taken approximately four seconds after the load was applied. With a fringe order of approximately twenty, locating both integral and half-order fringes provided approximately forty points for plotting a curve. This was increased to about seventy-eight points at 150 hours, after which the specimen fractured. The scatter of data points on this plot was again insignificant. Though a more dense moire grid would increase the number of points available for plotting, these additional points would not aid materially in defining the shape of the curve.

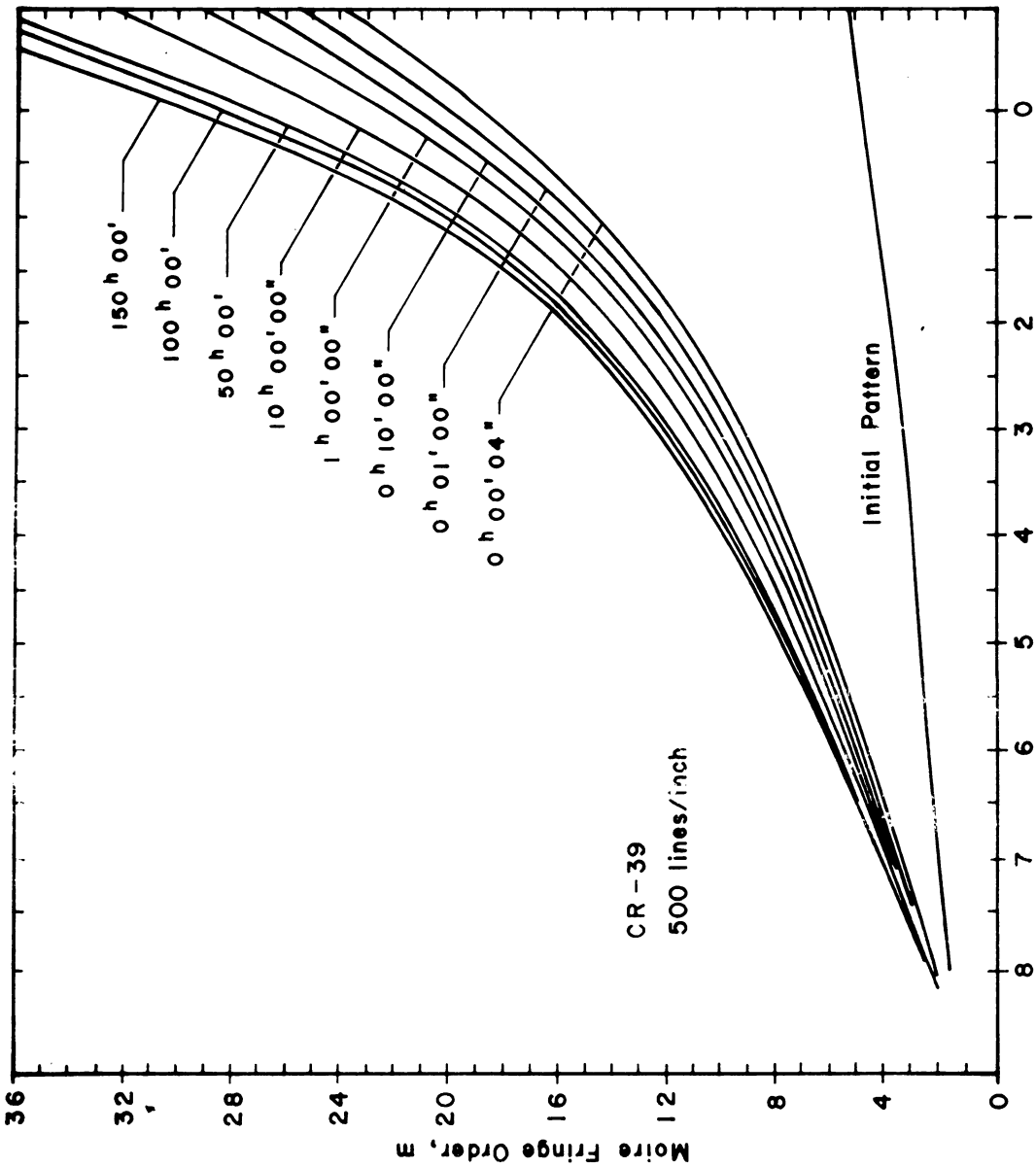

Fig. 3.4--Moire fringe order m vs. distance along centerline, $t = t_1, t_2, \ldots, t_n$ for CR-39.

Stress was plotted as a function of distance along the centerline of the specimen.

The strain at a given stress and time is represented by the slope of one of the curves at a particular point. Slopes were measured by a graphical technique, employing a set of mirrors mounted on a 90° machining block. One mirror was placed tangent to the line at the chosen point, the other perpendicular to it, thus yielding an image of the line tangent at the point and an image continuing the line at the point.

This method of measuring slope is, of course, susceptible to significant error. However, readings could be repeated to within about four percent. The possible increase in accuracy resulting from a sophisticated numerical evaluation of the slopes did not seem to be justified.

The slope evaluations yield data for plotting strain (or percentage elongation) as a function of stress for each of the times represented in Figure 3.4. Such a plot is shown in Figure 3.5 with the data points indicated. Some lack of smoothness is seen to exist. Because of the initial moire pattern, the data points actually represent the difference of two slope measurements, increasing the possible error. Despite this the scatter does not seem excessive, and the results are believed quite reliable.

Nonlinearity of the mechanical behavior at high stresses is again rather obvious. The departure from

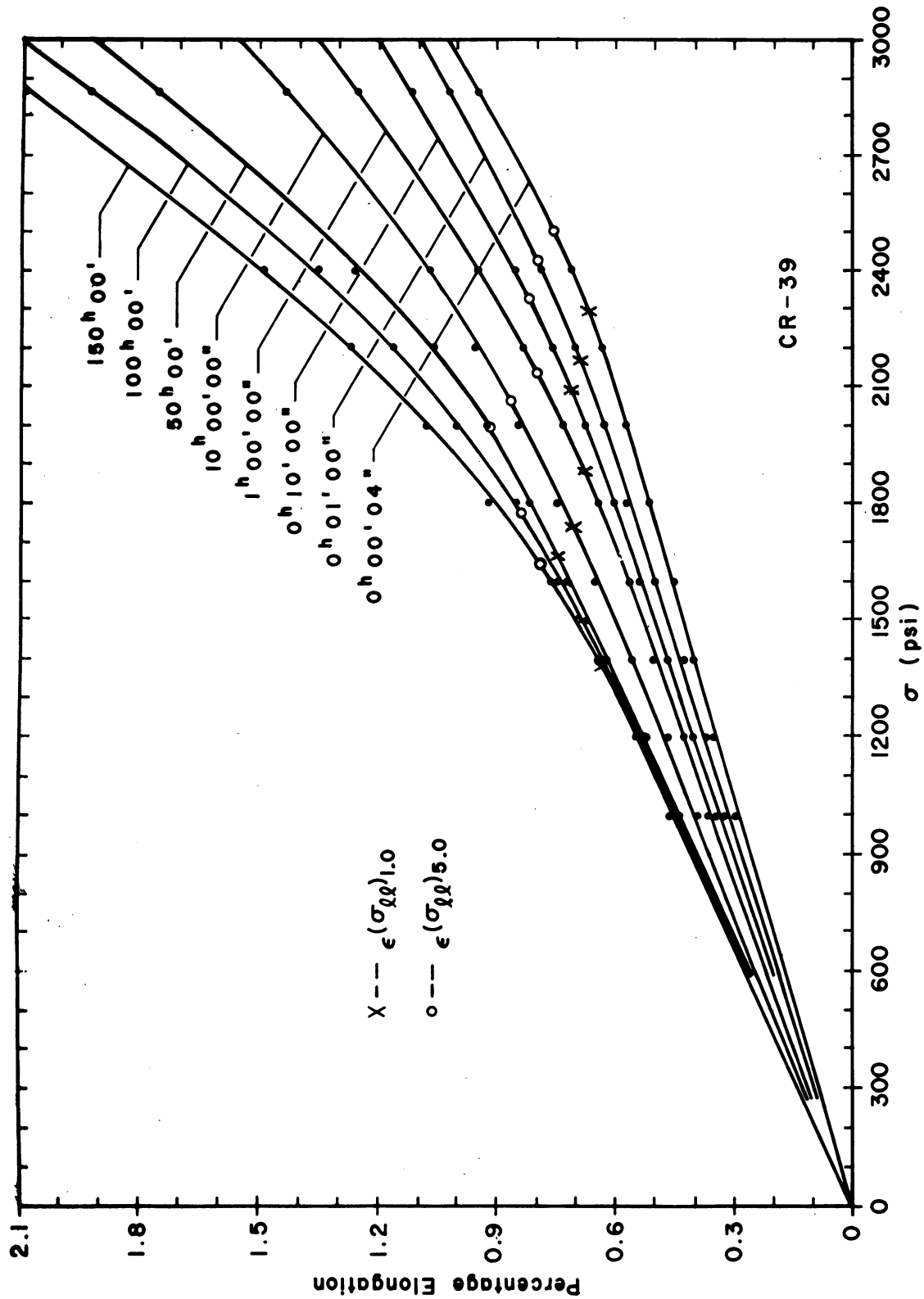

Fig. 3.5--Percentage elongation vs. stress, $t = t_1, t_2, \ldots, t_n$ for CR-39.

linearity (vertical deviation from extended straight line) seems more rapid than for birefringence, as indicated by comparison with Figure 3.2. The stress at one percent deviation from linearity $_{\varepsilon}(\sigma_{\ell\ell})_{1.0}$ is again marked by an "x" on each curve and $_{\varepsilon}(\sigma_{\ell\ell})_{5.0}$ by an "O." Linear limit stresses will be further discussed in a subsequent section.

Strain vs. Time, Stress Constant

From Figure 3.5 data can be deduced for a plot of strain (or percentage elongation) vs. time for a fixed stress level. Figure 3.6 shows such a plot for twelve levels of stress. Deviations from linearity again appear as increasing distances between consecutive curves at higher levels of stress.

Since the plot of Figure 3.5 "smooths" the measured strain data, the data points of Figure 3.6 furnish regular, well-defined curves.

Linear Limit Stress vs. Time

After the optical and mechanical linear limit stresses are determined from Figures 3.2 and 3.5, respectively, it is possible to show them as functions of time. This is done in Figures 3.7a and 3.7b; different time scales are necessary to show clearly their variation throughout the time interval for which they were determined.

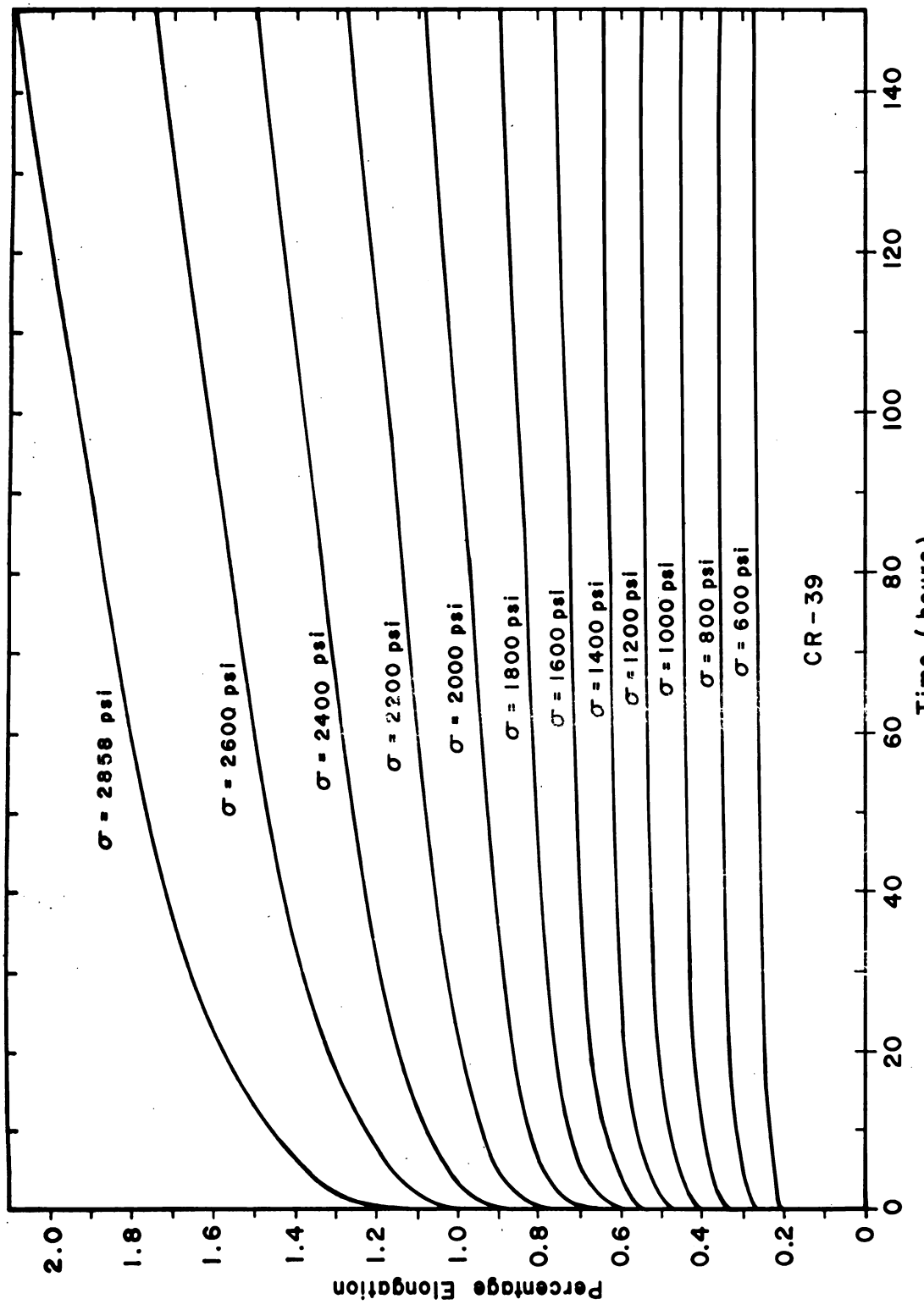

Fig. 3.6--Percentage elongation vs. time, $\sigma = \sigma_1, \sigma_2, \ldots, \sigma_n$ for CR-39.

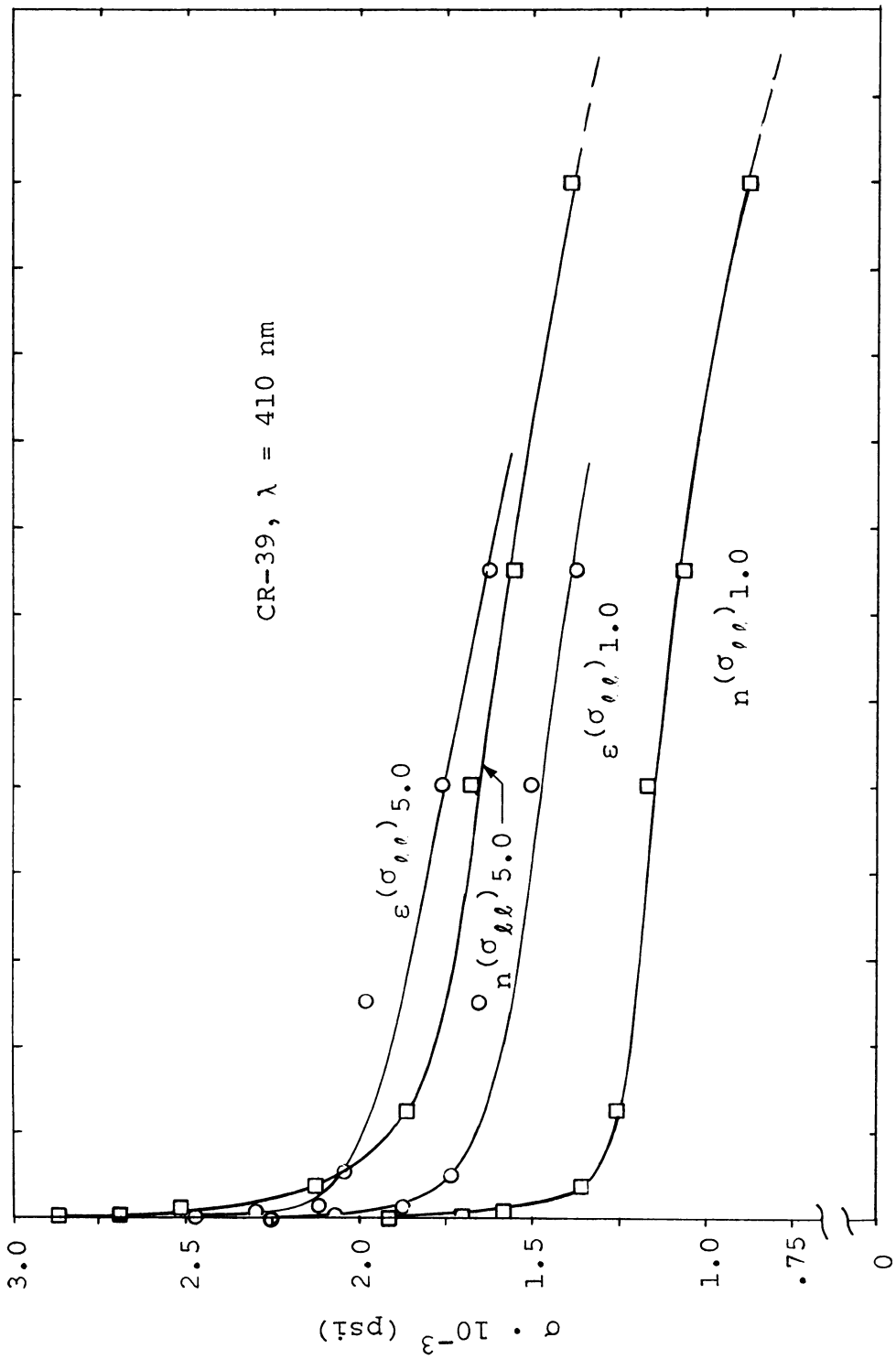

Fig. 3.7a--Linear limit stresses vs. time for birefringence and strain, time range: 0-240 hours, for CR-39.

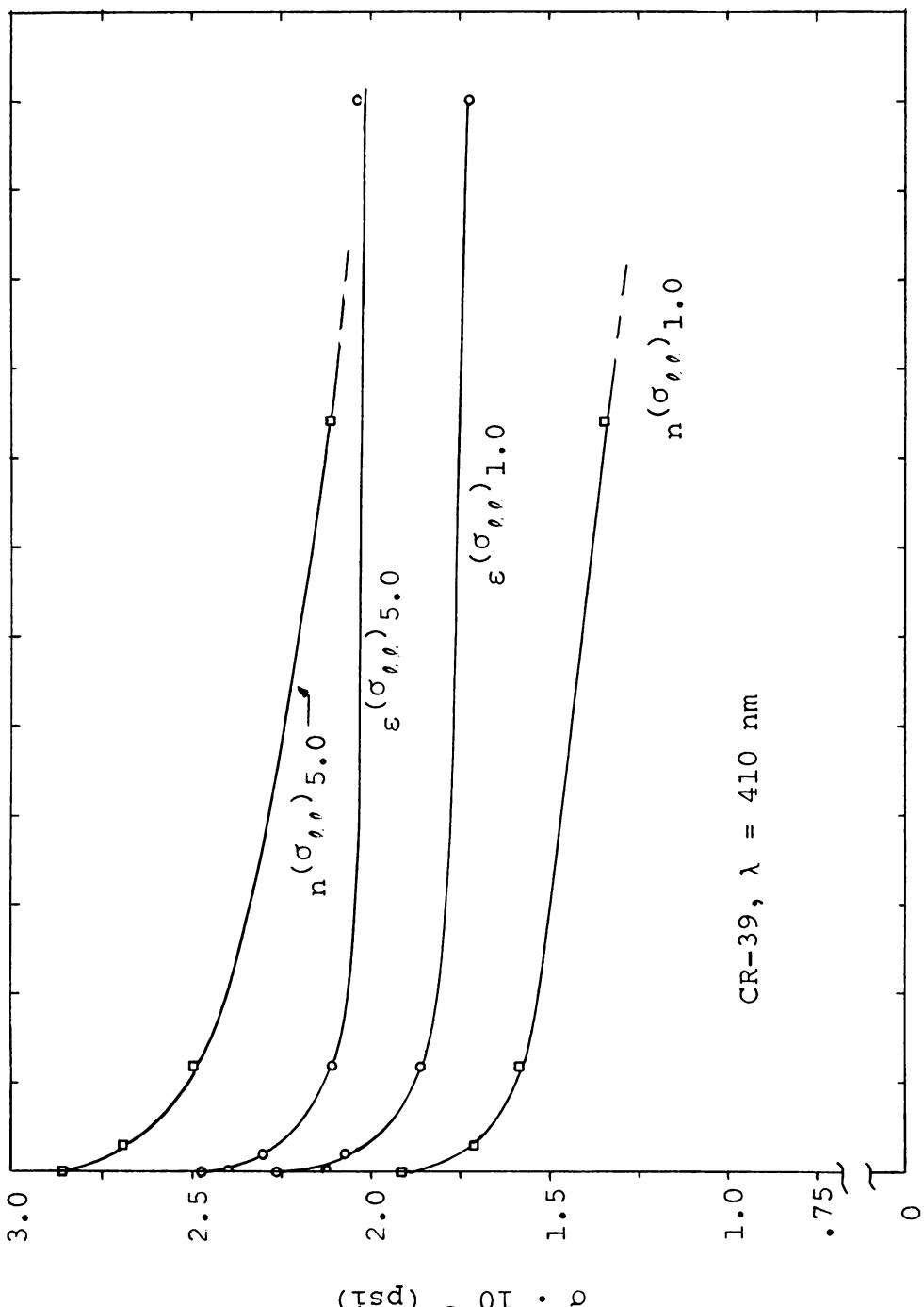

Fig. 3.7b--Linear limit stresses vs. time for birefringence and strain, time range: 0-10 hours, for CR-39.

The linear limit stress at one percent deviation from linearity is seen to be considerably lower for birefringence than for strain. Though little information is available for comparison, such a wide difference was not expected. Coolidge [7] reported that for a given rate of loading the stress-strain curve for CR-39 is a straight line up to about 3,000 psi, whereas linearity of the stress-fringe relation extends to "somewhere between 2,500 and 3,000 psi." The resin he tested was manufactured by the Pittsburgh Plate Glass Company. The method of testing employed in his investigation would not seem to permit adequate allowance for creep effects. Frocht [18] found that in Bakelite (BT-61-893) the "proportional limit" for birefringence is over twenty percent higher than for strain. Creep of this Bakelite was apparently considered negligible. Approximate values of $_{n}(\sigma_{\theta\theta})_{1.0}$ for CR-39 manufactured in Great Britain may be deduced from data presented by Pindera [47]. The values seem to be considerably higher than those of the American-made CR-39 tested in this study. However, the ultimate strength is also considerably higher for the British-made resin.

It must be concluded that the linear range of behavior, as well as other properties of CR-39, varies considerably with different manufacturers. Properties may vary from one lot to the next with the same manufacturer. Age and storage conditions may also affect some or all of

the properties. Pindera's CR-39 is known to have been stored for five years, whereas the material used in this study was tested within six months after purchase. The qualitative results of this study seem consistent with earlier findings; the quantitative differences emphasize the need for careful calibration.

Comparison of Figures 3.2 and 3.5 seems to indicate a more gradual departure from linearity in the birefringence-stress relation than in the strain-stress relation, especially at times greater than one hour. The linear limit stresses for birefringence and strain at five percent deviation from linearity are more nearly equal than those at one percent, except at very short times. This can be seen in Figures 3.7a and 3.7b. The crossing of the two curves at five percent deviation is puzzling and may be due to accumulated experimental error. Two quantities are being compared which are difficult to determine in the first place and which are of roughly the same magnitude. Irregularities are therefore not surprising. The crossing of the curves may actually portray the time behavior of the material. This does not seem entirely implausible but may be worthy of further detailed study.

Birefringence vs. Strain, Time Constant

From the plots previously shown, the relation of birefringence vs. strain at a given time after loading may

be deduced by the method outlined in Chapter II. Such a plot is shown in Figure 3.8. The largest strain encountered at one minute after loading was slightly greater than one percent. The relations are, of course, linear up to the fringe values or strains corresponding to the optical linear limit stress. Then there is a "breaking over" toward higher strain, indicating that at a given time after loading the strain increases faster than fringe value with increasing stress. Thus birefringence deviates more gradually than strain from linearity. No reference to such behavior could be found in the literature for CR-39, either to confirm or contradict these results.

The inflection of the curves at still higher values of strain (or birefringence) may warrant additional confirmation. It is not believed attributable to experimental error. An error analysis would be somewhat difficult to perform and would be of questionable accuracy. A statistical analysis of the scatter of the data points on the birefringence-stress and strain-stress plots might provide a meaningful estimate of the consistent error committed. Because of the regularity of the birefringence-stress plot, such analysis should seemingly be applied only to the strain-stress plot. But errors in measuring the slope of the moire fringe order vs. length curves are mostly responsible for the scatter of the strain-stress plot. The repeatability of the slope measurements (within

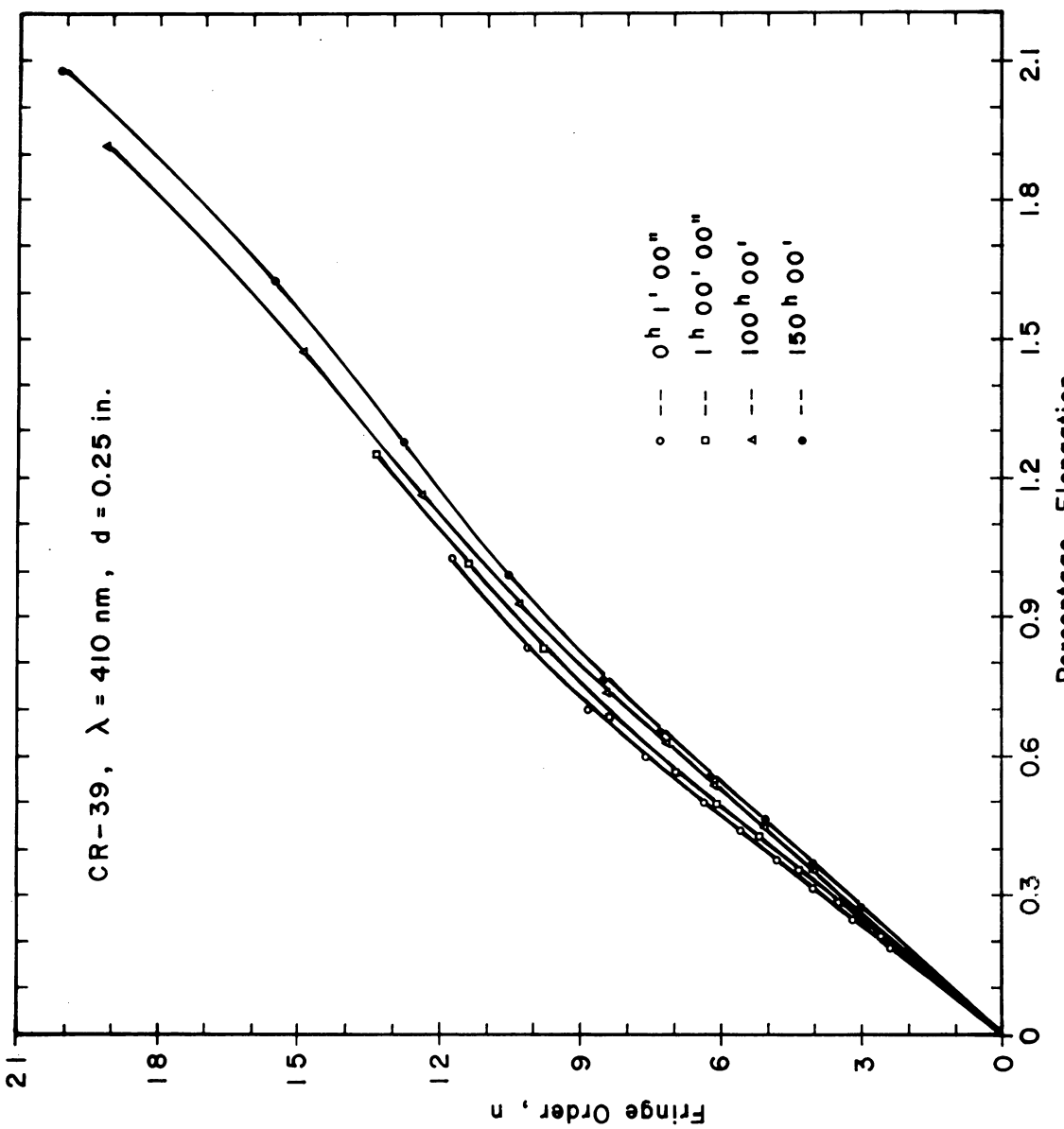

Fig. 3.8--Isochromatic fringe order n vs. percentage elongation, $t = t_1, t_2, \ldots, t_n$ for CR-39.

about 4%) offers some estimate of the possible errors in strain values. Consistent errors of $\pm$ 4% could cause the inflection, but errors of this magnitude are not believed present. Identical techniques were employed in testing the other materials (see Appendix III); no inflection appeared in birefringence-strain plots. Thus if consistent error is responsible for the inflection of the plot for CR-39, such error is apparently unique to this one test.

Further reduction of data, such as that necessary for a plot of fringe value vs. time for constant strain, does not seem advisable. Data for such a relation can be obtained directly from a relaxation test, and the plot of birefringence vs. strain for t = constant (as shown in Figure 3.8) can be obtained in a single step. Relaxation tests are thus recommended to determine whether the inflection indicated in Figure 3.8 is a true representation of this material's behavior.

At a given strain Figure 3.8 shows a decrease in birefringence with increasing time. This is expected for CR-39 by comparison with results presented by Clark [3] but, as he points out, is not true of all materials.

Material Coefficients in Linear Range

The photoelastic and mechanical material coefficients, such as $E(t)$, $f_\sigma(t)$, and $C_\sigma(t)$, can be deduced from the curves presented. As indicated, these

are functions of time, rather than constants as is sometimes assumed. It should further be emphasized that they are defined for the linear range of behavior.

From the slopes of the linear portions of the curves in Figures 3.2 and 3.5, f_σ yielding C_σ and E(t) are deduced. These functions are plotted in Figure 3.9. Their strong time-dependence during the first two or three hours, the time during which most static tests are performed, should be noted. The possible error which may result from assuming these functions to be constants, independent of time, is evident.

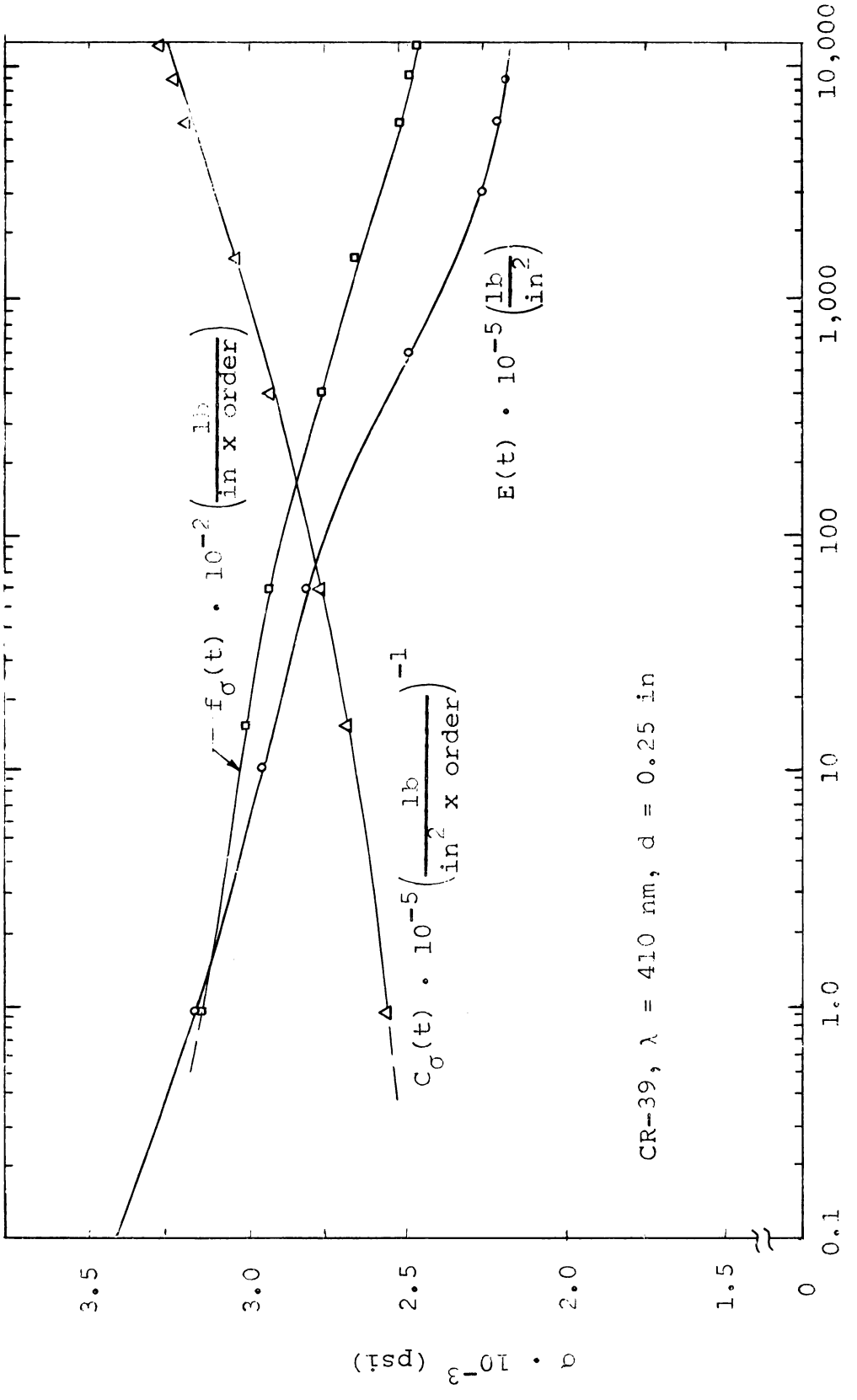

Fig. 3.9--The functions $C_\sigma(t)$, $f_\sigma(t)$, and E(t) for CR-39

CHAPTER IV

VISCOELASTIC STRESS ANALYSIS

Introduction

From the discussion and the graphical presentation of results in the two preceding chapters, the change with time of the mechanical and optical properties of the materials is quite apparent. This viscoelastic behavior is manifested as creep under constant stress or relaxation under constant strain. In most discussions, strain and stress are considered the time-dependent functions in creep and relaxation tests, respectively. The simplest way to describe the viscoelastic behavior is then to define the extension modulus D(t) or one of the shear or bulk compliances or moduli (to be defined) over the whole range of time and temperature. However, other time-dependent functions such as birefringence may be considered, with an analogous photoviscoelastic description given in terms of the stress-optic or strain-optic coefficients in creep or relaxation. In the following discussion of viscoelasticity, strain is usually considered the basic time-dependent function in the discussion of the creep tests performed in this study. Birefringence data was also obtained, and the isochromatic fringe order is considered the basic

time-dependent function in a similar discussion of photoviscoelasticity.

In this chapter some elements of the existing theories of linear viscoelasticity and photoviscoelasticity are discussed. Graphs of some "characteristic functions" defined by these theories are presented. Nonlinear theories are then discussed and applied to the optical creep test of CR-39.

Though viscoelasticity and photoviscoelasticity have much in common, discussions of them are separated in the following. The similarities and differences are pointed out where they do not seem obvious.

Aspects of the Problem

The problem of viscoelastic stress analysis has three aspects [11]: determination of material properties, interrelations among the various descriptions of viscoelastic behavior, and the methods of stress analysis. The first of these, determination of material properties, is the main concern in this study. The other two aspects warrant consideration even in a study of this type, since they determine the form of representation of material properties most suitable for a particular problem, as well as define the range of time, stress, temperature, etc. for which material properties must be determined. The first two aspects might indeed be considered as one [27]--namely, that of specifying the constitutive equations of the

material which are necessary for the analytical solution of boundary-value problems.

Most of the theoretical development of viscoelasticity, and surely most of the problems which have been solved, assume linear viscoelastic behavior--i.e., the time-dependent functions are approximately linearly proportional to the applied constant stresses or strains.[1] Many photoelastic and model materials, including those tested in this study, are found to be linearly photoviscoelastic or viscoelastic, provided the applied quantities do not exceed certain limiting values. The theory of linear viscoelasticity can then be applied to solution of boundary-value problems involving such materials.

Although there does not exist as yet a systematic or unified body of theoretical results on linear viscoelasticity comparable to that available in classical elasticity theory, it may be considered well-established. Work such as that of Gurtin and Sternberg [27] established a firm mathematical basis for the theory and gave a clear formulation of the problem.

---

[1] Since the linear limit stress (in a creep test) decreases with time, the designation "linearly viscoelastic" is more restrictive than "momentarily linear"--i.e., the former implies specification of a time interval throughout which behavior is linear. Within this time interval the behavior will be momentarily linear for a wider range of stress than that for which it is linearly viscoelastic. Reference to Figure 2.1, page 19, might clarify this assertion.

The isothermal stress analysis problem for an isotropic medium is formulated as follows: Given a body, occupying a closed region of space in its undeformed state, subjected to prescribed surface tractions $T_i(x_k,t)$ over part S_T of the boundary and to prescribed surface displacements $U_i(x_k,t)$ over the remaining part S_u of the boundary, determine the stress and strain distributions throughout the body. If the body is loaded or displaced at $t = 0$, then initial and boundary conditions take the form:

$$\sigma_{ij} = \varepsilon_{ij} = u_i = 0 \text{ for } t \leq 0 \tag{4.1}$$

$$\sigma_{ij}(x_k,t)n_j(x_k) = T_i(x_k,t) \text{ on } S_T \text{ for } t > 0 \tag{4.2}$$

$$u_i(x_k,t) = U_i(x_k,t) \text{ on } S_u \text{ for } t > 0, \tag{4.3}$$

where

u_i = displacement component in the direction of the i^{th} coordinate ($i = 1,2,3$),

n_j = unit outward normal vector on the boundary,

x_k = k^{th} coordinate of point.

The equations of motion and the (small) strain-displacement equations are:

$$\frac{\partial \sigma_{ij}}{\partial x_j} + X_i = \rho \frac{\partial^2 u_i}{\partial t^2} \tag{4.4}$$

$$\varepsilon_{ij} = \frac{1}{2}\left(\frac{\partial u_i}{\partial x_j} + \frac{\partial u_j}{\partial x_i}\right), \tag{4.5}$$

where

X_i = body force component in the direction of the i^{th} coordinate,

ρ = density of medium.

Finally, the constitutive equations of the viscoelastic material may be stated in general as:

$$P(s_{ij}) = Q(e_{ij}) \tag{4.6a}$$

$$P'(\sigma_{ii}) = Q'(\varepsilon_{ii}), \tag{4.6b}$$

where

$s_{ij} = \sigma_{ij} - \frac{1}{3}\delta_{ij}\sigma_{kk}$, the stress deviator,

$e_{ij} = \varepsilon_{ij} - \frac{1}{3}\delta_{ij}\sigma_{kk}$, the strain deviator,

P, P', Q, Q' = linear operators with respect to time (to be further explained).

The solution of the stress analysis problem consists of solving the system of Equations (4.2)-(4.6). Time variations, if any, of the traction and displacement boundaries must be prescribed. This can cause severe complications; in most solved problems such variations are not considered. In quasi-static problems the inertia terms in the equation of motion are negligible; the right-hand side of Equation (4.4) then becomes zero. Most problems so far solved are of this type.

In the methods of stress analysis mentioned at the beginning of this section--i.e., in arriving at a solution of Equations (4.2)-(4.6)--several possible approaches have emerged with, of course, a number of variations of each. In one such approach the governing equations are solved directly, which is sometimes possible by integrating separately with respect to the time and space variables. Lee [33] gave an example of this in an excellent survey article. A more common approach applies the Laplace transform to the system of equations, thus removing the time-dependence, so that the viscoelastic problem becomes an elastic one in the transformed variables. The so-called "correspondence principle" is thereby invoked. This method applies directly only to problems in which the portions S_T and S_u do not vary during the loading process [34]. A discussion of this approach, along with reference to a number of solved problems, may again be found in the survey article by Lee [33].

In addition to the mathematical complexities often encountered in the two methods mentioned above, they require the expression of material behavior in mathematical form--i.e., the viscoelastic operators of Equations (4.6a) and (4.6b) must be known. Such expressions can easily be too complicated to handle in a mathematical solution or can be too simple to adequately describe the behavior of the material, or both. This is particularly true in dynamics

problems where very short-time response is required. Physically meaningful solutions, nevertheless, have been obtained either by fitting mathematical functions to experimental data on material properties or by using such data directly in numerical solutions with the aid of a computer [34]. This latter method removes the limitation to the type of boundary-value problem which can be transformed into an associated elastic one.

Another approach is the completely experimental one. The importance of such an approach becomes apparent when the complexity of the viscoelastic stress analysis problem is considered. As in elasticity, solutions of only those problems with simple boundary conditions and geometry seem feasible analytically. When the correspondence principle is used, the viscoelastic solution indeed depends upon the availability of the solution to the associated elastic problem. It appears then that the problem of viscoelastic stress analysis is generally more complex than, or at best just as complex as, the elastic one.

One experimental approach for viscoelastic stress analysis is photoviscoelasticity--an extension of photoelasticity for elastic analyses--a logical extension indeed in view of the fact that most photoelastic model materials are inherently viscoelastic. Some aspects of this experimental approach are given in the following sections.

Stress, strain, and birefringence in a viscoelastic material are three uniquely interrelated second-order tensors. Mindlin [39] derived a stress-strain-optic law in the form of second-order linear differential operators for an idealized four-element model, assuming the material to be incompressible. Mindlin's work and that of others who followed are reviewed by Daniel [11] and extended to forms suitable for stress analysis purposes. Daniel gave the stress-optic law in both differential and integral form. The experimental approach necessary for calibration of the material and solution of the stress analysis problem was outlined and then applied to a dynamics problem.

The following sections give a rudimentary account of some methods of representation of the viscoelastic and photoviscoelastic properties of materials. Only a few of the many possible representations appear, and these are specialized to the needs of this study--namely, to the isothermal, quasi-static case. Reference is made to a number of sources where more general developments are given.

Forms of Representation of Linear Viscoelastic Behavior

Among the most comprehensive works in linear viscoelasticity are those by Leaderman [31], Alfrey [1], Gross [25], Staverman and Schwarzl [62], Ferry [17], and the three-volume one edited by Eirich [16]. Reference to many recent publications may also be found in Lee's paper [33].

Equations (4.6) gave the constitutive equations for a viscoelastic material in terms of deviatoric and dilatational parts of stress and strain. The corresponding equations for an isotropic elastic material are:

$$s_{ij} = 2Ge_{ij} \tag{4.7a}$$

$$\sigma_{ii} = 3K\varepsilon_{ii}, \tag{4.7b}$$

where

G = shear modulus,

K = bulk modulus.

Equations (4.6) may conveniently be written:

$$P(s_{ij}) = 2Q(e_{ij}) \tag{4.8a}$$

$$P'(\sigma_{ii}) = 3Q'(\varepsilon_{ii}), \tag{4.8b}$$

where P, P', Q, and Q' are again linear operators with respect to time, identical to those of Equations (4.6) except for the constant coefficients. Hereafter any reference to these operators assumes those of Equations (4.8).

In differential-operator form these operators are expressed as:

$$P = \sum_{r=0}^{m} p_r \frac{\partial^r}{\partial t^r}, \qquad Q = \sum_{r=0}^{n} q_r \frac{\partial^r}{\partial t^r}, \tag{4.9a,b}$$

$$P' = \sum_{r=0}^{m'} p'_r \frac{\partial^r}{\partial t^r}, \qquad Q' = \sum_{r=0}^{n'} q'_r \frac{\partial^r}{\partial t^r}, \qquad (4.9c,d)$$

where the coefficients p_r, q_r, p'_r, and q'_r are constants of the material. The number of such constants--i.e., the values of m, n, m', and n'--necessary to describe a material depends upon the viscoelastic behavior of the material and, of course, upon the accuracy desired. Frequently, the number required is high enough to make the mathematical treatment of the equations formidable.

The constants in the differential operators can be related to an idealized mechanical system composed of springs and dashpots. These mechanical systems then serve as pictorial representations of the material behavior. For such purposes the constants are usually specialized to correspond to the elements of simple mechanical systems, such as the Kelvin model (spring and dashpot in parallel), Maxwell model (spring and dashpot in series), or various combinations of these. The idea of the representation by mechanical models can be extended to an arbitrarily large number, indeed to an infinite number of elements. The operators are then characterized not by a finite number of constants but by continuous functions called distribution functions [62]--"distribution of retardation times" or "retardation spectrum" for the continuous Kelvin model used to describe creep, and "distribution of relaxation times"

or "relaxation spectrum" for the continuous Maxwell model used to describe relaxation.

The spectra give a picture of the springs and dashpots of the model which in turn can be thought of as representing molecular processes. Hence the spectra give a close representation of the molecular processes occurring in viscoelasticity, a fact which is important to the chemist or physicist relating chemical constitution of a material to its properties. Perhaps this is the best justification for their use to describe material behavior.

A more general representation is given by viscoelastic operators in integral form, which result from considering Boltzmann's superposition principle [1] for continuous stress or strain histories. Such a superposition principle is valid for (or equivalently describes) linear viscoelastic behavior. In integral-operator form, the deviatoric strain response to any time-varying stress $s_{ij}(t)$ is given by:

$$\varepsilon_{ij}(t) = \frac{1}{2}\int_{-\infty}^{t} J(t-\tau)\,\frac{ds_{ij}(\tau)}{d\tau}\,d\tau, \qquad (4.10)$$

where $J(t)$, called the "creep compliance" in shear, represents the strain response to a unit sustained shear stress.

A similar expression for pure dilatation is:

$$\varepsilon_{ii}(t) = \frac{1}{3}\int_{-\infty}^{t} B(t-\tau)\,\frac{d\sigma_{ii}(\tau)}{d\tau}\,d\tau, \qquad (4.11)$$

where B(t) is the "bulk compliance."

When the material has no stress or strain history--i.e., it is initially "dead"--then the lower limits of the integrals are replaced by zero.

Corresponding equations may be written in terms of "relaxation moduli" for the stress response to time-varying strain. Such moduli, as well as the compliances defined above, usually characterize the long-time behavior of materials. Though they could be used to describe dynamic behavior as well, provided their time variation for sufficiently short times were known, they are usually abandoned in dynamic studies in favor of complex moduli and compliances. These may be obtained from the response to sinusoidal loading of variable frequency. Since only creep tests were performed in the present study, only the creep compliances are of value here.

It should be mentioned that all of the moduli and compliances of an isotropic, viscoelastic medium are related and can, in principle, be found when only one of these so-called [62] "characteristic functions" is known for all times (or frequencies). Gross [25] presented many transformation formulas for this purpose. Not only are some of the transformations difficult to carry out, but

usually no one characteristic function is known for a sufficiently wide range of time or frequency to make all the transformations practicable. Some functions might then be thought of as complementing others for different time intervals rather than being equivalent.

The Equations (4.10) and (4.11) for deviatoric and dilatational strain response to time-varying stress may further be specialized for the case of uniaxial tension. An "extension compliance" D(t) can be deduced from the creep and bulk compliances, since a deviatoric and hydrostatic stress can be superposed to give uniaxial tension. In integral-operator form, the axial strain response to time-varying uniaxial stress is:

$$\varepsilon(t) = \int_0^t D(t-\tau) \frac{d\sigma(\tau)}{d\tau} d\tau. \qquad (4.12)$$

Note that the lower limit of zero has been employed, assuming no previous stress history.

If the loading consists of the sudden application of stress σ_0 at time zero which is then maintained constant, the strain response found from Equation (4.12) is:

$$\varepsilon(t) = \sigma_0 D(t). \qquad (4.13)$$

The extension compliance will be independent of σ_0 within the range of stress for which the material is linearly viscoelastic.

For relaxation-type tests the stress response to time-varying axial strain is:

$$\sigma(t) = \int_0^t E(t-\tau) \frac{d\varepsilon(\tau)}{d\tau} d\tau, \qquad (4.14)$$

where E(t) is the relaxation modulus or extension modulus. For a suddenly applied (at time zero) strain which is then maintained constant the stress response is given by:

$$\sigma(t) = \varepsilon_0 E(t). \qquad (4.15)$$

The extension compliance and modulus are formally related by:

$$\int_0^t E(t-\tau)D(\tau)d\tau = t. \qquad (4.16)$$

For moderate rates of creep an approximate relation is [11]:

$$E(t) \cong \frac{1}{D(t)}. \qquad (4.17)$$

To show how the creep and bulk compliances can be deduced from the extension compliance (and other easily accessible information) for the special case of sudden application of constant load at time zero, it is necessary simply to insert the deviatoric and dilatational parts of

the stress and strain tensors for uniaxial tension into the appropriate operators (4.10) and (4.11). The tensors are:

$$\sigma_{ij} = \begin{pmatrix} \sigma_0 & 0 & 0 \\ 0 & 0 & 0 \\ 0 & 0 & 0 \end{pmatrix}, \qquad \varepsilon_{ij} = \begin{pmatrix} \varepsilon_{11} & 0 & 0 \\ 0 & \varepsilon_{22} & 0 \\ 0 & 0 & \varepsilon_{33} \end{pmatrix}. \tag{4.18}$$

Now from Equation (4.10) the (deviatoric) shear creep compliance is (see also List of Symbols):

$$J(t) = \frac{2e_{ij}(t)}{s_{ij}} = \frac{2e_{11}(t)}{s_{11}} = \frac{2\varepsilon_{11}(t) - \varepsilon_{22}(t) - \varepsilon_{33}(t)}{\sigma_0}; \tag{4.19}$$

and the bulk compliance from Equation (4.11) is:

$$B(t) = \frac{3\varepsilon_{ii}(t)}{\sigma_{ii}} = \frac{3[\varepsilon_{11}(t) + \varepsilon_{22}(t) + \varepsilon_{33}(t)]}{\sigma_0}. \tag{4.20}$$

Thus if one of the transverse strains is measured along with the axial strain, then the other transverse strain can be computed (assuming isotropy); or equivalently, Poisson's ratio[1] $\mu(t)$ may be obtained. When Poisson's ratio is employed, the above equations become:

$$J(t) = \frac{2\varepsilon_{11}(t)[1 + \mu(t)]}{\sigma_0} \tag{4.21}$$

---

[1] "Poisson's ratio" is generalized beyond its normal meaning and is here defined simply as the negative ratio of the lateral to the axial strain. For other definitions see page 73 of Stuart [63].

and

$$B(t) = \frac{3\varepsilon_{11}(t)[1 - 2\mu(t)]}{\sigma_0}. \qquad (4.22)$$

For many polymers Poisson's ratio is found to be nearly constant with time. Unplasticized high polymers at room temperature are in their glassy state [64]. It is known [62] that Poisson's ratio may quite accurately be assumed constant over a wide range of time for such materials. Daniel [10] found it to vary little over four decades of time in a low-modulus material with true axial strains as high as fifteen percent. Equations (4.21) and (4.22) are even further simplified if the time-dependence of Poisson's ratio is neglected. A simple tension test, yielding the extension compliance, along with the known or measured value of Poisson's ratio, then suffices to completely characterize the linear viscoelastic, mechanical behavior of an isotropic material.

Before proceeding to the forms of representation of photoviscoelastic properties, one further point regarding the mechanical behavior should be noted. In the most general case of loading, the principal axes of stress do not coincide with the principal axes of strain in a viscoelastic medium. This could be expected from a comparison with plasticity theory, where such coincidence breaks down unless the directions of principal stresses are constant. Although few examples of this have been observed in

plastics, Frocht and Thomson [23] found such a lack of coincidence in cellulose nitrate when the loading was such that the directions of principal stress rotated.

Both stress and strain enter only one set of equations in the formulation of a viscoelasticity problem [Equations (4.1)-(4.6)]--namely, the constitutive equations. There the stresses and strains are divided into deviatoric and dilatational parts. Hence it would seem, in principle, possible to solve analytically the general viscoelastic problem wherein principal axes of stress and strain do not coincide. The method used to solve the equations, however carefully chosen, would likely lead to a lengthy and involved analysis. Experimental methods, one of which is briefly discussed in the following section, offer an alternative approach. Even here, a number of complications arise.

On the other hand, Mindlin [39] showed that if the stress can be represented as a product of two functions, one of which depends only on position coordinates (x_k) and the other only on time, i.e.,

$$\sigma_{ij}(x_k,t) = \sigma'_{ij}(x_k)f(t); \qquad (4.23)$$

then the principal axes of stress and of strain coincide. This condition excludes, for example, moving loads, which would cause principal stress directions to change, and

initial stresses, unless these stresses are of the same type as those represented in Equation (4.23).

Forms of Representation of Linear Photoviscoelastic Behavior

As stated previously, stress, strain, and birefringence are three uniquely interrelated second-order tensors. Daniel's representation [11] in integral form of the stress-optic law for viscoelastic materials seems most practical for stress analysis purposes. Though his work draws upon that of Mindlin [39] and others, his formulation seems to be the best suited for inclusion in this study. A slightly different notation is used in the equations presented below, reflecting that of Theocaris [64].

If the direction of light propagation is considered the z-direction of a cartesian system of axes, then the relative retardation (birefringence) observed in the usual applications of two-dimensional photoelasticity is the maximum difference of birefringence in two mutually perpendicular directions in the x-y plane. These directions are called the secondary principal optical directions, and the corresponding values of the index of refraction are called the secondary principal values. Similar terminology is used for stresses and strains.

Stress-birefringence relations may now be written as:

$$\sigma_{xx} - \sigma_{yy} = \int_0^t \beta_\sigma(t-\tau) \frac{d}{d\tau} (n_{xx} - n_{yy}) \, d\tau, \qquad (4.24)$$

where

σ_{xx}, σ_{yy} = normal stresses along axes of coordinates,

n_{xx}, n_{yy} = indices of refraction along coordinate directions,

$\beta_\sigma(t)$ = time-varying difference in secondary principal stresses for unit sustained birefringence;

or as:

$$\sigma_{xx} - \sigma_{yy} = \int_0^t \beta_\sigma(t-\tau) \frac{d}{d\tau} [n_\sigma(\tau) \cos 2\varphi_n(\tau)] \, d\tau, \qquad (4.25)$$

where

$n_\sigma(t) = (n_1 - n_2)$ = difference in secondary principal values of index of refraction (relative birefringence),

$\varphi_n(t)$ = angle between secondary principal optical directions and coordinate axes.

The secondary principal stress difference $(\sigma_1 - \sigma_2)$ may be related directly to the relative birefringence by:

$$\sigma_1 - \sigma_2 = \left\{ \left[\int_0^t \beta_\sigma(t-\tau) \frac{d}{d\tau} [n_\sigma(\tau) \sin 2\varphi_n(\tau)] \, d\tau \right]^2 \right.$$

$$\left. + \left[\int_0^t \beta_\sigma(t-\tau) \frac{d}{d\tau} [n_\sigma(\tau) \cos 2\varphi_n(\tau) \, d\tau] \right]^2 \right\}^{\frac{1}{2}}. \quad (4.26)$$

The principal stress directions are available from:

$$\tan 2\varphi_\sigma(t) = \frac{\int_0^t \beta_\sigma(t-\tau) \frac{d}{d\tau} [n_\sigma(\tau) \sin 2\varphi_n(\tau)] \, d\tau}{\int_0^t \beta_\sigma(t-\tau) \frac{d}{d\tau} [n_\sigma(\tau) \cos 2\varphi_n(\tau)] \, d\tau}, \quad (4.27)$$

where $\varphi_\sigma(t)$ = angle between secondary principal stress directions and coordinate axes.

Finally, the shear stress is given by:

$$\sigma_{xy} = \frac{1}{2} \int_0^t \beta_\sigma(t-\tau) \frac{d}{d\tau} [n_\sigma \sin 2\varphi_n(\tau)] \, d\tau. \quad (4.28)$$

Thus the photoviscoelastic determination of the secondary stress difference at a point in a viscoelastic body, as a function of time, requires a continuous record of birefringence and isoclinic data in addition to

knowledge of the stress-optic coefficient $\beta_\sigma(t)$. This is in contrast to photoelasticity where such a stress difference is determined by the momentary values of fringe order and $C_\sigma(t)$.

To separate the principal stresses the shear difference or oblique incidence methods commonly used in photoelasticity can be applied [21]. Some modifications accounting for the difference of Φ_n and Φ_σ may be necessary. This accomplished, the strain can be determined using the theory already presented. An alternative procedure for determining strain is to measure it directly, possibly by employing the moire method. Such an approach would require no prior knowledge of mechanical properties.

Evaluation of $\beta_\sigma(t)$, the time-varying difference in principal stresses for unit sustained birefringence, in principle, could be determined directly from an optical relaxation test. But such a test, wherein birefringence is maintained constant, is very difficult to conduct. However, if $\alpha(t)$ represents the time-varying birefringence for a unit sustained difference in secondary principal stresses (creep test), then $\alpha(t)$ and $\beta_\sigma(t)$ are related as follows:

$$\int_0^t \alpha(t-\tau)\beta_\sigma(\tau)d\tau = t \qquad (4.29a)$$

or

$$\int_0^t \alpha(\tau)\beta_\sigma(t-\tau)d\tau = t. \qquad (4.29b)$$

For moderate rates of creep,

$$\beta_\sigma(t) \cong \frac{1}{\alpha(t)}, \qquad (4.30)$$

which permits the determination of $\beta_\sigma(t)$ by means of a relatively easy-to-perform creep test such as the one performed in this study. For a body with symmetrical shape and loading $\varphi_n(t)$ can be made zero and Equation (4.26) becomes:

$$\sigma_1 - \sigma_2 = \int_0^t \beta_\sigma(t-\tau) \frac{d}{d\tau} [n_\sigma(\tau)] \, d\tau. \qquad (4.31)$$

For a suddenly attained birefringence n_0 which is maintained constant from time zero (optical relaxation test) Equation (4.31) becomes:[1]

$$\sigma_1 - \sigma_2 = \beta_\sigma(t)n_0. \qquad (4.32)$$

The analagous equation for an optical creep test is:

$$n(t) = \alpha(t)(\sigma_1 - \sigma_2). \qquad (4.33)$$

---

[1] Comparison with Equation (2.8) reveals that $\beta(t) = \frac{2f_\sigma(t)}{d}$.

In the present study a uniaxial stress state was employed and $\alpha(t)$ was determined from

$$n(t) = \alpha(t)\sigma, \tag{4.34}$$

which, by use of Equation (4.30), determined $\beta_\sigma(t)$.

Plots of $\beta_\sigma(t)$ and $D(t)$[1] as functions of time are shown in Figure 4.1. Since these characteristic functions are defined for linear optical and mechanical behavior, they can describe the behavior only for a limited range of stress and time as determined in the previous chapter.

Some similarities and differences in the treatment of linear viscoelasticity and linear photoviscoelasticity may be noted. It has been pointed out that, generally, mechanical coincidence in a viscoelastic body does not prevail--i.e., the principal-stress and principal-strain axes do not coincide. This is in contrast to elasticity where they do coincide, at least for isotropic media. Furthermore, in photoelasticity the principal-optical axes coincide with the principal-stress axes so that the meaning of isoclinics is clear. But the question now arises whether the breakdown in mechanical coincidence is accompanied by a breakdown in optical coincidence; or equivalently, what is the meaning of the isoclinic parameters in the presence of general viscoelastic or plastic behavior. Do the isoclinic parameters give the directions of the

---

[1]Refer to Equation (4.13) for definition of D(t).

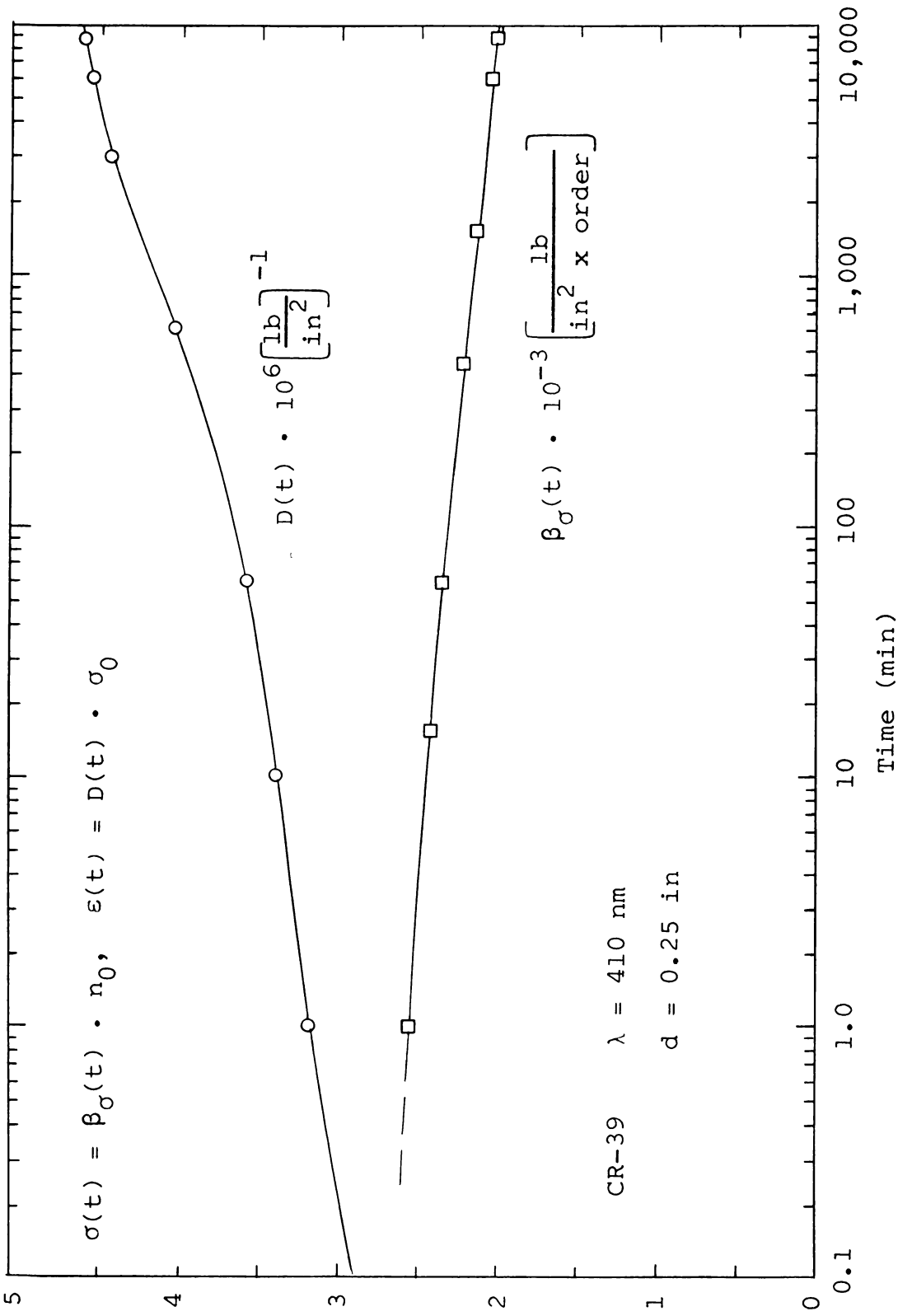

Fig. 4.1--Functions $\beta_\sigma(t)$ and D(t) for CR-39.

secondary principal stresses, the secondary principal strains, or neither? The theory above assumes neither.

Equations for the strain-optic laws similar to the stress-optic ones above would require the introduction of another angle φ_ε, the angle between the secondary principal-strain axes and the coordinate axes. The above question, rephrased, becomes: is $\varphi_n = \varphi_\sigma$, or is $\varphi_n = \varphi_\varepsilon$, or is $\varphi_\sigma \neq \varphi_n \neq \varphi_\varepsilon$? In the most general case it must be assumed that the last condition prevails. Theocaris [64] pointed out, however, that the "glassy" region of viscoelastic behavior, where deformation is predominantly elastic, and the "rubbery" region, where the creep rate is quite low, correspond to quasi-elastic conditions wherein the axes of secondary principal stress, strain, and birefringence coincide. He observed marked deviations from coincidence in the "transition" range, where creep rate is high, in a highly (60%) plasticized epoxy polymer.

Frocht and Thomson [22] found similar deviations in an American cellulose nitrate but found that after several hours the secondary principal optical directions coincided with secondary principal stress directions--i.e., $\varphi_n = \varphi_\sigma$. But in a German cellulose nitrate Frocht and Cheng [19,20] noted no such time delay. Although mechanical coincidence broke down when principal stresses underwent rotation, optical coincidence ($\varphi_n = \varphi_\sigma$) continued to exist. Such results are quite remarkable and far-reaching in regard to

the applications of photoviscoelasticity or photoplasticity. It appears that time spent in material selection might be profitably invested.

Nonlinear Viscoelasticity

The theories of linear viscoelasticity and photoviscoelasticity, which were briefly introduced in preceding sections, describe the mechanical and optical behavior for only limited ranges of stress and time. Even within these ranges some anomalies are probably present but cannot easily be detected. Thus the descriptions "linear" and "nonlinear" are somewhat arbitrary. The nonlinear region might be defined as that region where deviations from linearity can definitely be detected or cannot be overlooked. That such a region exists for some of the materials tested in this study becomes quite evident from inspection of the plots of Chapter III or Appendix III. Though considerable effort has gone into formulating theories of nonlinear viscoelasticity, the subject is not yet well-developed nor is there agreement on the most satisfactory approach. This is to be expected in view of the relatively recent beginning of any concentrated research efforts, the many types and causes of deviations from linearity, and the mathematical complexity of the subject relative to its linear counterpart.

One factor limiting development is the lack of accurate experimental data. As late as 1965 Theocaris [64]

wrote, concerning nonlinear behavior of polymers in their glassy state where strains are relatively small: "Experimental evidence is rather sparse and the only significant contributions which exist concern the nonlinear behavior in the rubbery zone." This study hopefully provides some evidence of the type mentioned.

Most attempts to describe nonlinear behavior fall into one of the three categories: (1) empirical power laws (see Marin and co-workers [38]), (2) postulated behavior in terms of models (with nonlinear springs and modified dashpots), and (3) integral representation in the form of a modified superposition principle. All three of these have their roots in corresponding representations of linear behavior. Of the three, the last one seems most natural and most successful; further discussion will be limited to it.

Green, Rivlin, and Spencer [24] established the basis for the nonlinear theory in a series of highly mathematical articles. Quoting Theocaris again, ". . . it seems that only simple cases may be satisfactorily considered by this theory." The theory has been successfully applied by a number of investigators to such simple cases. Ward and Onat [69] presented a clear and concise summary of the theory as it applies to the behavior under simple stress conditions. Some elements of their presentation are reflected in the one below. Lockett [35] considered a more

general case and showed how the material functions (properties) for a general triaxial loading can be determined experimentally for a material whose response can be adequately expressed by a constitutive equation involving integrals of the first, second, and third orders. The constitutive equation is expressed in matrix form; the number of tests shown necessary for completely determining the material functions appears to be quite impracticable.

Onaran and Findley [46] specialized Lockett's results to simple stress states and presented examples to show the effectiveness of a multiple integral functional relationship for describing the response of polyvinyl chloride. The same approach is used at the end of this chapter.

The assumption that the elongation of a simple tension specimen at time t depends on all the previous values of the rate of loading can be expressed mathematically by:

$$\varepsilon(t) = \left[F \frac{d\sigma(\tau)}{d\tau} \right]_{\tau=-\infty}^{t}, \tag{4.35}$$

where

$\varepsilon(t)$ = unit strain of specimen at time t,

$\sigma(\tau)$ = time-dependent uniaxial stress,

F = a functional.

Should the functional F be linear and continuous, this response can be represented by Equation (4.12).

It has been shown (see [69] for references) that if F is continuous and nonlinear it may be represented to any desired degree of accuracy by:

$$\varepsilon(t) = \int_{-\infty}^{t} D_1(t-\tau_1) \frac{d\sigma(\tau_1)}{d\tau_1} d\tau_1$$

$$+ \int_{-\infty}^{t}\int_{-\infty}^{t} D_2(t-\tau_1, t-\tau_2) \frac{d\sigma(\tau_1)}{d\tau_1} \frac{d\sigma(\tau_2)}{d\tau_2} d\tau_1 d\tau_2 + \cdots$$

$$+ \int_{-\infty}^{t} \cdots \int_{-\infty}^{t} D_n(t-\tau_1, \ldots, t-\tau_n) \frac{d\sigma(\tau_1)}{d\tau_1} \cdots$$

$$\frac{d\sigma(\tau_n)}{d\tau_n} d\tau_1 \cdots d\tau_n. \qquad (4.36)$$

Spencer and Rivlin [61] showed that for an initially isotropic material the number of such integrals required does not exceed five. For most applications thus far attempted two or three have proven sufficient for acceptable accuracy.

If the material has no load history prior to time t = 0, the lower limit of the integrals can be replaced by zero. Furthermore, if the stress--say σ_i--is suddenly applied at time zero and subsequently maintained constant (creep test), then Equation (4.36) becomes:

$$\varepsilon(t,\sigma_i) = D_1(t)\sigma_i + D_2(t,t)\sigma_i^2 + \ldots$$

$$+ D_n(t, \ldots ,t)\sigma_i^n. \qquad (4.37)$$

The first term is linear in stress; subsequent terms might be regarded as corrections to the linear one to account for nonlinear behavior.

A number of investigators, including Onaran and Findley [46], have found three terms of Equation (4.37) sufficient to adequately describe the behavior of several polymers for a reasonably wide range of stress and time. Then:

$$\varepsilon(t,\sigma_i) = D_1(t)\sigma_i + D_2(t,t)\sigma_i^2 + D_3(t,t,t)\sigma_i^3. \qquad (4.38)$$

Hence loading programs having three independent values of σ_i provide three equations for determining the functions $D_1(t)$, $D_2(t,t)$, and $D_3(t,t,t)$. The function $D_1(t)$ is determined completely, while the other two are determined only where their arguments take on equal values. Though $D_1(t)$ is determined completely, it should be noted [35] that it depends on each of the constants σ_i and therefore will not be identical with the function obtained in the linear theory from a single value of σ_i.

If experimental values of $\varepsilon(t_1,\sigma_i)$ for the three chosen values of σ_i are used in Equation (4.38), then

values for D_1, D_2, and D_3 are obtained only for t_1, the time represented by the data. When such values are computed at enough different times, the form of the functions $D_1(t)$, $D_2(t,t)$, and $D_3(t,t,t)$ can be determined.

Alternatively, if analytical curves can be fitted to the data for the three chosen values of σ_i, then analytical expressions can be used in Equation (4.38) to yield the functions $D_1(t)$, etc. directly. Though this approach is somewhat empirical, it extends the purely empirical approach by providing the functions $D_1(t)$, $D_2(t,t)$, and $D_3(t,t,t)$, which are the kernels of the more general "superposition" integrals in Equation (4.36).

The problem in this latter approach is to find the analytical expression which satisfactorily fits the data for the three chosen levels of stress. The accuracy of such a fit depends upon the range of stress and time employed, as well as upon the form of the expression and upon the behavior of the material itself--e.g., upon the "smoothness" of the transition from the linear to the nonlinear region.

Onaran and Findley [46] have found an expression of the form

$$\varepsilon(t) = \varepsilon_0 + gt^h, \tag{4.39}$$

where

ε_0 = a curve-fit constant,

g,h = constants (to be explained),

to yield satisfactory results for several polymers. After rearranging Equation (4.39) and taking the logarithm of both sides, it becomes:

$$\log (\varepsilon - \varepsilon_0) = \log g + h \log t. \qquad (4.40)$$

Hence on a full logarithmic plot of $(\varepsilon - \varepsilon_0)$ vs. t, h is the slope of the line at time t and g is an intercept. The constants ε_0 may be chosen to make the curve a straight line of best fit, thereby making h a constant. When these constants are determined for three independent stress levels σ_i, Equation (4.39) can be used with Equation (4.38) to determine the functions (kernels) $D_1(t)$, $D_2(t,t)$, and $D_3(t,t,t)$.

Nonlinear Photoviscoelasticity

Virtually all work on nonlinear behavior reported in the literature deals with the mechanical properties of the materials tested. Similarity of the strain-stress and birefringence-stress plots of Chapter III seems to imply that any analytical description of the mechanical behavior would parallel that of the optical behavior--i.e., birefringence is very closely related to strain throughout the linear and into the nonlinear range. Observing this and considering birefringence data of this study more accurate than the strain data, it was decided to apply the scheme

outlined above to determine similar kernels for an integral-type representation of the photoviscoelastic properties of the material tested.

Since axial tension tests were used in this study, questions regarding coincidence of optical and mechanical axes do not enter. In all of the equations of the previous section n(t) might simply be substituted for $\varepsilon(t)$ where:

$$n(t) = n_1(t) - n_2(t), \tag{4.41}$$

so that n(t) is the difference of secondary principal indices of refraction--i.e., the relative birefringence or simply the fringe value.

Equation (4.38) then implies:

$$n(t,\sigma_i) = D_1(t)\sigma_i + D_2(t,t)\sigma_i^2 + D_3(t,t,t)\sigma_i^3. \tag{4.42}$$

Equation (4.39) suggests:

$$n(t) = n_0 + gt^h; \tag{4.43}$$

and Equation (4.40) leads to:

$$\log (n - n_0) = \log g + h \log t. \tag{4.44}$$

The largest stress plotted in the optical test of CR-39 was 2,858 psi. The stress levels 600 psi, 1,600 psi, and 2,600 psi were chosen for the three independent values of stress for use in Equation (4.42). The time range

available was one minute to 240 hours (14,400 min). The range one minute to 10^4 minutes was chosen for representation because of its convenience on the logarithmic time scale.

The method of determining n_0 in Equation (4.44) to cause a "best fit" straight line is not apparent in the literature surveyed. The following scheme was therefore devised. Using data from the curves of birefringence vs. stress at t = constant (Chapter III), a plot of n vs. log t was made[1] for the three stress levels mentioned above. From this plot values of n were read at one minute, 10^2 minutes, and 10^4 minutes at each of the three stress levels. With these three values of n, at a given stress, n_0 was then computed to force a straight line on the log $(n - n_0)$ vs. log t plot through the three points. Figure 4.2 shows this plot. Then g was evaluated as the ordinate at one minute and h as the slope of the line for each stress[2] in accordance with Equation (4.44). This yielded the desired expressions for the left side of Equation (4.42) which may then be written in matrix form, using the values found, as:

---

[1]The plot of n vs. t at σ = constant in Chapter III does not yield sufficient accuracy at 10^2 minutes.

[2]In all publications reviewed the slopes were found to be the same for all values of stress. The variation of h in the present case is evident in the exponents on t in Equation (4.45).

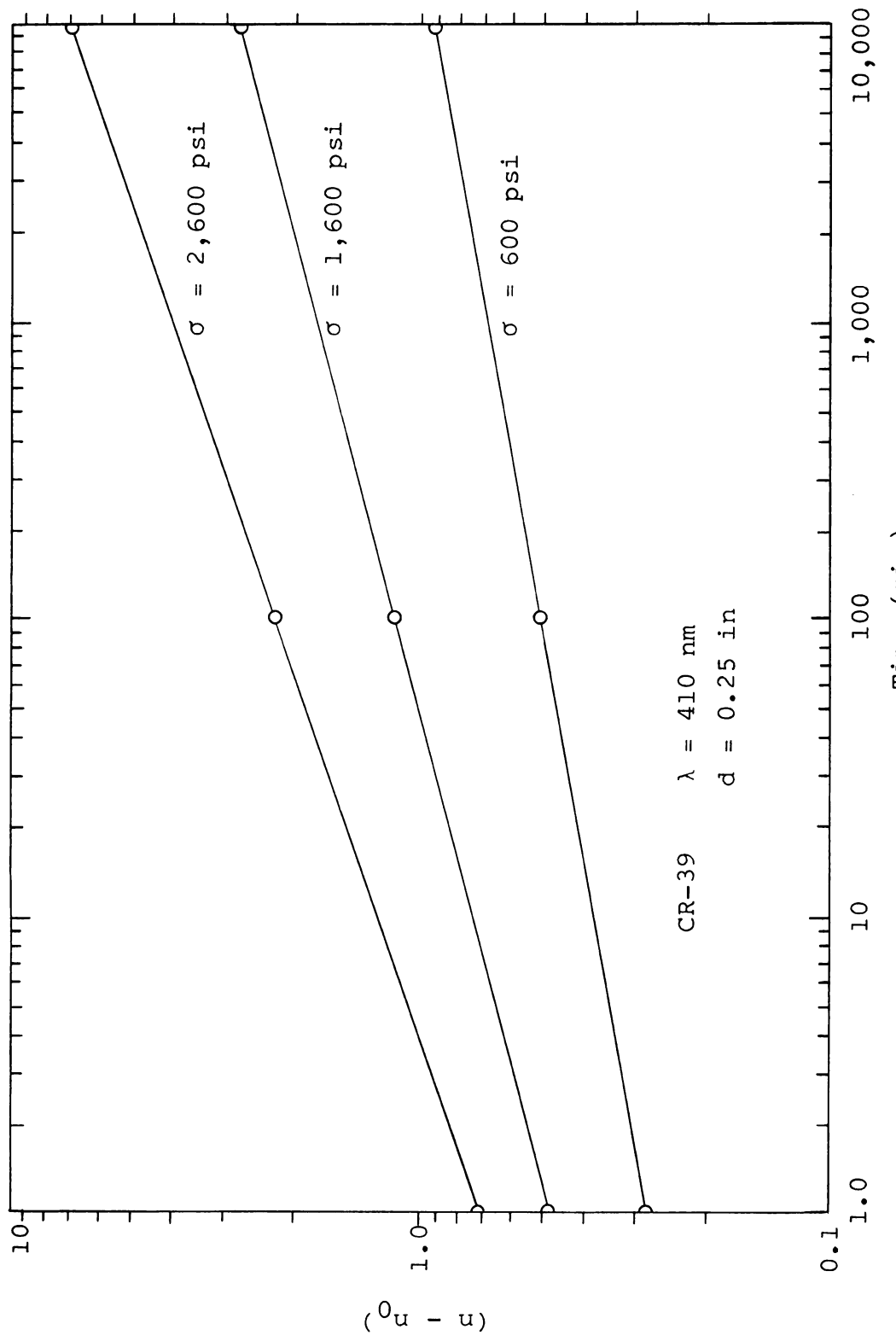

Fig. 4.2--Plot of $(n - n_0)$ vs. time for three stress levels for CR-39.

$$\begin{bmatrix} 2.10 + .28t^{.1291} \\ 5.86 + .48t^{.1895} \\ 9.77 + .76t^{.2386} \end{bmatrix} = \begin{bmatrix} 600 & 600^2 & 600^3 \\ 1{,}600 & 1{,}600^2 & 1{,}600^3 \\ 2{,}600 & 2{,}600^2 & 2{,}600^3 \end{bmatrix} \begin{bmatrix} D_1 \\ D_2 \\ D_3 \end{bmatrix} . \tag{4.45}$$

When the first matrix on the right is inverted, the desired expressions for the kernels are found.

The kernels are shown as functions of time in Figure 4.3. It should be noted that $D_2(t,t)$ is negative throughout.

Greater insight into the contribution of each kernel to the total birefringence is afforded by Figure 4.4, where the three terms on the right side of Equation (4.42) are shown separately, along with their sum and the experimentally determined curve of birefringence vs. time at 2,600 psi. The nonlinearity is seen to be quite pronounced; and the deviation between the linear viscoelastic contribution, given by the $D_1(t)$ kernel, and the actual behavior is seen to increase with increasing time. The calculated curve with all three kernels gives excellent agreement with the experimental results. Recall, however, that the stress of 2,600 psi was used in determining the kernels.

The accuracy of the calculated values of birefringence for a wide range of stress can be judged from Figure 4.5, where the curve of n vs. t (σ = const) from Chapter III is shown, along with calculated values of n. Agreement is seen to be quite good (throughout the time

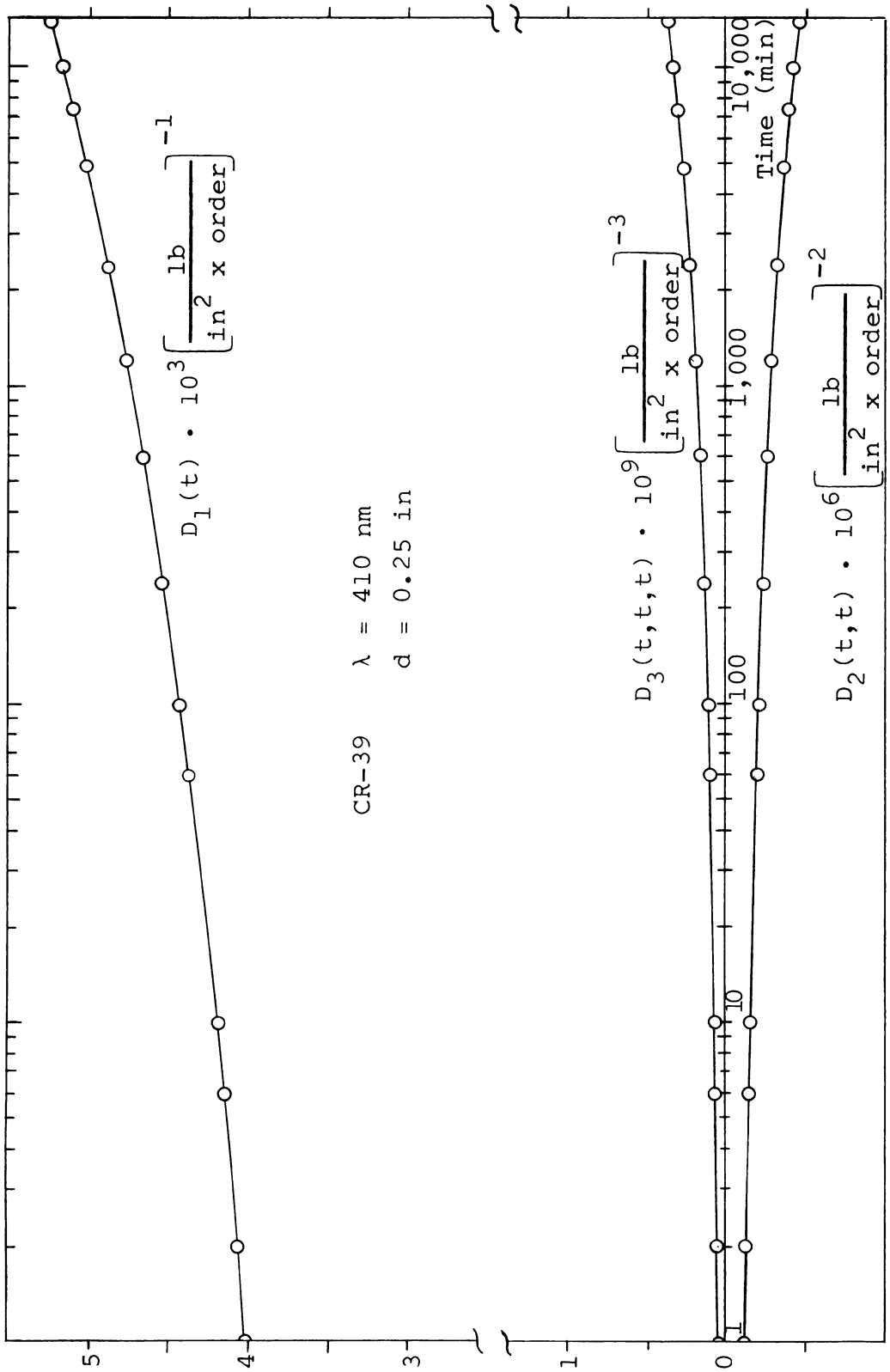

Fig. 4.3--Kernels $D_1(t)$, $D_2(t,t)$ and $D_3(t,t,t)$ for CR-39.

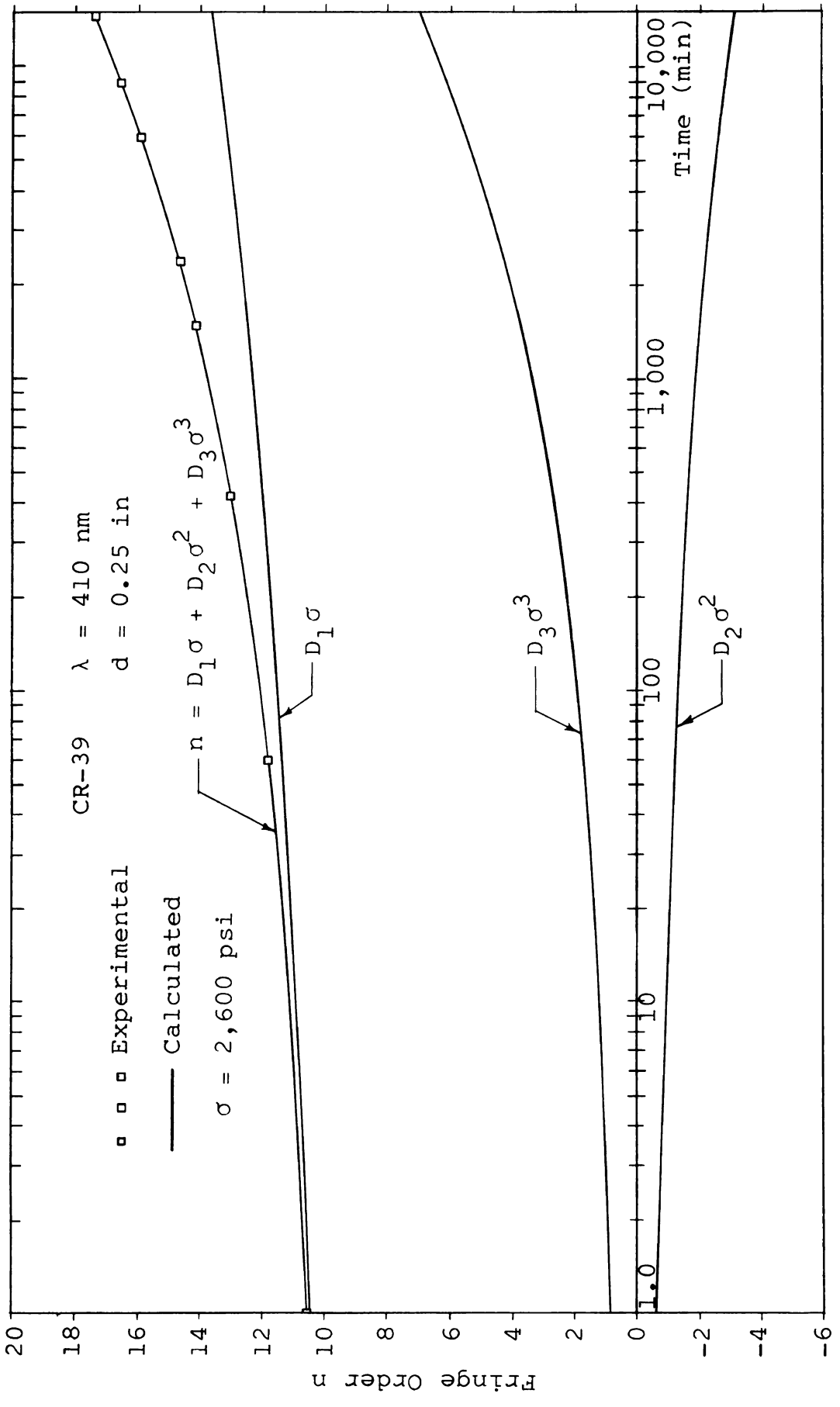

Fig. 4.4--Isochromatic fringe order n vs. time, experimental and calculated values, σ = 2,600 psi, for CR-39.

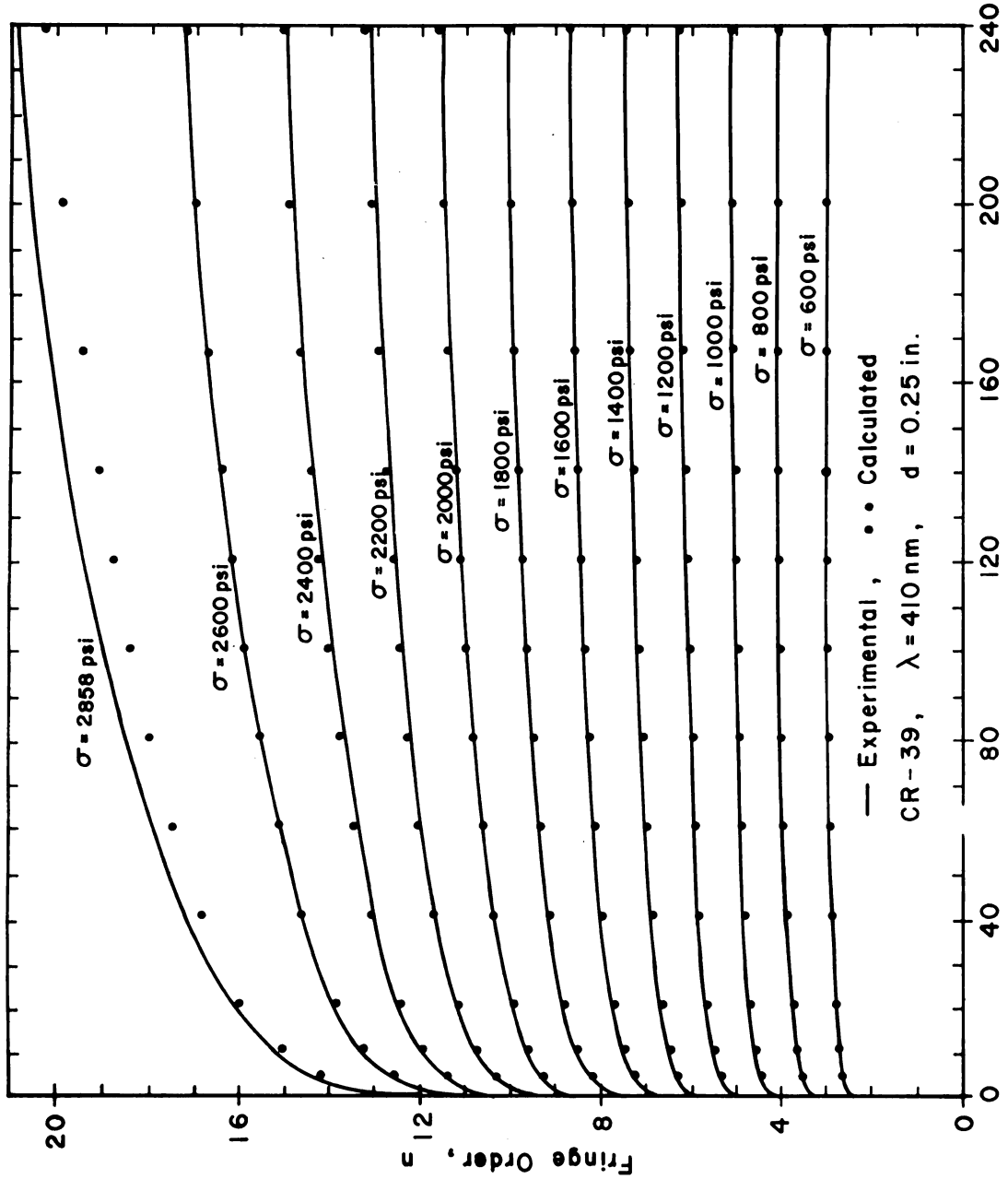

Fig. 4.5--Isochromatic fringe order n vs. time, experimental and calculated values, $\sigma = \sigma_1, \sigma_2, \ldots, \sigma_n$ for CR-39.

range) for the stress range of 600 psi to 2,600 psi but poor for the stress of 2,858 psi. This is not surprising, since the stresses of 600, 1,600, and 2,600 psi were used to determine the kernels. Furthermore, the nonlinearity becomes very pronounced at stresses above 2,600 psi. This may be observed either in Figure 4.5 or in Figure 3.2 of Chapter III.

Closer agreement between experimental and calculated results for the higher stress level of 2,858 psi, of course, is possible by using this value of stress as one of the three for calculating the kernels. However, this would probably cause greater discrepancies at the lower levels of stress.

Modifying Equation (4.42) to yield closer agreement with experimental results is also possible. Onaran and Findley suggested the following form:

$$n(t,\sigma_i) = D_1(t)\sigma_i + D_2(t,t)(\sigma_i^*)^2 + D_3(t,t,t)(\sigma_i^*)^3, \tag{4.46}$$

where

$\sigma_i^* = \sigma_i - \sigma_{\ell\ell}$ when $\sigma_i > \sigma_{\ell\ell}$,

$\sigma_i^* = 0$ when $\sigma_i < \sigma_{\ell\ell}$.

As previously pointed out, the kernel $D_1(t)$ represents the linear contribution to the response, and the other two represent the deviations from linearity. Since this deviation is more pronounced at higher levels of stress, the above modification can be expected to improve considerably

the representation at these higher levels without loss of accuracy at lower levels, where behavior is essentially linear.

Since the linear limit stress $\sigma_{\ell\ell}$ changes significantly with time, some question arises concerning the proper value to use in Equation (4.46). It seems that the lowest value, corresponding to the longest time to be considered in the representation, should be used.

This modified theory was not used for the CR-39 reported here, because the former representation seemed adequate for the stress range of 600 psi to 2,600 psi. For the time range of 240 hours, 2,600 psi is dangerously near the fracture strength of the material. Although it carried a stress of 3,085 psi for the full 240 hours in the optical test, it fractured in less than 167 hours at a stress of 2,858 in the mechanical test. The latter specimen was probably damaged while applying the moire grid, though such damage was not apparent. In earlier optical tests the material fractured in less than 47 hours at 3,700 psi and in less than 2 hours at 4,170 psi.

Limitations of Results Presented

All results given above are based on constant uniaxial stress sustained for 240 hours. Hence no information on the behavior of the material in recovery or upon unloading is given, even though such data was collected.

Furthermore, this study makes no attempt to determine whether the stress-optic law for more general stress states differs materially from the one for uniaxial stress. On the basis of some published results, significant differences are not expected even in the nonlinear range. For example, in cellulose nitrate Frocht and Thomson [23] found that for equal values of principal stress difference essentially the same birefringence was obtained under a biaxial state of stress as under a uniaxial state, although strains of nearly twenty percent were encountered. As pointed out previously, a thorough investigation of behavior under combined stress states extending into the nonlinear region requires an exhaustive testing program.

CHAPTER V

VARIATION OF OPTICAL PROPERTIES WITH WAVE LENGTH

Investigation Performed

All results presented in previous chapters involving the relative retardation or birefringent properties of CR-39 were based upon one wave length of radiation--namely, 410 nm. The photoelastic coefficients, such as C_σ and f_σ, in the linear range for this one wave length were determined as functions of time. The extent of the linear range--i.e., ${}_n(\sigma_{\ell\ell})_{1.0}$ or ${}_n(\sigma_{\ell\ell})_{5.0}$--was likewise determined as a function of time for one wave length.

Most optical material properties depend to some degree upon wave length of radiation. An extreme example is the high transmission of some wave lengths and complete blocking out of others, a phenomenon useful in the production of filters and in x-ray techniques, to name only two familiar cases. The birefringent properties are likewise known to depend upon wave length. This dependence is known as dispersion of birefringence. Since a number of wave lengths, ranging from 410 nm to 800 nm, were employed in this investigation, data on this phenomenon was obtained. Further discussion and some data on dispersion of birefringence are given in the following section.

In view of the dependence of birefringence on wave length, it seems logical to question whether the linear limit stress at a given deviation from linearity--say $_n(\sigma_{\ell\ell})_{1.0}$--might also depend upon wave length. This was, in fact, the primary purpose of using several wave lengths. Although the results of this investigation are not conclusive in answering the question, some useful results were obtained and are presented in the last section of this chapter.

Dispersion of Birefringence

The time-dependence of the photoelastic coefficients in Equations (2.7)-(2.9) was previously discussed. Dispersion of birefringence implies that the coefficient C_σ is not independent of wave length, nor is the coefficient f_σ directly proportional to wave length. It is equivalent to say that the fringe order n is not inversely proportional to wave length.

Dispersion of birefringence may be regarded as a source of error, a nuisance, or an asset, depending upon its recognition and utilization. If several wave lengths are employed in a photoelastic investigation and the dispersion of birefringence ignored, significant errors may result even though a relatively narrow range of wave lengths is employed. Such errors, of course, can be avoided by careful calibration tests employing the same wave lengths used in the investigation, resulting then in

some inconvenience. For at least one material, dispersion of birefringence was successfully used to measure the degree of plastic deformation in photoplasticity investigations [42]. In this case dispersion might well be considered an asset.

Several types of measurements and descriptions of dispersion of birefringence have been employed. Coker and Filon [6] reported the results of their many investigations on glass and referenced the work of several other investigators. Though their methods of measurement varied considerably, results obtained were sufficiently consistent that a description of dispersion of birefringence was possible. For many glasses they found that the variation with wave length of the stress-optic coefficient C_σ was adequately described by:

$$C_\sigma = \frac{C_0}{\left(1 - \frac{\lambda_0}{\lambda}\right)}, \tag{5.1}$$

where C_0 and λ_0 are constants for a given glass. The authors pointed out that "the formula is not to be regarded as of universal application" and that even some glasses must be considered outside the range of applicability of the formula.

Mönch [41] expressed dispersion of birefringence as a percentage by the equation:

$$D = \frac{(n\lambda)_{Na} - (n\lambda)_{Hg}}{(n\lambda)_{Na}} \cdot 100, \qquad (5.2)$$

where $(n\lambda)_{Na}$ and $(n\lambda)_{Hg}$ are the products of fringe order and wave length for yellow sodium (λ = 589.3 nm) and blue mercury (λ = 435.8 nm) radiation, respectively. In later work Mönch and Loreck [42] substituted red light (λ = 655 nm) for the yellow sodium above, resulting in greater values of D and therefore greater accuracy. Although the above description with either value served the desired purpose--namely, representing the degree of plastic deformation in celluloid--the arbitrariness of the choice of wave lengths employed should be noted. No insight is given into the fundamental nature of dispersion of birefringence at any wave lengths other than those used in the description, covering a rather narrow range.

The shortcomings of previous descriptions as general measures of dispersion of birefringence were discussed by Pindera and Cloud [49]. A new description, called "Normalized Dispersion of Birefringence," was developed which removed most of the shortcomings of those previously presented. Perhaps most significant, it allows dispersion of birefringence to be determined as a continuous function of wave length. The procedure outlined below follows closely that given by the authors cited. Some

modifications, reflecting mostly personal preference, are introduced in the following.

In the creep test performed on CR-39 a sequence of pictures at various wave lengths was taken, beginning at 100 hours after the constant load was applied. Since the entire sequence was obtained in about six minutes, creep effects were negligible. From these pictures data was obtained for the plot of fringe order vs. length along the tapered specimen. Since the stress was known as a continuous function of the length, fringe order could then be plotted as a function of stress at each of the wave lengths. This plot is shown in Figure 5.1 for eight wave lengths.[1]

Then at σ = 1,200 psi (within the linear range of behavior) the fringe order n was read for each wave length. These values and the "relative retardation" R ($R = n\lambda$) were tabulated. In the linear range these values are, of course, linear functions of stress. The ratios

$$r = \frac{R(\lambda)}{R(\lambda_0)}, \tag{5.3}$$

where λ_0 = 546 nm is an arbitrarily chosen "reference" wave length, were then computed and tabulated.

---

[1]Pictures at 500 nm and 700 nm exhibited irregular intensity fringes and therefore were not used.

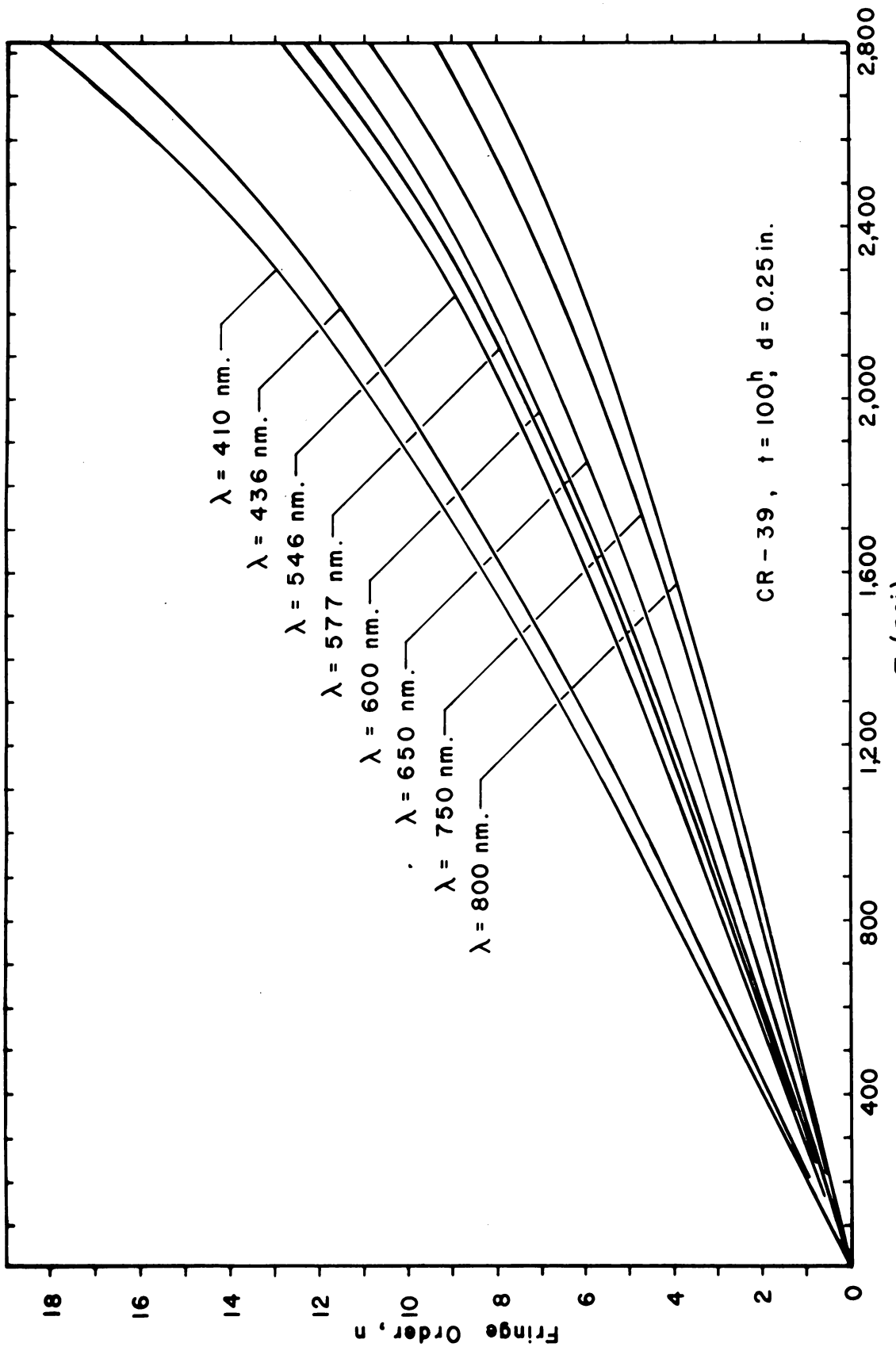

Fig. 5.1--Isochromatic fringe order n vs. stress, $\lambda = \lambda_1, \lambda_2, \ldots, \lambda_n$ for CR-39.

The ratios of Equation (5.3) were plotted as a function of wave length. Pindera and Cloud called this a "Normalized Retardation Curve." The rate of change of normalized retardation with respect to wave length was then defined as the "Normalized Dispersion of Birefringence" and denoted by D_λ. Thus

$$D_\lambda = \frac{dr}{d\lambda}. \tag{5.4}$$

Both r and D_λ, as defined by Equation (5.3) and Equation (5.4), respectively, are independent of stress in the linear range but may well depend upon stress in the nonlinear range. This might be expected on the basis of the previously mentioned results for celluloid. In fact, the dependence of r on stress could seemingly be an indication of nonlinearity.

To investigate this possibility for CR-39, normalized retardation curves at one level of stress in the linear range (1,200 psi) and several levels in the nonlinear range were plotted. Figure 5.2 shows a reduction of such a plot in which only two levels of stress in the nonlinear range are included. Some variation with stress is evident.

The curve for the stress in the linear range is similar in many respects to the one given by Cloud [4] for CR-39. Cloud found no systematic variations with uniaxial stress: variations were random. He analyzed his results

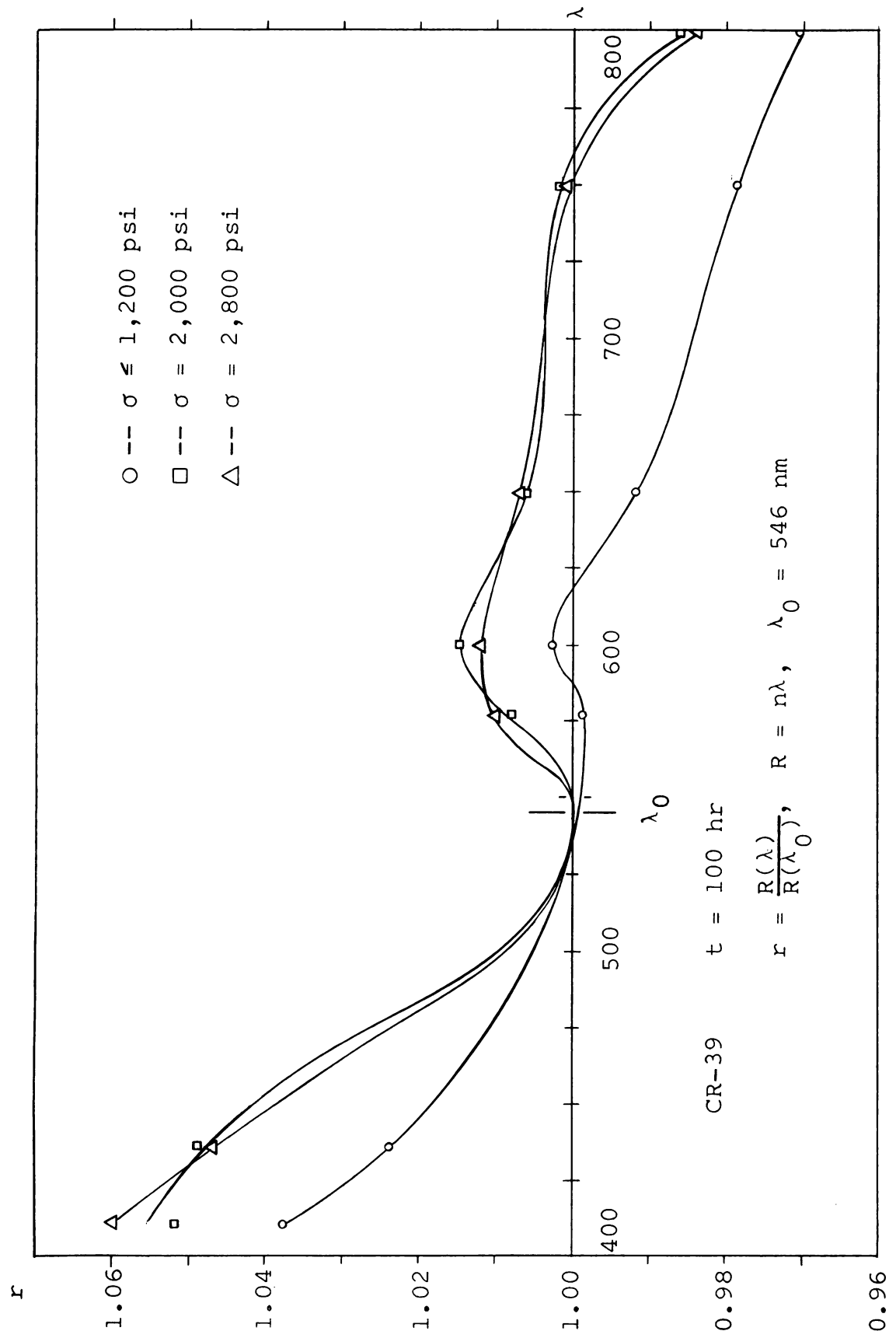

Fig. 5.2--Normalized retardation curves for CR-39.

statistically and showed a range of r values at each wave length employed.

Results of this study are subject to significant error because of the sensitivity of r to wave length and the lack of precise determination of the wave lengths used. Manufacturer's specifications of filters employed were checked using a hand spectroscope (Zeiss) and the values were accepted.

The slope of the normalized retardation curve in the linear range of stress was evaluated at several points. From these slopes the normalized dispersion of birefringence curve, Figure 5.3, was plotted. Again some similarities to the corresponding curve obtained by Cloud for CR-39 are evident, as well as some striking differences. The dispersion found by Cloud was negative throughout the range of wave lengths employed at 66 hours after the load was applied. Although the increased time of 100 hours used in this study could account in part for the differences, it could not be solely responsible for them. Further investigations seem necessary to reconcile the differences.

In an attempt to correlate dispersion of birefringence phenomena to the degree of nonlinearity of birefringence, a plot of normalized retardation vs. stress was constructed for each wave length. Readings were taken at several values of stress in the nonlinear range. However, since no conclusions could be drawn from the plot, it is

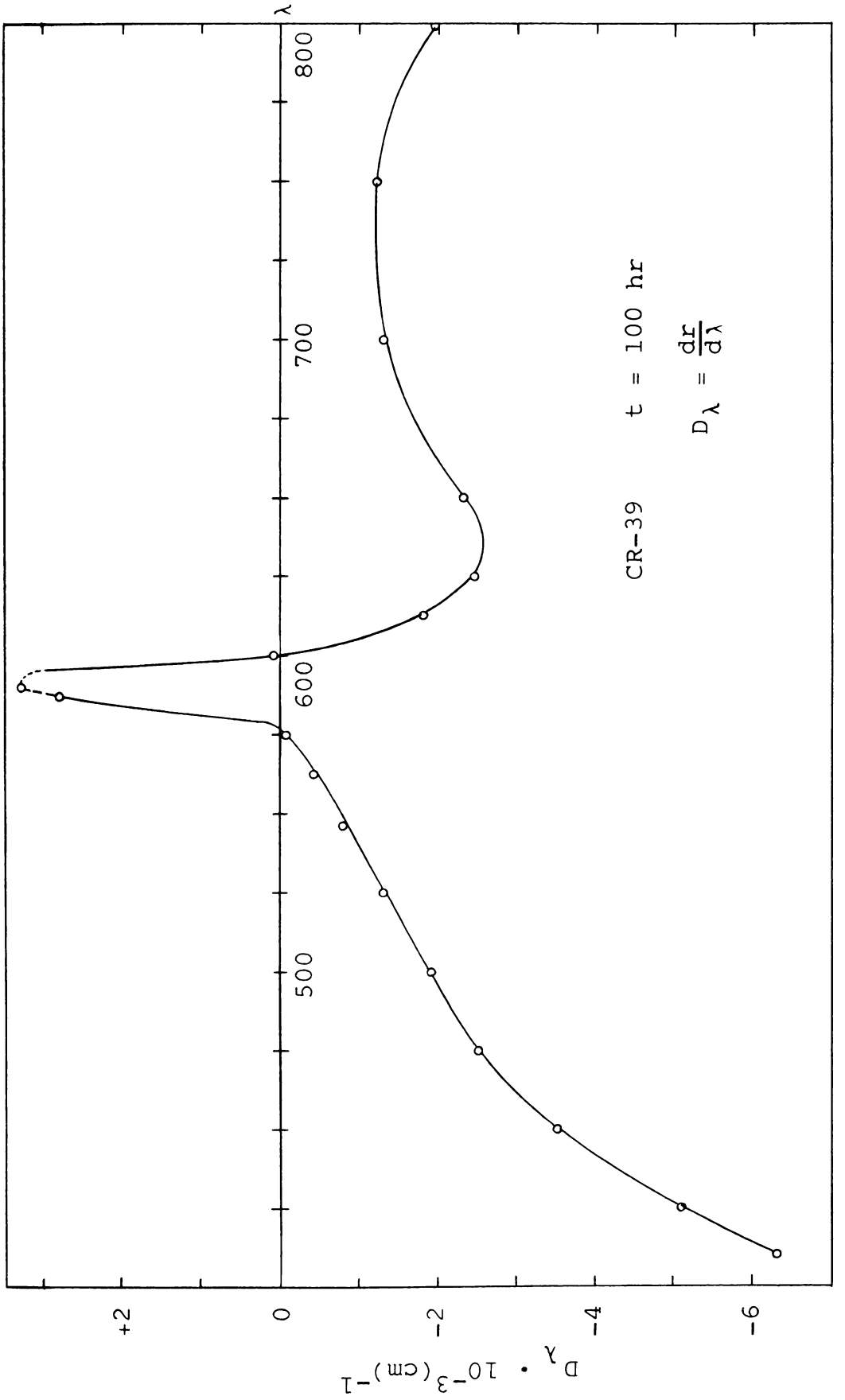

Fig. 5.3--Normalized dispersion of birefringence for CR-39.

not shown. Figure 5.2 provides a glimpse of the difficulty encountered. The curves for 2,000 psi and for 2,800 psi are hardly distinguishable from each other, despite wide differences in the degree of nonlinearity.

It must be concluded that the normalized retardation and hence the normalized dispersion of birefringence are not effective measures of the nonlinearity of CR-39, even though they cannot be assumed independent of stress.

The magnitude of the error committed in assuming that photoelastic coefficients are independent of wave length (in the linear range) can be estimated from Figure 5.2. The possible error in the visible spectrum (390 nm to 770 nm) for CR-39 appears to be about seven percent.

Variation of Linear Limit Stress with Wave Length

Figure 5.1 readily yields data on the dependence of the linear limit stress on wave lengths. This is presented in Figure 5.4, where $_{n}(\sigma_{\ell\ell})_{1.0}$ and $_{n}(\sigma_{\ell\ell})_{5.0}$ are given for each wave length.

Considerable variation of the linear limit stress values may be observed. Values of $_{n}(\sigma_{\ell\ell})_{1.0}$ are within about ten percent of a "mean" value of 1,355 psi; values of $_{n}(\sigma_{\ell\ell})_{5.0}$ are within seven percent of 1,720 psi. These variations seem quite random, however, perhaps indicating only the magnitude of experimental error rather than any

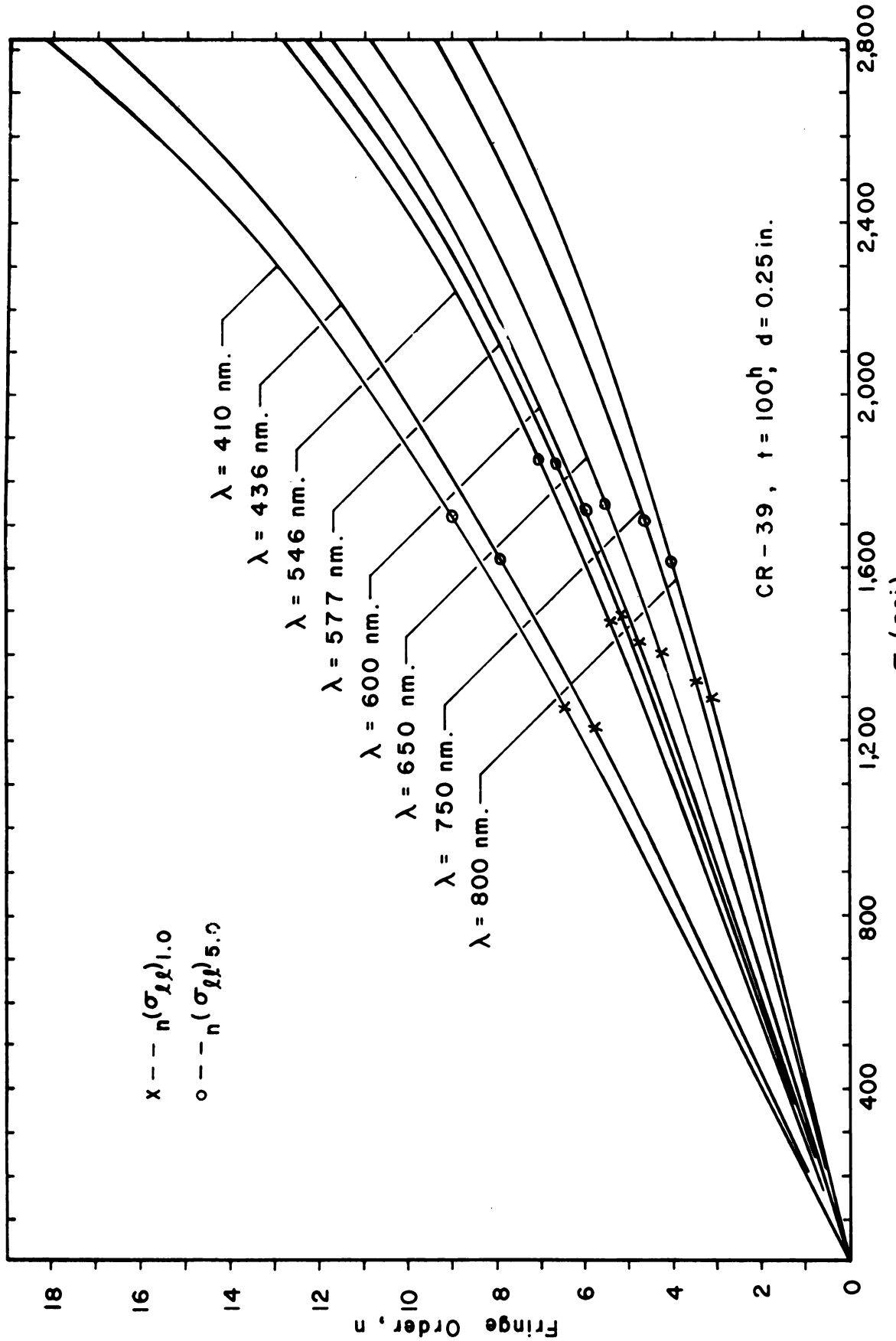

Fig. 5.4--Isochromatic fringe order n vs. stress, $\lambda = \lambda_1, \lambda_2, \ldots, \lambda_n$, showing linear limit stresses for CR-39.

dependence on wave length. Such dependence cannot be detected in the results of this study.

Causes and consequences of the irregularities of linear limit stress values are further discussed in the next chapter. It might here be mentioned that some irregularities must be expected. Limiting-value types of material properties (such as proportional limit, endurance limit, or ultimate strength) are not easily determined. Usually a large number of specimens is tested and the data is subjected to a statistical analysis. Precise values of such properties cannot be obtained from a single specimen.

CHAPTER VI

DISCUSSION, CONCLUSIONS, AND RECOMMENDATIONS FOR FURTHER RESEARCH

Achievement of Objective

The primary objective of this study--to investigate the effect of time upon the birefringent and mechanical properties of several plastics--was achieved. The isothermal, quasi-static behavior under constant, uniaxial stress conditions was examined quite exhaustively--for approximately five decades of logarithmic time, and for a range of stress sufficiently broad to cover not only the linear region but also much of the nonlinear region for those materials exhibiting nonlinear behavior.

Data is presented graphically for all materials. Certain characteristic functions defined by viscoelastic and photoviscoelastic theories are determined for CR-39 in both the linear and the nonlinear regions. Such characteristic functions can be deduced from data presented in Appendix III for the other materials tested.

The linear limit stresses--i.e., the stresses limiting the momentarily linear range of behavior--were determined as functions of time for the response to stress of both strain and birefringence. The linear limit

stresses at both one percent and five percent deviation from linearity were determined. For CR-39 these stresses are plotted as functions of time in Chapter III. They are shown on birefringence-stress and strain-stress plots in Appendix III for the other materials. Further discussion of specific properties of each material appears later in this chapter.

A number of wave lengths of radiation were employed in the birefringence investigations, providing data for the study of two phenomena: dispersion of birefringence and variation of linear limit stresses with wave length. Such data was analyzed only for CR-39.

Experimental Techniques

Tapered models were successfully employed to obtain optical and mechanical data essential to this study. Few references can be found to the use of such models by other investigators. Their use in conjunction with the moire method for collecting mechanical strain data is believed to be without precedent.

Tapered models offer the advantage over most commonly used calibration models of allowing measurement of the response to stress over a broad range of stress. In principle, the response can be measured as a continuous function of stress within the existing range. This avoids the necessity of testing a large number of models or of using repeated or step loadings (which would be necessary

for prismatic models) to obtain data such as that required by this study. Because stresses near the ultimate strength were reached, neither repeated nor step loadings would have been appropriate. The use of tapered models thus made feasible a very extensive investigation into the effects of time on the materials tested. More general use of such models for studies of material behavior is recommended.

Although the models and techniques employed yielded results acceptably accurate for this study, some improvement in models and techniques is possible. The equipment available for this study would have allowed longer models. Somewhat less than a 10-inch-long gage portion of both the photoelastic and the mechanical specimens was actually useful because of the interference produced by the load in the stress distribution near the ends. The fields of both the polariscope and the optical system employed in observing moire fringes were thirteen inches in diameter. The use of longer models would permit a slightly more accurate determination of stresses and would reduce the significance of errors in determining fringe locations. However, this improvement would be very small in the present case.

A small improvement might also result from using higher-density line arrays in the moire analysis. A sufficient number of points was available for plotting very smooth curves of fringe order vs. length. But higher-density arrays would yield not only a larger number but

also narrower fringes, permitting more accurate fringe location determinations. The same advantage could be gained by using an optical sensing device in conjunction with an x-y recorder, as described in Appendix II.

Improvement in technique is needed chiefly in slope determinations of the moire fringe order vs. length curves. Better results might be obtained by use of an analytical (numerical) approach wherein smooth curves are fitted to the experimental data points and the slopes of these curves are evaluated numerically at desired points to yield the desired strains. These strains could then be related to stresses at the points where strains are known and stress-strain curves could be plotted. Birefringence-stress curves could be plotted in much the same way. From these curves linear limit stresses for any chosen deviation from linearity could be evaluated.

It seems that the most reliable check of the over-all accuracy of such an ambitious numerical program would be a comparison with results obtained by the procedures followed in this study. The proposed numerical approach might conceivably reduce the irregularity of data point locations on some plots, such as those for strain vs. stress or linear limit stress vs. time. The effects of such irregularity were minimized by the graphical techniques employed in this study. It was felt that the increase in accuracy, if any, which might have resulted

from using a numerical approach rather than a graphical one, could not justify the expenditure of time required by both the computer and the programmer to pursue such an approach.

The results of the study of dispersion of birefringence in CR-39 are not conclusive, even though they compare quite favorably with some results previously published by other authors. The main source of error is believed to be in the determination of the wave lengths--a very crucial determination for such studies. A hand-held spectroscope was used to check the manufacturer's specifications of the filters used. Although no deviations from the specifications were detected, the sensitivity of the spectroscope readings (about $\pm$ 2 nm) was not considered adequate for the purpose at hand.

Some variation with stress of the normalized retardation curve was detected. The variation was not consistent enough, however, to indicate a definite relationship between normalized retardation and stress, or between normalized retardation and degree of nonlinearity in the birefringence response to stress.

No dependence upon wave length of the linear limit stresses could be detected. There is probably no good reason to expect such dependence, at least within the limited range of wave lengths employed. However, this part of the study yielded valuable information regarding the

magnitude of possible error in all previous determinations of linear limit stresses. Apparently the ${}_n(\sigma_{\ell\ell})_{1.0}$ values found for CR-39 might be in error by as much as ten percent. But this does not mean that a serious error would result from assuming linearity to extend to a stress level that is ten percent higher than the actual value of ${}_n(\sigma_{\ell\ell})_{1.0}$. It simply means that the deviation from linearity of the response (birefringence or strain) might be, say, two percent rather than one percent.

Hence the errors which may be present in the reported values of the linear limit stresses do not seriously limit the usefulness of the results of this study. No serious errors will result from assuming the behavior of the materials to be linear up to the linear limit stresses reported, even if these values are not precisely determined. Serious errors can result, however, from assuming that a material such as CR-39 exhibits linear behavior up to the ultimate strength. Hopefully this point has been made eminently clear by this study.

Material Property Descriptions

One fundamental aspect of the forms of material property descriptions and of their interpretation deserves further discussion. Suitable viscoelastic and photoviscoelastic forms of representation were discussed in Chapter IV. In Chapter II it was implied that the characteristic functions describing the mechanical properties might be

thought of as time-dependent elastic coefficients and might be used in a modified, time-dependent Hooke's law. The strain response to one-dimensional constant stress was given as:

$$\varepsilon(t) = \frac{\sigma}{E(t)}. \tag{6.1}$$

The quantity E(t) was called a relaxation modulus, but the resemblance to a time-dependent Young's modulus was pointed out.

Similarly, the commonly used birefringence-stress relations were stated as:

$$n = \frac{d}{2f_\sigma} (\sigma_1 - \sigma_2) \tag{6.2}$$

and

$$n = \frac{C_\sigma d}{\lambda} (\sigma_1 - \sigma_2). \tag{6.3}$$

It was shown that the coefficients f_σ and C_σ actually vary with time. Again in this case it was implied that "momentary" values of these coefficients, as determined by one-dimensional tests, can be used in the more general stress situations represented by Equations (6.2) and (6.3). Thus a "momentary-photoelastic" condition of the material is implied, although the materials tested are admittedly photoviscoelastic.

The accuracy of many previously conducted photoelastic investigations, using materials such as those

tested in this study, indicates that the assumption of momentary "photoelasticity" is valid. This furthermore suggests that the assumption of momentary elasticity is valid in the case of mechanical properties. In this study no serious effort was directed toward establishing a firm theoretical basis for such assumptions, nor was an intensive search made of the literature for possible establishment by other investigators. Some ideas or first impressions are believed to be worth stating and are therefore given below.

In the discussion of viscoelasticity (Chapter IV) the relationship between the relaxation modulus E(t) and the extension compliance D(t) was given as:

$$\int_0^t E(t-\tau)D(\tau)d\tau = t. \tag{6.4}$$

But for "moderate rates of creep" an approximate relation is:

$$E(t) \cong \frac{1}{D(t)}. \tag{6.5}$$

Then the one-dimensional strain response to stress is given by Equation (6.1). But this equation assumes a modified form of "Hooke's law"; the relaxation modulus E(t) is considered simply to be a time-dependent Young's modulus. Hence the accuracy of the approximation involved in

Equation (6.5) is believed to be closely (if not directly) related to the momentary-elastic assumption.

Some insight into the problem might be gained by approaching it from another point of view. Differentiating with respect to time the one-dimensional Hooke's law equation

$$\sigma = E\varepsilon, \tag{6.6}$$

we obtain:

$$\dot{\sigma} = \dot{E}\varepsilon + E\dot{\varepsilon}, \tag{6.7}$$

where the dots denote time derivations and E is Young's modulus. Now if the behavior is truly elastic, $\dot{E}$ must be zero, since E is a constant. Then Equation (6.7) becomes:

$$\dot{\sigma} = E\dot{\varepsilon}. \tag{6.8}$$

For a momentary-elastic material the sequel to Equation (6.8) must be:

$$\dot{\sigma} = E(t)\dot{\varepsilon}. \tag{6.9}$$

But by starting with a time-dependent Hooke's law

$$\sigma = E(t)\varepsilon, \tag{6.10}$$

we obtain by differentiation:

$$\dot{\sigma} = \dot{E}(t)\varepsilon + E(t)\dot{\varepsilon}. \tag{6.11}$$

For Equation (6.11) to be identical to Equation (6.9) we

must have:

$$\dot{E}(t) \equiv 0. \tag{6.12}$$

Thus if the time-dependent Hooke's law assumption is to yield satisfactory results, the condition

$$\dot{E}(t) \cong 0 \tag{6.13}$$

must prevail. This condition is implied by the "moderate rates of creep" condition leading to Equation (6.5). Whether or not the two are more rigorously and fundamentally related, both are believed to be applicable to the behavior of the materials tested in this study.

Properties of Particular Materials

Polyester Resin CR-39.--The properties of this material were discussed from many viewpoints in Chapters III-V. It was selected for testing and for extensive discussion because it is probably the most widely used photoelastic material in this country. It has many desirable properties: It is clear and very smooth-surfaced, thus possessing excellent transmission properties and yielding very distinct, regular fringes. Furthermore, it is in an intermediate range of optical sensitivity and exhibits linear behavior throughout a reasonably wide range. It is inexpensive and readily available in sheets of various sizes and thicknesses. It will undoubtedly continue to be widely used.

However, this material must be carefully calibrated, not only for the effects of time upon the photoelastic coefficients and the mechanical characteristic functions but also for the extent of the linear range of behavior. This is particularly important because CR-39 is available from a number of suppliers and its properties are known to vary with the manufacturer.

The results of this study show that the linear limit stresses vary greatly with time after loading. Furthermore, within a few minutes after load is applied the linear limit stresses are much lower than the ultimate strength. This makes an analysis based on the assumption of linearity up to near-failure vulnerable to serious error, since large deviations from linearity are clearly possible.

Polyester Resin PS-1.--Although this material is intended primarily for photoelastic coatings, its properties make it very useful for models also. The results obtained from the tests on this material are presented graphically in Figures A3.1-A3.5 of Appendix III.

The material is seen to exhibit a distinct linear range of behavior, both mechanical and optical. The change of linear limit stress with time is small. The values of $_{n}(\sigma_{\ell\ell})_{1.0}$ are lower than the corresponding values for strain $_{\varepsilon}(\sigma_{\ell\ell})_{1.0}$. This is the same result herein reported for CR-39.

Deviations from linearity are relatively "slow": that is to say, errors would be small in assuming linearity to extend well beyond the linear limit stresses reported. Furthermore, the birefringence-strain plot (Figure A3.5) is very nearly linear up to the highest strains encountered, about two percent. This is a very important property in regard to the material's potential as a photoelastic coating.

Figures A3.2 and A3.4 show that time effects are extremely small after the load has been applied for three or four hours--i.e., the creep rate is very low.

The material is very nearly clear; some roughness of the surface detracts from its otherwise good transmission characteristics. It is very sensitive optically and is easily machined. It was found to yield (not fracture) at a stress above 9,000 psi. Therefore, it may be a useful material for photoplasticity studies. Its lack of brittleness reduces the hazards normally associated with stress concentrations.

Over-all, PS-1 is considered to be an excellent photoelastic model and coating material.

Epoxy Resin PS-2.--The behavior of PS-2 is similar in many respects to that of CR-39. It exhibits a much lower creep rate, however, and a smaller variation with time of linear limit stresses. Curves showing the data obtained for this material appear in Figures A3.6-A3.10.

No deviation from linearity in either the optical or mechanical response to stress was detected within the first few minutes after load was applied. This is contrary to earlier findings of the optical behavior as reported in [50]. A different lot number of the material was used in this study than in the earlier investigation.

The linear limit stresses at one percent deviation from linearity for optical behavior are slightly lower than the corresponding ones for mechanical behavior.

The creep rate of PS-2 is somewhere between those of CR-39 and PS-1. Figure A3.10 shows that the birefringence-strain relation is linear for a wide range of strains (above 1%) and deviates very little from linearity for strains up to nearly two percent. Like PS-1, it is very useful for coatings. Birefringence is seen to decrease with time at a given strain.

The material is ductile: it fails in shear at a uniaxial tensile stress above 12,000 psi. It has a deep amber color, which presents some problems concerning fringe definition (low contrast). It has very smooth surfaces and is very sensitive optically (comparable to PS-1). Like PS-1, it is available in sheets of various sizes and thicknesses.

Polyester Resin Palatal P6-K.--Figures A3.11-A3.15 show the optical and mechanical properties of P6-K. No deviation from linearity was detected in the optical

behavior within the ranges of stress and time employed. Some nonlinearity was observed in the mechanical behavior, but the deviations from linearity are seen (Figure A3.13) to be small and to occur only after constant stress was maintained for several hours.

The specimens used for the two investigations (optical and mechanical) were from different plates which were cured separately. Although the plates were taken from the same "lot" and approximately the same curing cycle was used, the differences in the behavior (mechanical and optical) might be due to variations in the handling of the specimens.

The creep rate is very low. Birefringence is seen (Figure A3.15) to decrease rapidly with time at a given strain.

The material was donated by the manufacturer in liquid form. It was mixed in the following proportions by weight: 100 parts resin, 1.50 parts catalyst, and 0.05 parts activator. It was cast between glass plates in sheets of nominal 1/4-inch and 3/8-inch thicknesses. A curing temperature of 90°C was maintained for 40 hours. The material was tested after it was stored, at room temperature, for over a year.

Though relatively insensitive optically, the broad range of linearity in the birefringence response to stress makes it a very useful photoelastic model material.

Fracture occurred in the photoelastic specimen after 200 hours at a stress of 5,950 psi. The test for mechanical properties was terminated after 100 hours because of an air conditioner failure.

Palatal P6-K exhibits good optical transmission characteristics with only a slight amber tint. It is quite brittle and is susceptible to chipping during the machining process.

Recommendations for Further Research

Several suggestions for continuing or extending the work of this study seem in order. These are given below:

1. Constant strain, relaxation-type tests, both optical and mechanical, should be conducted to check some results deduced from the creep tests of this study. Such tests on CR-39 would be particularly enlightening in view of the possible inflection in the birefringence-strain plot (Figure 3.8). A direct check could be made on the moduli, compliances, and photoelastic coefficients reported in this study.
2. Only quasi-static loadings were employed in this investigation. Yet accurate calibration tests are equally or even more important to dynamic studies using models. Some experimental studies of wave propagation, for example, have been reported with wholly inadequate calibrations, or even a complete

absence of them. Thus, the short-time response to periodic and/or impact loadings should be accurately determined. Constant strain rate loadings might also be employed. Such studies would constitute a valuable extension to the results here reported, if the same materials were used.

3. Photoviscoelasticity promises to become a powerful tool in viscoelastic stress analysis. An intensive search for suitable model materials must be conducted if the method is to achieve prominence. These materials must, of course, be carefully examined (calibrated). Photoviscoelastic theories and techniques must be scrutinized, tested, and further developed.
4. The momentary-elastic assumption, discussed at various points throughout this writing, seems justified for high-modulus materials exhibiting a low creep rate. But the question remains open of when (for what creep rate, say) the momentary-elastic theory must be abandoned in favor of a more general viscoelastic theory. Theoretical and/or experimental studies to help answer this question would be very valuable.
5. Linear limit stresses and certain other characteristic functions describing material behavior were determined in this study for the response to

one-dimensional stress. The ability of these quantities or functions to predict behavior under more general stress states should be checked.

6. Little experimental evidence has been provided for the study of nonlinear viscoelasticity under combined stress states. A number of theories and assumptions, therefore, lack experimental verification. This is particularly true for nonlinearities associated with small strains. Nonlinearities of this type are obviously exhibited by some of the materials (e.g., CR-39) tested in this study. Further investigations, employing combined stress states extending into the nonlinear range, might provide valuable data for further theoretical and experimental studies.
7. The moire method of strain (displacement) analysis has been the subject of very intensive study during the past few years. Further development is believed needed, particularly in the techniques of grid production and application. The possible use of diffraction gratings, especially, should be further investigated and developed.

LIST OF REFERENCES

1. Alfrey, T., Mechanical Behavior of High Polymers, vol. VI, Interscience Publishers, Inc., New York, 1948.

2. Bell, J. F., "Diffraction Grating Strain Gage," Proc. Soc. Exptl. Stress Anal., 17, 2 (1960), 51-64.

3. Clark, A. B. J., "Static and Dynamic Calibration of a Photoelastic Model Material, CR-39," Proc. Soc. Exptl. Stress Anal., 14, 1 (1956), 195-204.

4. Cloud, G. L., "Infrared Photoelasticity: Principles, Methods, and Applications," Ph.D. dissertation, College of Engineering, Michigan State University, 1966.

5. Clutterbuck, M., "The Dependence of Stress Distribution on Elastic Constants," Brit. Jour. Applied Phys., 9, 8 (1958), 323-29.

6. Coker, E. G., and L. N. G. Filon, A Treatise on Photo-elasticity, The University Press, Cambridge, Gr. Brit., 1957.

7. Coolidge, D. J., Jr., "An Investigation of the Mechanical and Stress-optical Properties of Columbia Resin, CR-39," Proc. Soc. Exptl. Stress Anal., 6, 1 (1948), 74-82.

8. Crisp, J. D. C., "The Measurement of Plane Strains by a Photoscreen Method," Proc. Soc. Exptl. Stress Anal., 15, 1 (1957), 65.

9. Dally, J. W., and W. F. Riley, "Experimental Stress Analysis with the Moire Fringe Method," Product Eng., 36, part 2 (1965), 41-48.

10. Daniel, I. M., "Quasi-static Properties of a Photo-viscoelastic Material," Exptl. Mech., 5, 3 (1965), 83-89.

11. Daniel, I. M., "Static and Dynamic Stress Analysis in Viscoelastic Materials," Ph.D. dissertation, Illinois Institute of Technology, 1964.

12. Diruy, M., "L'Analyse des Contraintes par la Methods des Reseaux Optiques," Docaero, no. 55 (March, 1955), pp. 1-18.

13. Dolan, T. J., and W. M. Murray, "Photoelasticity," Handbook of Experimental Stress Analysis, ed. M. Heteinyi, John Wiley and Sons, New York, 1950.

14. Douglas, R. A., C. Akkoc, and C. E. Pugh, "Strain-field Investigation with Plane Diffraction Gratings," Exptl. Mech., 5, 7 (1965), 233-38.

15. Durelli, A. J., and V. J. Parks, "Moire Fringes as Parametric Curves," presented at 1966 S.E.S.A. spring meeting, Detroit, Michigan, May 4-6, 1966.

16. Eirich, F. R., Rheology, Theory and Applications, vols. I, II, and III, Academic Press, New York, 1960.

17. Ferry, J. D., Viscoelastic Properties of Polymers, John Wiley and Sons, New York, 1961.

18. Frocht, M. M., Photoelasticity, vols. I and II, John Wiley and Sons, Inc., New York, 1941.

19. Frocht, M. M., and Y. F. Cheng, "An Experimental Study of the Laws of Double Refraction in the Plastic State in Cellulose Nitrate--Foundations for Three-dimensional Photoplasticity," Photoelasticity, ed. M. M. Frocht, Pergamon Press, New York, 1963, pp. 195-216.

20. Frocht, M. M., and Y. F. Cheng, "On the Meaning of Isoclinic Parameters in the Plastic State in Cellulose Nitrate," Jour. Applied Mech., 29 (1962), 1-6.

21. Frocht, M. M., and R. Guernsey, Jr., "Further Work on the General Three-dimensional Photoelastic Problem," Jour. Applied Mech., 22, 2 (1955), 183-89.

22. Frocht, M. M., and R. A. Thomson, "Further Work on Plane Elastoplastic Stress Distributions," Photo-elasticity, ed. M. M. Frocht, Pergamon Press, New York, 1963, pp. 185-93.

23. Frocht, M. M., and R. A. Thomson, "Studies in Photo-plasticity," Proc. Third U.S. Natl. Cong. Applied Mech. (1958), 533-40.

24. Green, A. E., and R. S. Rivlin, "The Mechanics of Nonlinear Materials with Memory," Archive for Rational Mech. and Anal., Part I, 1 (1957), 1-21; Part II, with A. J. M. Spencer, 3 (1959), 82-90; Part III, 4 (1959-60), 387-404.

25. Gross, B., Mathematical Structure of the Theories of Viscoelasticity, Hermann, Paris, 1953. See also: Jour. Applied Phys., 18, 212 (1947); 19, 257 (1948); and 22, 1035 (1951).

26. Guild, J., The Interference Systems of Crossed Diffraction Gratings, Clarendon Press, Oxford, 1956.

27. Gurtin, M. E., and E. Sternberg, "On the Linear Theory of Viscoelasticity," Archive for Rational Mech. and Anal., 11, 4 (1961), 291-356.

28. Jessop, H. T., and F. C. Harris, Photoelasticity Principles and Methods, Dover Publications, New York, 1949.

29. "Kodak Wratten Filters," Scientific and Technical Data Book B-3, Eastman Kodak Co., Rochester, N.Y., 1965.

30. Kolsky, H., "Experimental Studies of the Mechanical Behavior of Linear Viscoelastic Solids," Technical Report No. AM-18, Dept. of Defense, ARPA, Materials Research Program, April, 1965.

31. Leaderman, H., Elastic and Creep Properties of Filamentous Materials, Textile Foundation, Washington, 1943.

32. Leaderman, H., "Viscoelastic Phenomena in Amorphous High Polymeric Systems," Rheology, vol. II, ed. F. R. Eirich, Academic Press, New York, 1958.

33. Lee, E. H., "Viscoelastic Stress Analysis," Proc. First Symposium on Naval Structural Mech., Pergamon Press, New York, 1960, pp. 456-82.

34. Lee, E. H., and T. G. Rogers, "Solution of Viscoelastic Stress Analysis Problems Using Measured Creep or Relaxation Functions," Jour. Applied Mech., 30 (1963), 127-33.

35. Lockett, F. J., "Creep and Stress-relaxation Experiments for Non-linear Materials," Int. Jour. Eng. Sci., 3 (1965), 59-75.

36. Low, I. A. B., "The Moire Method Using Diffraction Gratings," presented at 1966 S.E.S.A. spring meeting, Detroit, Michigan, May 4-6, 1966.

37. Low, I. A. B., and J. W. Bray, "Strain Analysis Using Moire Fringes," Engineering, 213 (1962), 566.

38. Marin, J., and J. E. Griffith, "Creep Relaxation of Plexiglas IIA for Simple Stresses," Jour. Eng. Mech. Div., Proc. A.S.C.E., 82, EM-3 (1956), Paper 1029, 1-20.

39. Mindlin, R. D., "A Mathematical Theory of Photoviscoelasticity," Jour. Applied Phys., 20 (1949), 206-216.

40. Mindlin, R. D., "Analysis of Doubly Refracting Materials with Circularly and Elliptically Polarized Light," Jour. Optical Soc. Am., 27 (1937), 288.

41. Mönch, E., "Die Dispersion der Doppelbrechung bei Zelluloid als Plastizitätsmas in der Spannungsoptik," Zeitschrift für angewandte Physik, 6, 8 (1954), 371-75.

42. Mönch, E., and R. Loreck, "A Study of the Accuracy and Limits of Application of Plane Photoplastic Experiments," Photoelasticity, ed. M. M. Frocht, Pergamon Press, New York, 1963, pp. 169-84.

43. Morse, S., A. J. Durelli, and C. Sciammarella, "Geometry of Moire Fringes in Strain Analysis," Jour. Eng. Mech. Div., Proc. A.S.C.E., EM-4 (1960), pp. 105-126.

44. Nielson, L. E., Mechanical Properties of Polymers, Reinhold Publishing Corp., Chapman and Hall, Ltd., London, 1962.

45. O'Haven, C. P., and J. F. Harding, "Studies of Plastic Flow Problems by Photo-grid Methods," Proc. Soc. Exptl. Stress Anal., 2, 2 (1944), 59-70.

46. Onaran, K., and W. N. Findley, "Combined Stress-creep Experiments on a Nonlinear Viscoelastic Material to Determine the Kernel Functions for a Multiple Integral Representation of Creep," Trans. Soc. Rheology, 9, 2 (1965), 299-327.

47. Pindera, J. T., "Einige rheolgische Probleme bei spannungsoptischen Untersuchungen," Internationales spannungsoptischen Symposium, Berlin, April, 1961, Akademie-Verlag, Berlin, 1962.

48. Pindera, J. T., "Remarks on Properties of Photoviscoelastic Model Materials, Exptl. Mech., 6, 7 (1966), 375-80.

49. Pindera, J. T., and G. L. Cloud, "On the Description of Dispersion of Birefringence of Photoelastic Materials," Exptl. Mech., 6, 9 (1966), 470-80.

50. Pindera, J. T., and E. W. Kiesling, "On the Linear Range of Behavior of Photoelastic and Model Materials," Proc. Third Int. Cong. Exptl. Stress Anal., West Berlin, March, 1966, VDI-Berichte No. 102, 1966, pp. 89-94.

51. Post, D., "The Moire Grid-analyzer Method of Strain Analysis," Exptl. Mech., 5, 11 (1965), 368-77.

52. Ross, B. E., C. A. Sciammarella, and D. Sturgeon, "Basic Optical Law in the Interpretation of Moire Patterns Applied to the Analysis of Strains--Part 2," Exptl. Mech., 5, 6 (1965), 161-66.

53. Sciammarella, C. A., "Basic Optical Law in the Interpretation of Moire Patterns Applied to the Analysis of Strains--Part 1," Exptl. Mech., 5, 5 (1965), 154-60.

54. Sciammarella, C. A., "Techniques of Fringe Interpolation in Moire Patterns," presented at Second Int. Cong. Exptl. Mech., Washington, D.C., September 28-October 1, 1965.

55. Sciammarella, C. A., and F. Chiang, "The Moire Method Applied to Three-dimensional Elastic Problems," Proc. S.E.S.A., 4, 11 (1964), 313-19.

56. Sciammarella, C. A., and A. J. Durelli, "Moire Fringes as a Means of Analyzing Strains," Jour. Eng. Mech. Div., Proc. A.S.C.E., 87, EM-1 (1961), 582-601.

57. Sciammarella, C. A., and N. Lurowist, "Interpolation of Moire Fringe Orders by a Purely Optical Technique, Moire Fringe Multiplication," presented at Fourth Int. Cong. Applied Mech., Minneapolis, Minnesota, June 14-17, 1966.

58. Sciammarella, C. A., and D. Sturgeon, "Substantial Improvements in the Processing of Moire Data by Optical and Digital Filtering," Proc. Third Int. Cong. Exptl. Stress Anal., West Berlin, March, 1966, VDI-Berichte No. 102, 1966.

59. Shepherd, R., and L. M. Wensley, "The Moire-fringe Method of Displacement Measurement Applied to Indirect Structural-model Analysis, Exptl. Mech., 5, 6 (1965), 167-76.

60. Shimada, H., and M. Chiba, "Photoelastic Investigation of Large Deflections by Low-modulus Materials," Exptl. Mech., 5, 10 (1965), 340-44.

61. Spencer, A. J. M., and R. S. Rivlin, "Further Results in the Theory of Matrix Polynomials," Archive for Rational Mech. and Anal., 4 (1959-60), 214-30.

62. Staverman, A. J., and F. Schwarzl, "Linear Deformation Behavior of High Polymers," Die Physik der Hochpolymeren, vol. IV, ed. H. A. Stuart, Springer-Verlag, Berlin, 1956, chaps. 1 and 2.

63. Stuart, H. A., Die Physik der Hochpolymeren, vol. IV, Springer-Verlag, Berlin, 1956.

64. Theocaris, P. S., "A Review of the Rheo-optical Properties of Linear High Polymers," Exptl. Mech., 5, 4 (1965), 105-114.

65. Theocaris, P. S., "Creep and Relaxation Contraction Ratio of Linear Viscoelastic Materials," Jour. Mech. Phys. Solids, 12 (1964), 125-38.

66. Theocaris, P. S., "Moire Fringes: A Powerful Measuring Device," Applied Mech. Revs., 15, 5 (1962), 333-39.

67. Theocaris, P. S., and H. H. Kuo, "The Moire Method of Zonal and Line Gratings," Exptl. Mech., 5, 8 (1965), 267-72.

68. Timoshenko, S., and J. N. Goodier, Theory of Elasticity, 2d ed., McGraw-Hill Book Co., New York, 1951.

69. Ward, I. M., and E. T. Onat, "Non-linear Mechanical Behavior of Oriented Polypropylene," Jour. Mech. Phys. Solids, 11 (1963), 217-29.

APPENDIX I

ANALYSIS OF STRESS DISTRIBUTION IN TAPERED MODEL

As stated in Chapter II, any model for which there is a known analytical solution for the stress distribution can be used for calibration. Such a solution for a wedge loaded with a concentrated force at the apex is given below. Combining this with experimental evidence obtained for a material with known properties, the value of radial stress along the centerline of the tapered model used throughout this study is obtained.

Timoshenko and Goodier [68] obtained the solution by assuming stresses which satisfy the boundary conditions. An unknown constant is evaluated from equilibrium considerations. Frocht [18] used the Airy stress function

$$\Phi = Cr\theta \sin \theta \tag{A1.1}$$

to obtain the stresses

$$\sigma_r = 2C \frac{\cos \theta}{r}, \tag{A1.2}$$

$$\sigma_\theta = 0, \tag{A1.3}$$

$$\tau_r = 0, \tag{A1.4}$$

where θ is measured from the centerline and r from the apex as shown in Figure A1.1. The boundary conditions are satisfied by such stresses, and it may easily be verified that the stress function satisfies the necessary compatibility equation.

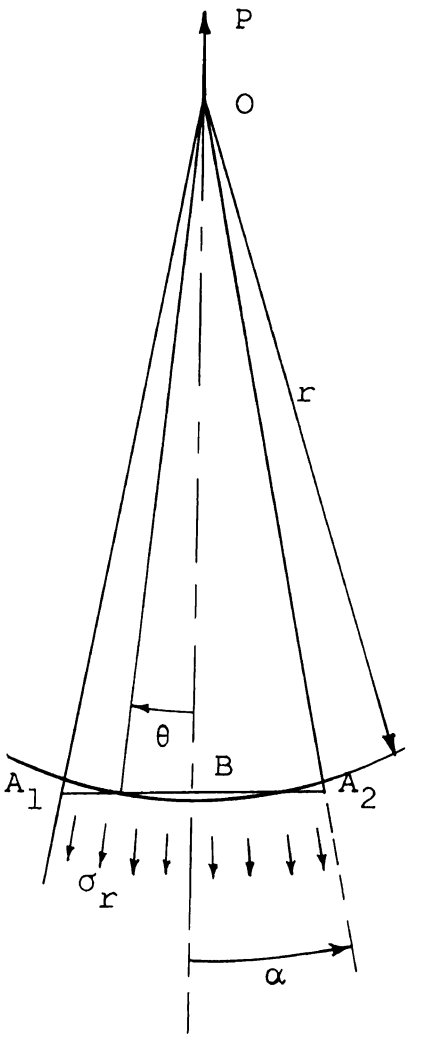

Fig. A1.1--Sketch of wedge with concentrated load at the apex.

The constant C is evaluated by considering the equilibrium of a portion of the wedge bounded by the

straight sides and the surface r = constant. The constant C is thus found to be:

$$C = \frac{P}{d(2\alpha + \sin 2\alpha)}, \tag{A1.5}$$

where d is the thickness of the model.

Combining Equations (A1.2) and (A1.5) yields:

$$\sigma_r = \frac{2P \cos \theta}{rd(2\alpha + \sin 2\alpha)}. \tag{A1.6}$$

The equation relating order of isochromatic and stress was given in Chapter II as:

$$n = \frac{C_\sigma d}{\lambda} (\sigma_1 - \sigma_2). \tag{A1.7}$$

In the case of the wedge,

$$\sigma_1 = \sigma_r \quad \text{and} \quad \sigma_2 = 0,$$

so

$$n = \frac{C_\sigma}{\lambda} \frac{2P \cos \theta}{r(2\alpha + \sin 2\alpha)}. \tag{A1.8}$$

Equation (A1.8) shows that on the centerline of the model, when $\theta = 0$, the isochromatic fringe of a given order is circular. For the model used in this study $\alpha = 7.12°$. Since $\cos 7.12° = 0.9922$, the fringes may be regarded as circular for the entire wedge portion of the model used.

It is interesting that the solution presented above, through Equation (A1.8), does not restrict the value of the angle α to being small. Hence the solution applies as well to a semi-infinite plate, where $\alpha = \frac{\pi}{2}$.

For the modified wedge used in this study (soon to be described), the small part of the wedge is transformed to a section of uniform width. Hence the apex of the wedge is not on a boundary. The radius r, therefore, is not easily measured. However, the width of the model can be measured with accuracy and speed. This can be used to determine the nominal stress which can in turn be related to the radial stress σ_r as follows:

$$\sigma_{nom} = \frac{P}{d(\overline{A_1A_2})} \quad \text{from Figure A1.1,}$$

$$\overline{OB} = r \cos\theta, \quad \overline{A_1B} = \overline{OB} \tan\alpha = \overline{A_1A_2}/2,$$

$$\overline{A_1A_2} = 2\,\overline{OB} \tan\alpha = 2r \cos\theta \tan\alpha,$$

$$\sigma_{nom} = \frac{P}{2rd \cos\theta \tan\alpha}. \tag{A1.9}$$

Let

$$\sigma_r = k\sigma_{nom}, \tag{A1.10}$$

where k is a stress concentration factor. From Equations (A1.6), (A1.9), and (A1.10),

$$\frac{2 \cos \theta}{2\alpha + \sin 2\alpha} = (k) \frac{1}{2 \cos \theta \tan \alpha},$$

from which

$$k = \frac{4 \cos^2 \theta \tan \alpha}{2\alpha + \sin 2\alpha}. \qquad \text{(A1.11)}$$

Along the centerline of the model (wedge), where the fringe order for birefringence or moire patterns is read, $\theta = 0$ and

$$(k)_{\theta=0} = \frac{4 \tan \alpha}{2\alpha + \sin 2\alpha} \qquad \text{(A1.12)}$$

For models used, $\alpha = 7.13°$. The value of k along the centerline becomes:

$$(k)_{\theta=0} = 1.011. \qquad \text{(A1.13)}$$

Thus

$$\sigma_r = 1.011\sigma_{nom}. \qquad \text{(A1.14)}$$

The above analysis is valid only in that portion of the wedge-shaped portion of the specimen where no disturbance in the stress distribution exists. The expression for σ_r shows that $\sigma_r \rightarrow \infty$ as $r \rightarrow 0$; hence it is necessary to modify the wedge shape in such a way that the smallest cross-section is capable of carrying a load sufficient to cause a meaningful stress in the largest portion of the wedge. This is accomplished by transforming the smaller portion of the wedge into a prismatic "shank," as shown in

Figure A1.2. This shank is long enough to provide a uniform axial stress over a length sufficient to accurately measure order of isochromatic, longitudinal strain, and transverse strain. On the end of the prismatic portion opposite the wedge, smooth transition to a corner is made, thus providing a point of zero stress where the zero-order isochromatic is found. The small holes near each end were used only to align and hold the model for machining, as discussed in Chapter II.

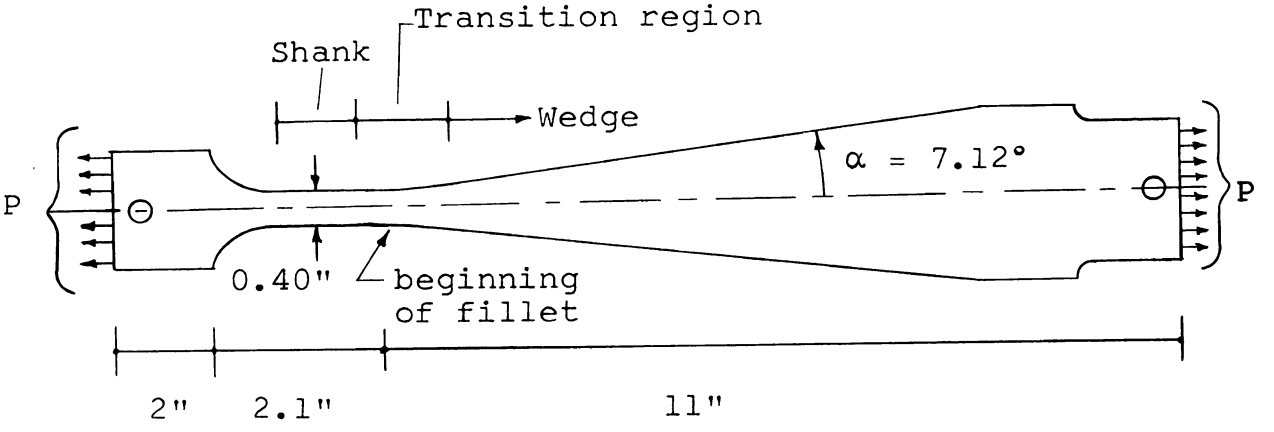

Fig. A1.2--Sketch showing shape and approximate dimension of tapered model used.

Since the region of transition from the wedge to the shank does not lend itself to mathematical analysis for the stress distribution, an experimental method is used. The stress concentration factor k, defined by Equation (A1.10), is determined continuously from the wedge portion, where its value is 1.011, through the transition region and into the shank portion, where its value is 1.00. This

experimental determination is easily made with a material known to have a momentarily linear stress-birefringence relation for stresses below those encountered in the shank during the determination. Polyester Resin Palatal P6-K in the cured state was known from previous tests[1] to possess such properties and was therefore selected.

Because the stress-birefringence relation is linear, each integral-order isochromatic fringe represents a given difference in principal stresses. But since the distribution is radial in the wedge, this given difference is simply an increment of the radial stress σ_r. On a picture of the isochromatic fringe pattern, taken with a constant load on the model, the location of each integral fringe was determined on the centerline. In the wedge portion, where k is known to be 1.011, the radial stress at each fringe location is computed from the nominal stress. Now, when the increment of σ_r represented by each integral isochromatic fringe is known, the value of the apparent σ_r can be determined at each point on the centerline where a fringe crosses, through the transition region and into the shank. At each of these points the nominal stress is computed. Now the stress concentration factor k is determined at the

---

[1]Since both stress distribution and isochromatics are radial in the wedge portion of the model (Fig. A1.2), the momentary linearity of the stress-birefringence relation can be checked up to the maximum stress in the wedge portion. This stress should not be exceeded in the shank during the test for determination of the stress concentration factor.

discrete points where fringes cross the centerline. The known value of k in the shank affords a check.

The value of k may now be plotted against the distance along the centerline. The plot used throughout the photoelastic calibration studies is shown in Figure A1.3. The beginning of the fillet, located by means of a micrometer caliper, served as a reference point. Two scales are shown on the abscissa because in scribing the scale on some models metric units were employed; on others the scale was in inches.

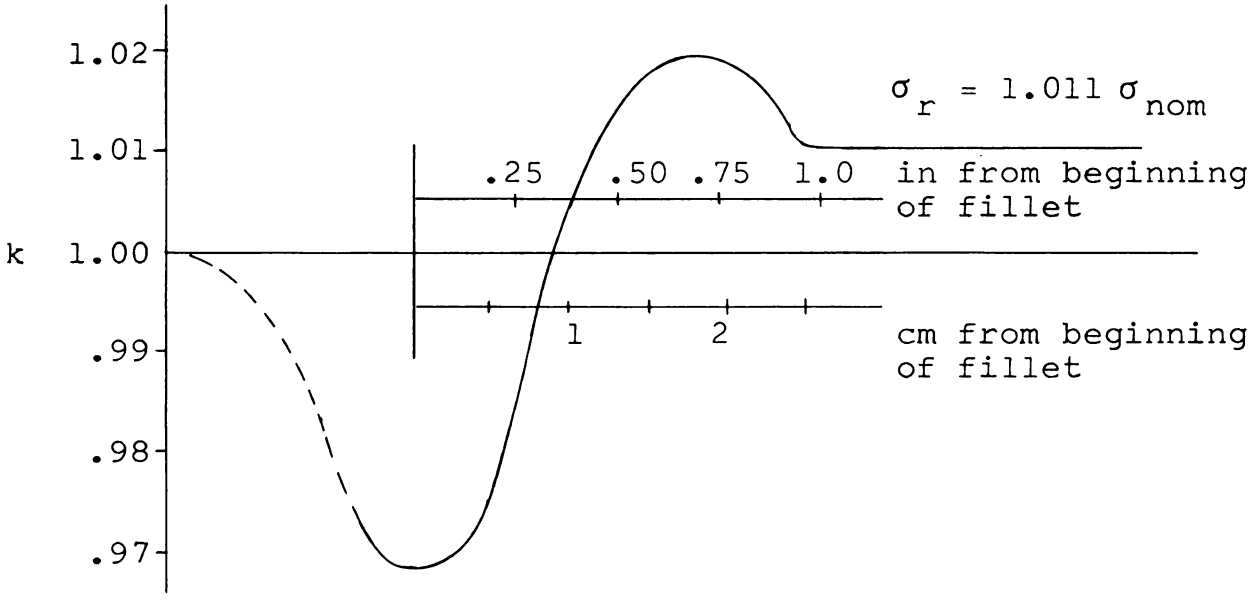

Fig. A1.3--Plot showing variation of the stress concentration factor k along the centerline of the photoelastic model.

Additional points on the plot may be obtained by considering half-order fringes or by changing the load on the model.

The external load at the large end of the taper disrupts the radial distribution of stress as given by Equation (A1.6) near the end. The width there is approximately 2.5 inches. The isochromatic fringes are very broad in the largest portion of the taper, due to the small stress gradient, making fringe location difficult. Hence no readings were taken in the portion 3-4 inches from the large end. The lowest useful stress was then approximately twenty percent of that in the shank.

A similar calibration could be performed for the strain distribution. It is more complicated because an integral moire fringe does not represent a particular strain but only a certain displacement relative to another fringe. Furthermore, the effect on the moire pattern is not as pronounced as on the isochromatic pattern for the following reason. The isochromatic order is related to the difference in principal stresses $(\sigma_1 - \sigma_2)$ or, in this case, $(\sigma_r - \sigma_\theta)$. Hence any small transverse stress σ_θ affects the isochromatic order directly. The strain in the radial direction would, on the other hand, be affected by a transverse stress component only through the Poisson effect. Since Poisson's ratio cannot exceed the value of 0.5 (in an elastic material), the effect of such a transverse stress component on axial strain is less pronounced than upon the isochromatic fringe pattern.

Poisson's ratio is less than 0.4 for the materials tested in this study. Irregularities of the moire fringe pattern in the transition region were not apparent. On the mechanical models the stress concentration factor was therefore assumed 1.00 in the shank and up to the point of crossing in Figure A1.3, and 1.011 for the remainder of the model.

Typical isochromatic and moire fringe patterns are shown in Figure A1.4.

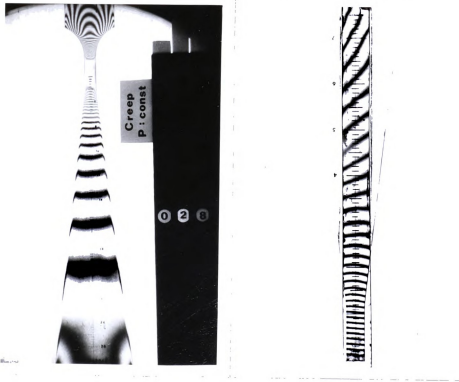

(a) (b)

Fig. A1.4--Photographs of (a) isochromatic fringe pattern and (b) moire fringe pattern.

APPENDIX II

TECHNIQUES OF MOIRE STRAIN ANALYSIS

Difficulties Presented by a "Conventional" Method

In order to plot strain as a function of stress, at a given time after loading, including not only the linear but also a portion of the nonlinear region, at least eight points seem necessary (see Figure 3.5). Though the general shape of the stress-strain curve can be established with only a few points, the accurate evaluation of the linear limit stress value at a specified deviation from linearity of strain requires eight or more.

These considerations led to the attempt at measuring the average strain over a 4-inch gage length by means of a mechanical extensometer on eight tension specimens of uniform width. The extensometer consists of an invar steel bar attached at one of its ends to the specimen, with the bar resting lightly in a guide cemented to the specimen near the other end. The displacement of a fine line scratched on the bar, 4 inches from the attached end, relative to a similar line on the guide, was measured with a telemicroscope supplied by Gaertner Scientific Corporation.

This method promised three distinct advantages: (1) high sensitivity (better than 1 x 10^{-4} in/in); (2) no adverse effects, such as stiffening or indentation of the specimen; and (3) repeated use of a single extensometer.

Inherent in this method are some disadvantages. Only one specimen at a time can be tested without special load frames, designed to accommodate multiple specimens, and provision for readily and accurately moving the telemicroscope to obtain successive readings on all specimens is also necessary. A load frame holding nine specimens was used by Marin and Griffith [38], with electrical resistance gages measuring strain. The expense of building such a load frame, with the additional telemicroscope carriage, was beyond the means of the present study.

The series of eight or more separate tests require at least eighty days for obtaining the creep data desired in this study; nevertheless, it was attempted. Eight specimens of Polyester Resin PS-1, with a prismatic portion exceeding 5.2 inches in length and a width of 0.40 inch, were cut from a plate approximately 0.130 inch thick. From the data obtained by separate tests at different stress levels curves of strain vs. time were drawn for each stress level. Six tests at successively higher stress levels, extending well into the nonlinear region, were followed by two at stress levels by then known to be near the linear limit stress. Although it was difficult to repeat readings

closely, little scatter was evident in the data. From this plot data was deduced for strain vs. stress at selected times.

In this strain-stress plot glaring discrepancies appeared. The eight points available for plotting each curve were scattered excessively for purposes of accurately determining the linear limit stress. The points corresponding to the last two tests appeared four to five percent above the curve established by the other six points.

Several causes, acting alone or in combination, might be responsible for such erratic behavior. As mentioned in Chapter II, when more than one specimen is used in a calibration test, they must all be machined and handled identically. For convenience and consistency all eight specimens were machined at once. But then how are they to be handled identically when they must be stored for various periods of time awaiting testing? Since the time-edge effect was known to be significant on some plastics, the machined surfaces were coated with silicone grease and the specimens were stored in tightly closed polyethylene bags. Perhaps this precaution was not necessary--or perhaps it was necessary but not effective. Possibly it even caused a degradation of the data.

Lack of homogeneity could also cause the discrepancies. Frocht and Thomson [23] found variations of up to seven percent in birefringence, in eight different models

cut from a single sheet of celluloid. Some variation in mechanical properties seems just as likely.

Reloading for shorter time periods produced roughly the same magnitudes of strain response but a different rate of creep, particularly at the highest stresses encountered. No data of value to this study was obtained.

Suitability of Moire Method

Because of the time required by further attempts to use the method discussed above, it was abandoned in favor of one employing the moire method on a tapered specimen with a shape identical to that used in the optical test. Its use on such a model yields strain data for any (every) value of stress within a certain range, this range quite naturally being about the same as for the test of optical properties on the same material. Hence one model yields all the stress-strain data required by this study.

The theory and methods of interpretation of moire patterns are well-established [15,43,51,55,56]. Theocaris [66] recently reported on past efforts and presented an extensive bibliography on the moire method.

Low sensitivity has generally limited the usefulness of the method to the measurement of the relatively large strains. With two initially identical line arrays of density 500 lines/inch each fringe, formed by superposition of the two arrays after one is deformed, represents a relative displacement of 0.002 inch. By counting half fringes

a relative displacement of 0.001 inch can be detected. Since strain in a given direction is given by the displacement gradient in that direction, fringes must be closely spaced in regions where the gradient is small or changes rapidly if serious errors are to be avoided. Fortunately, no such rapid changes were present in the tapered specimen used for this study.

Accuracy of the moire method can be improved by many techniques [9]: (1) Higher-density (i.e., smaller-pitch) arrays produce more fringes with consequent increase in precision. (2) Variable-pitch arrays allow compensation-type determinations of fractional fringe orders, thus increasing accuracy. This is essentially the same as using an initial mismatch of pitches, producing an initial pattern, and subsequently yielding a larger number of fringes. (3) Photocells can be used to measure light intensity at a point. The intensity, in turn, can be related [53] to the maximum and minimum intensities corresponding to integral and half-order fringes, thereby yielding a continuous relationship between light intensities and displacements, and hence strains. Sciammarella and associates [52] obtained better results by this method using a 300 line/inch grid, yielding minimum strains of 20×10^{-6} inch/inch, than by the conventional method using 1,000 lines/inch in a previous test under similar conditions. (4) Various methods of fringe interpolation have been successfully employed

[54,58]. Sciammarella and Lurowist [57] obtained partial fringes by observing the normal moire pattern in a field of polarized light, thus taking advantage of the diffraction characteristics of line arrays. Low [36] achieved the same result using diffraction gratings instead of ordinary line arrays. These gratings promise several advantages other than the one mentioned.

None of these refinements seemed necessary in this study. The investment in time and auxiliary equipment required to utilize them seemed unwarranted. As mentioned above, no rapid changes in the displacement gradient occurred. It was seen in Chapter III that a 500 line/inch array yielded an adequate number of points for plotting a smooth curve of fringe order vs. length along the specimen. Loss of accuracy resulted mostly from evaluating the slope of this line rather than in constructing it, and this evaluation might be improved by means of a suitable data-smoothing technique if necessary.

The choice of 500 lines/inch as the density for model and analyzer was somewhat arbitrary. The pitch most appropriate for a given application can be specified only within some range. It should be small enough to yield sufficient response for the smallest strains anticipated but should not be so small as to produce so many fringes in regions of highest strain that they can no longer be clearly distinguished. The difficulty and expense inherent

in producing fine arrays will usually dictate that the largest permissible pitch be used.

Production of Line Arrays-- General Methods

Methods of producing line arrays vary widely, depending upon such factors as the density of the array, type of model material used, equipment available, and the number of arrays required. Reference arrays in various densities are available on a stable transparent backing, such as glass, with cost depending upon the density and over-all size. Duplicates of these can be made by contact printing. Suitable arrays can also be made by photographing larger, inexpensive, coarse screens.

Line arrays on the model are much more difficult to produce. Of course, they must be accurate in line width and spacing and must follow the model perfectly during deformation yet offer no significant resistance to deformation. Model arrays are usually produced in one of five ways: (1) The array is scribed or indented into the surface. (2) An array is photographed or contact printed on stripping film, and a very thin film carrying the emulsion is cemented to the specimen. (3) The array is printed, by contact, in a layer of light-sensitive emulsion coating the specimen. (4) Commercially available gages with arrays etched in thin metal may be cemented to the specimen. When the cement has cured, a metal backing is

stripped off, leaving only a series of thin metal filaments attached to the specimen. (5) A diffraction grating is "printed" by contact in a layer of liquid resin, coating the specimen.

The problem of choosing the method most suitable for a particular application has many aspects, some of which were mentioned at the beginning of this section. Application of an array on plastics presents problems not present for metals: chemicals used for etching may attack the plastics, scribing may introduce stress concentrations or fail to yield sufficient contrast for observable fringes, and the heating required for the cure of some coatings is excessive for plastics.

The first method mentioned above--namely, scribing or indenting the array into the surface--can hardly be considered for plastics. It has, however, been used quite successfully on other materials. Using the mechanism from a rotary microtome, Douglas, Akkoc, and Pugh [14] obtained consistently successful gratings of line densities to 12,700 lines/inch on flat metal specimens. Bell [2] obtained rulings in the form of cylindrical threads with densities as high as 30,720 lines/inch using a specially modified lathe.

The use of stripping film, as mentioned secondly above, offers the advantage of using directly an array on film, thus eliminating the additional step of contact

printing on the emulsion-covered specimen as required by (3). Since stripping film was used extensively in this study, its use will be further discussed in the following section.

Before a suitable cement for bonding the stripping film to the specimen was found, the third method was tried. In this method the specimen is coated with a light-sensitive emulsion which is, in turn, exposed by contact printing to the desired array on glass or film. Because most of the available emulsions are relatively insensitive and because intimate contact is required, a vacuum printing frame and carbon-arc lamp are usually used in the operation. These were made available for use in this study by two local firms--one a lithographer, the other a photo-engraver.

Although this method is probably the most widely used for applying arrays to models, success was not achieved in the course of this study. The greatest difficulty was the lack of an inexpensive array on glass or film which transmitted the light exposing the emulsion with uniform intensity. Glass plates with the desired 500 line/inch array scratched into the surface were known to be available. Their cost was prohibitive ($16 per square inch from one manufacturer) for the size required in this study (approximately 10-inch length). Film reproductions of these arrays,

which were later purchased, were not known to be available at the time the method was attempted.

An array of 500 lines/inch was, however, obtained on film by photographing a coarse, inexpensive screen of 65 lines/inch. The lack of uniform light transmission by the screen caused a corresponding nonuniformity in the film, which was further magnified in the array printed on the specimen. The exposure of the emulsion coating the specimen ranged from too low, so that the emulsion was removed in developing, to too high, so that the lines could not be distinguished. The images on film, however, were sufficiently uniform in intensity for the production of high quality and high contrast moire fringes when two such films were placed in contact. Since these images could successfully be produced on stripping film, the method employing such film directly was again pursued and finally used successfully. Before discussing the technique used in applying the stripping film, the last two methods mentioned above--i.e., use of commercially available, bondable gages and diffraction gratings--will be briefly discussed.

Bondable gages promise the advantages of easy application, lack of stiffening since the grid is advertised as consisting of a series of unconnected "dots," and extremely high contrast since the array is formed in metal which is transferred to the specimen. Their chief disadvantages would seem to be relatively high cost and

limited size (e.g., at present the largest available 500 line/inch grid is 3.6 in x 3.6 in at $55). Application in this study, where an area of 0.40 inch by 10 inches was needed, required cutting the largest available grid into strips and joining three strips end to end.

In view of the promised advantages, one of the bondable gages described above was purchased and bonded, in strips, to two specimens, one of which was to serve as the analyzer to measure the strain response of the other. After testing it was discovered that instead of a series of square dots the grid actually consisted of a series of crossed lines, thus aborting some of its greatest potential advantages--those of offering no resistance to deformation and of following arbitrarily large strains. Though the slight stiffening was not believed significant, no further use was made of the bondable gages, since cross-lined metal screens of the same density were found to be available from another manufacturer in an 11-inch by 11-inch size for approximately the same cost as quoted above for the bondable gage of one-ninth the area. One of the metal screens was purchased to make contact prints on film of the cross-lined grid, but it was not used directly as a gage.

The diffraction-grating method used by Low [36] offers at least three distinct advantages: ease of application, high density, and inherent fringe-interpolation potential. The grating is available as a series of

"grooves" in hardened gelatin on a glass backing plate. The specimen to which the grating is to be applied is coated with a liquid resin into which the grooves are pressed and held until the resin "sets" or cures. The master grating is then removed and can be used again. Gratings with 5,000 rulings per inch have been successfully employed; 2,500 rulings per inch are more common and generally adequate.

With the proper optical system the fundamental moire fringes are reduced to fine sharp lines, thus facilitating accurate location. But in addition, subsidiary fringes can be produced which are fractional-order fringes. These are useful for interpolating displacements within the fundamental period, an important factor for very small strains or high-strain gradients.

Although the increased accuracy of such a method was not required in the present study, the low cost and apparent ease of grid production might have dictated its use. Unfortunately, information about the method came too late for inclusion in this study.

Grid Application
Method Employed

Of the five previously mentioned methods of applying arrays to the specimen and analyzer, three were tried but only one proved successful--namely, the one employing stripping film. In this method the desired array is

imprinted in the emulsion of the film, either by photography or by contact printing. A coarse screen of 65 lines/inch was photographically reduced to 500 lines/inch on stripping film in the first attempts of this study. Later the commercial availability of a 500 line/inch film reproduction was recognized, and one was purchased. It was used to make contact prints on stripping film. These prints were more uniform but gave slightly less contrast than the photographs.

The stripping layer or membrane carrying the emulsion is quite stable, considering its thickness (between 0.0004 and 0.0005 in). This stability is necessary for the usual transfer process of stripping (wet or dry) and cementing to a new base. While its stiffness is not significant in stiffening the specimens to which it was applied, it is also inadequate for allowing one inexperienced in its handling to transfer, after stripping, a piece 0.40 inch by 10 inches to a specimen without extensive distortion! If, however, a cement could be found giving adequate adhesion to allow the backing of the stripping film to be peeled off after cementing, then the problem of distortion would be drastically reduced. The stability of the membrane creates further demands upon the cement, since no creep of the cement is allowed if the bonded membrane is to follow the specimen upon straining.

Eastman 910 cement was found adequate for the task. Its "instant" curing adds another advantage. A liquid cement of the same material as the specimen has been used [12]. Besides the lack of availability in liquid form of some materials, the excessive curing time of most materials handicaps their use as a cement.

The procedure used in cementing the thin strip to the specimen was developed without the advantages of prior experience or any instructions. The specimen to which the membrane was to be bonded was thoroughly "degreased" and cleaned with powdered abrasive. The strip of film was cleaned with a cloth moistened with a very mild acetic acid solution. The film, both membrane and backing, was then positioned and one side taped. The exposed part of the specimen surface, as well as the edges and the film backing, was then coated with a releasing agent to prevent the "squeezed out" cement from adhering to the specimen. Care was necessary to avoid getting the releasing agent under the film.

The film was then raised with the taped edge acting as a hinge. The catalyst was applied to the film and a layer of the cement was applied to the specimen near the taped edge of the film. The specimen, film side down, was then placed on a surface plate, and uniform pressure, via weight on a straight bar, was applied from the back (top) of the specimen. With high pressure applied for a few

seconds the cement cured. Excess cement was then wiped off, along with the releasing agent. The backing was stripped from the membrane making the specimen, with line array attached, ready for testing. Other details of the testing procedure are given in Chapter II, Part B.

APPENDIX III

DATA FOR OTHER MATERIALS TESTED

Polyester Resin PS-1

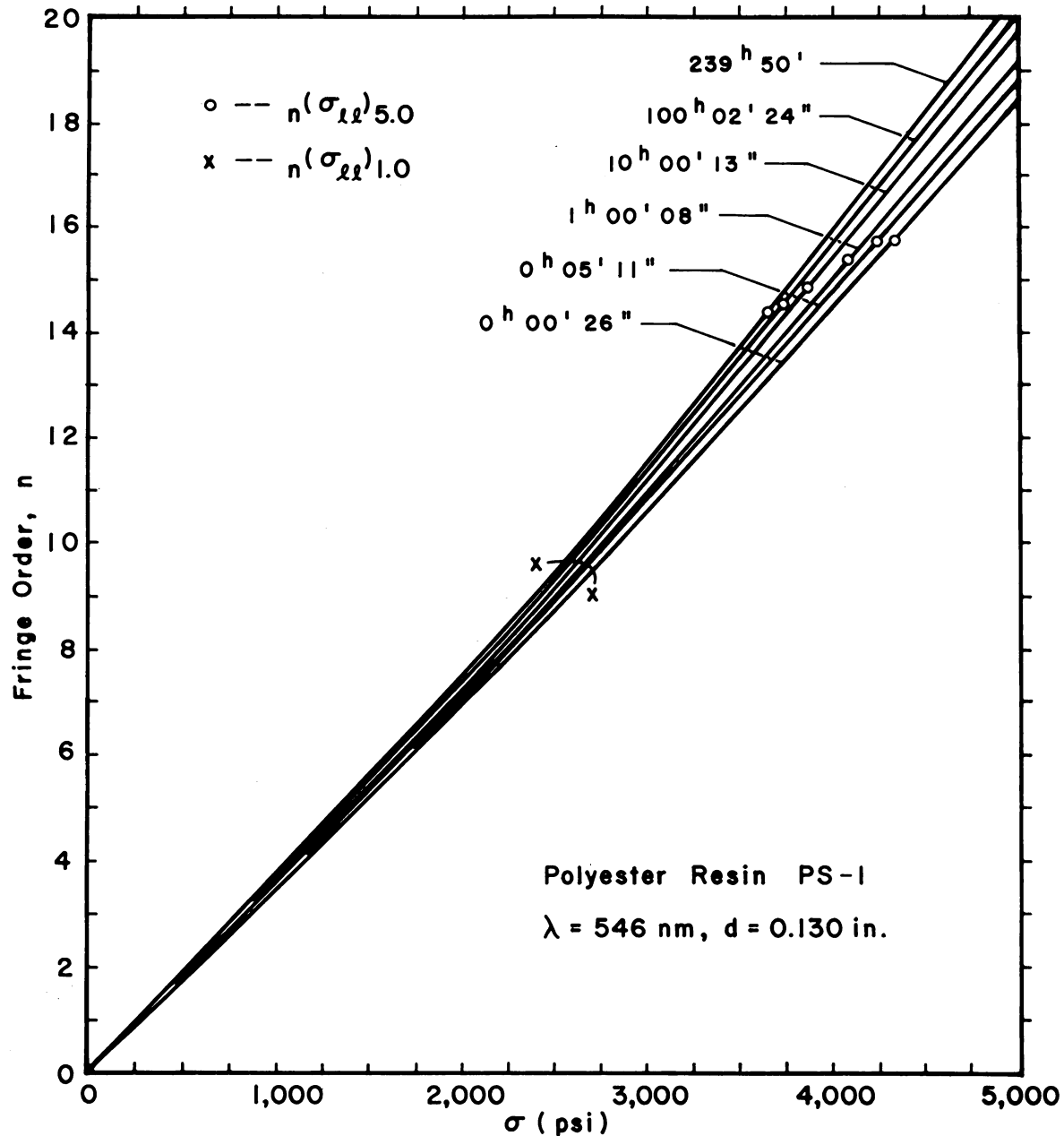

Fig. A3.1--Isochromatic fringe order n vs. stress, $t = t_1, t_2, \ldots, t_n$ for PS-1.

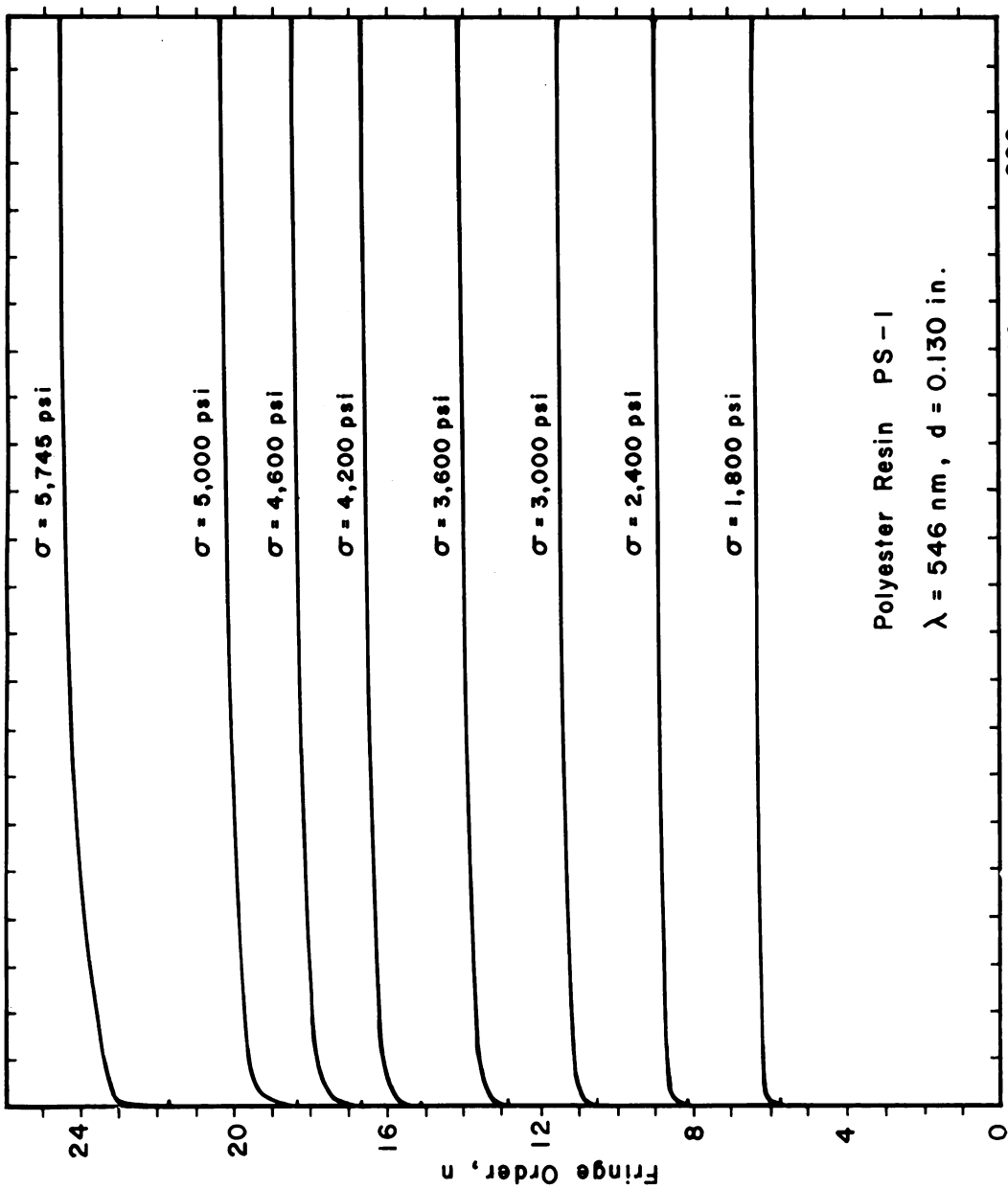

Fig. A3.2--Isochromatic fringe order n vs. time, $\sigma = \sigma_1, \sigma_2, \ldots, \sigma_n$ for PS-1.

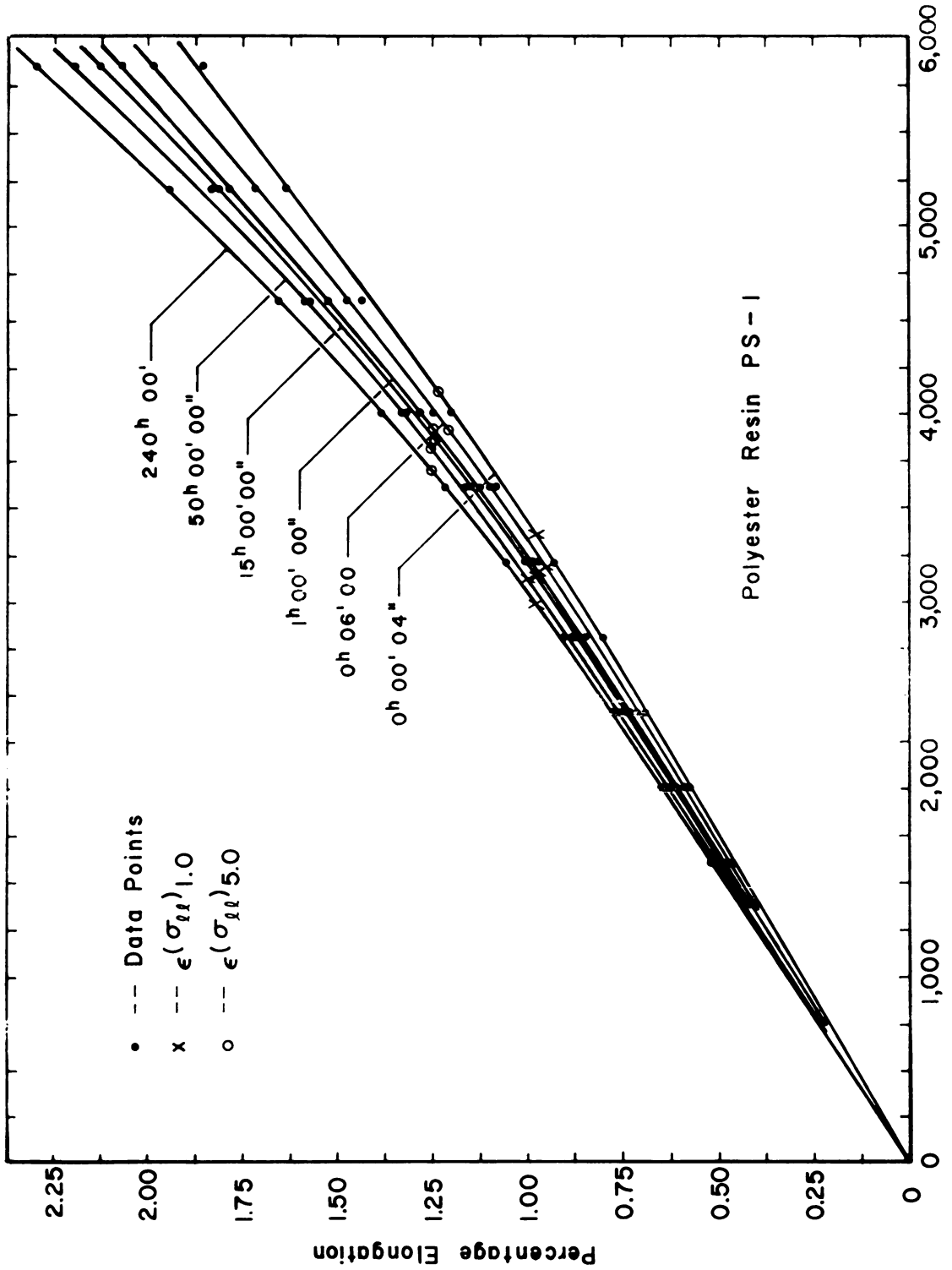

Fig. A3.3--Percentage elongation vs. stress, $t = t_1, t_2, \ldots, t_n$ for PS-1.

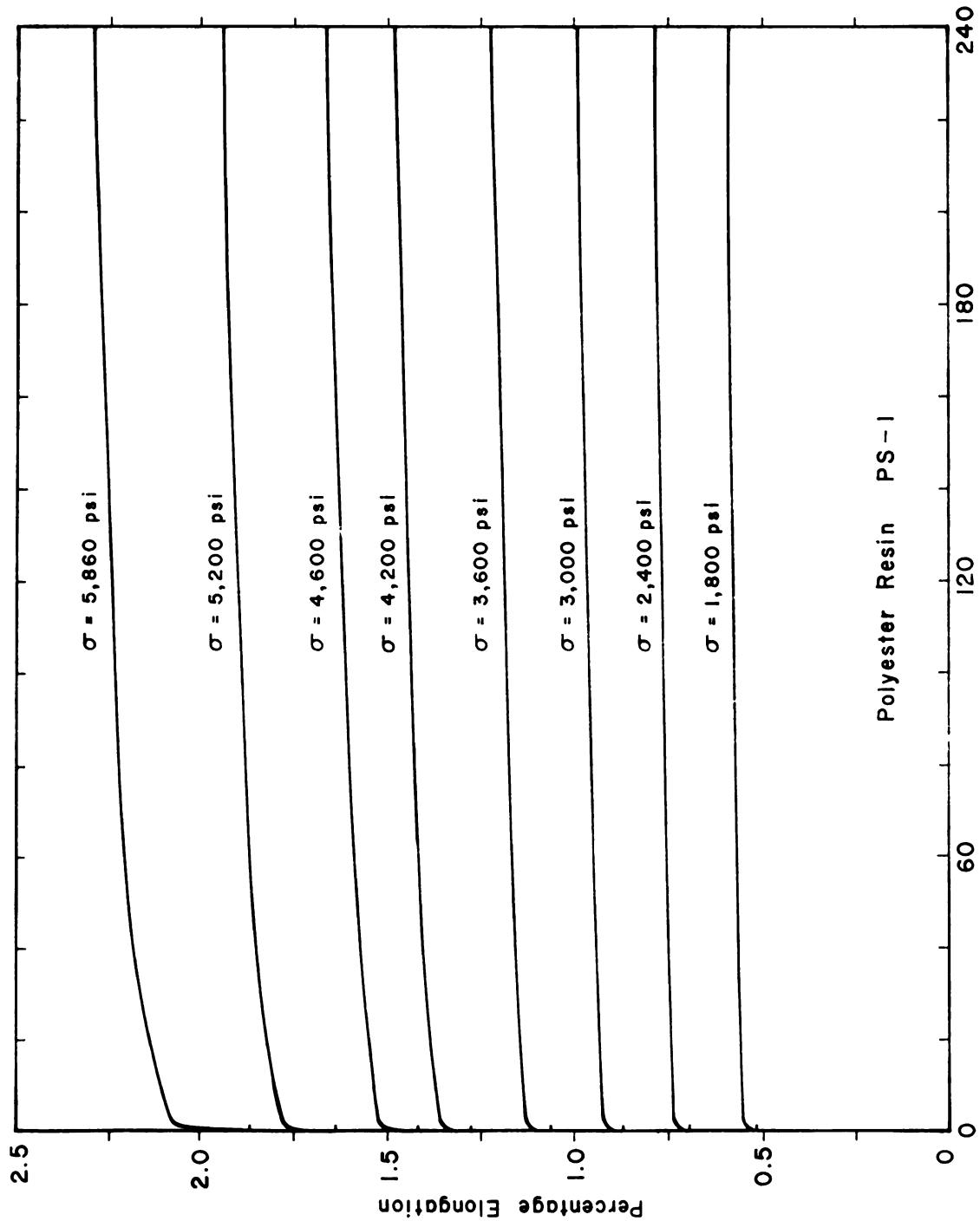

Fig. A3.4--Percentage elongation vs. time, $\sigma = \sigma_1, \sigma_2, \ldots, \sigma_n$ for PS-1.

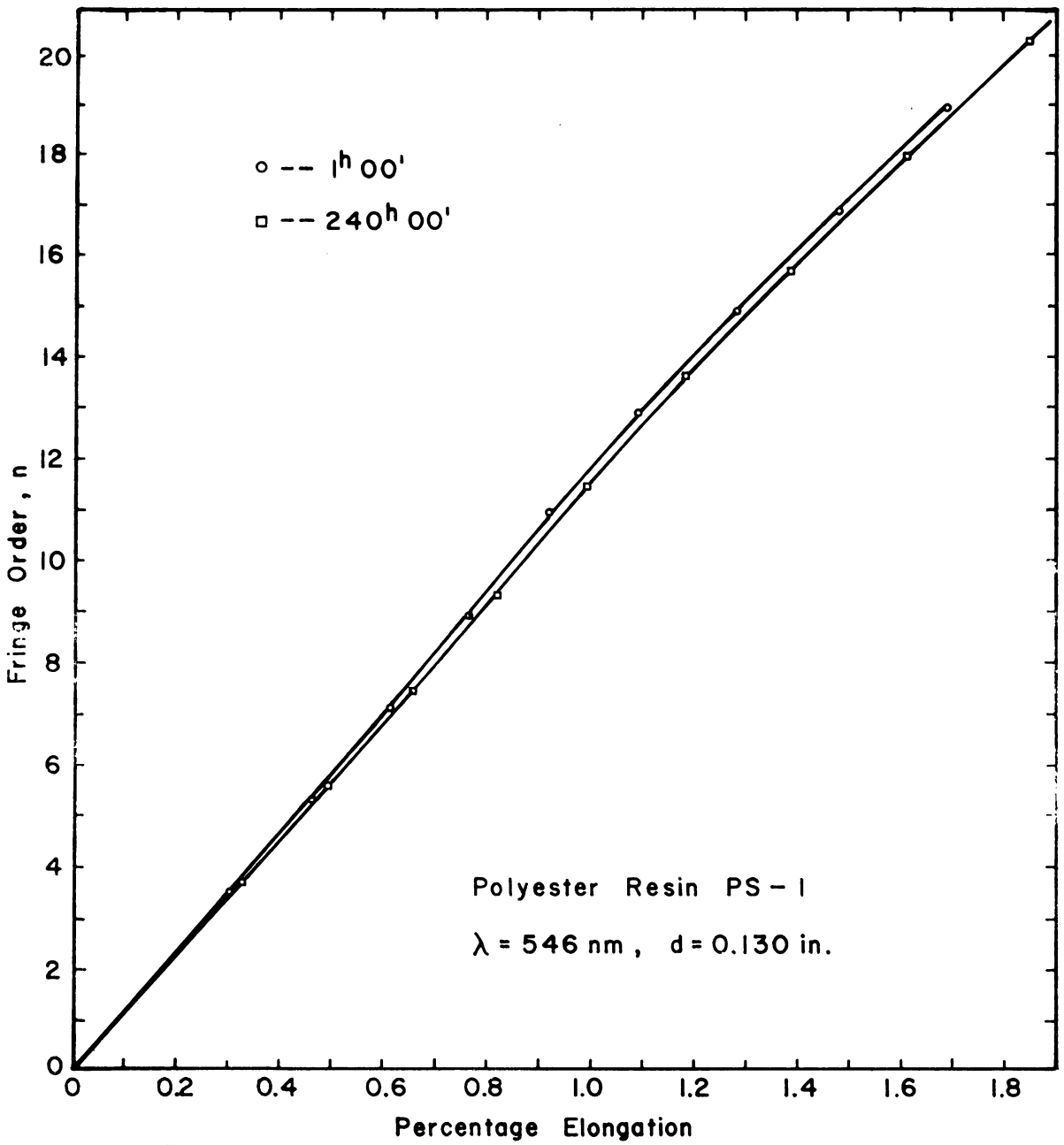

Fig. A3.5--Isochromatic fringe order n vs. percentage elongation, $t = t_1, t_2, \ldots, t_n$ for PS-1.

Epoxy Resin PS-2

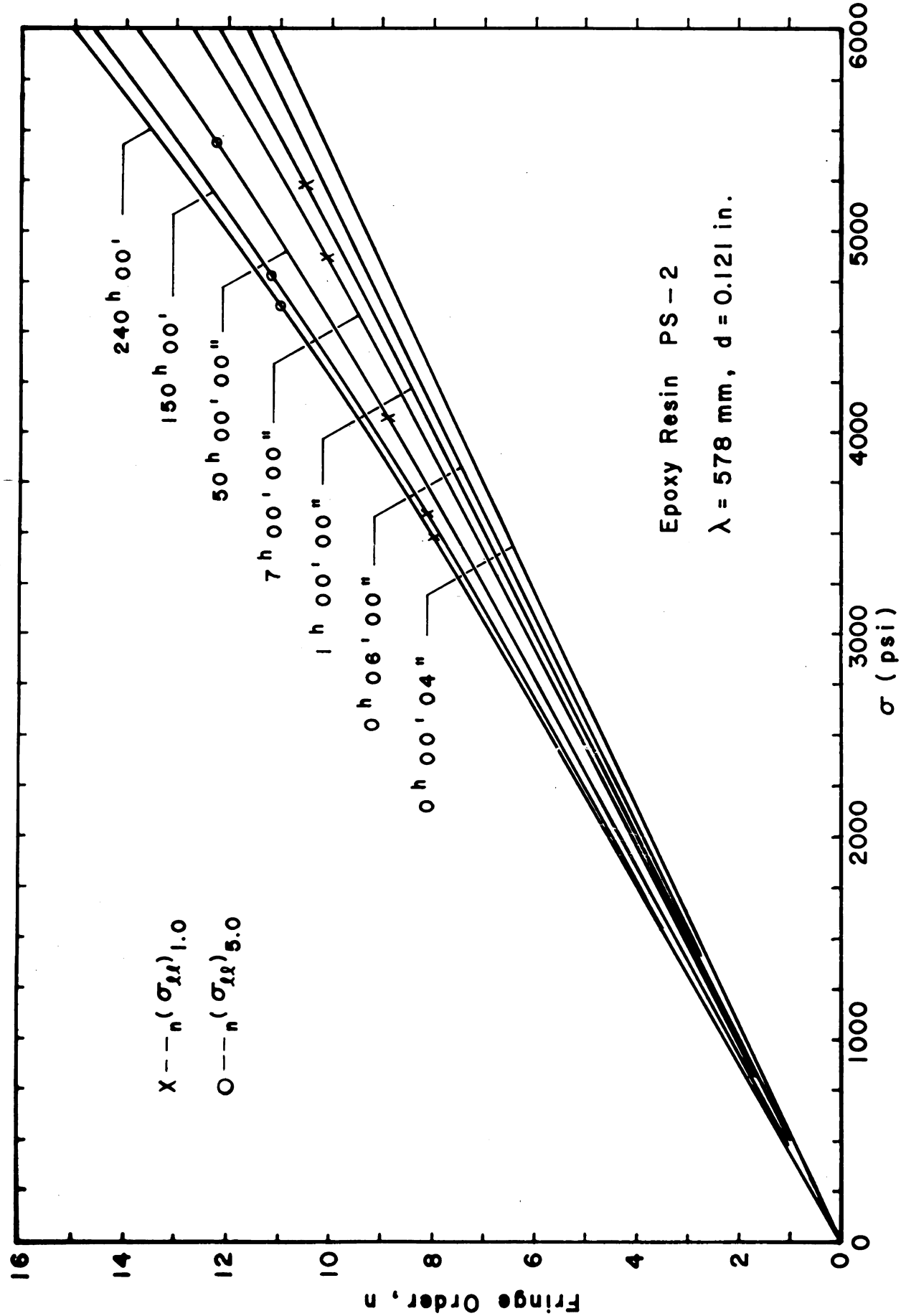

Fig. A3.6--Isochromatic fringe order n vs. stress, $t = t_1, t_2, \ldots, t_n$ for PS-2.

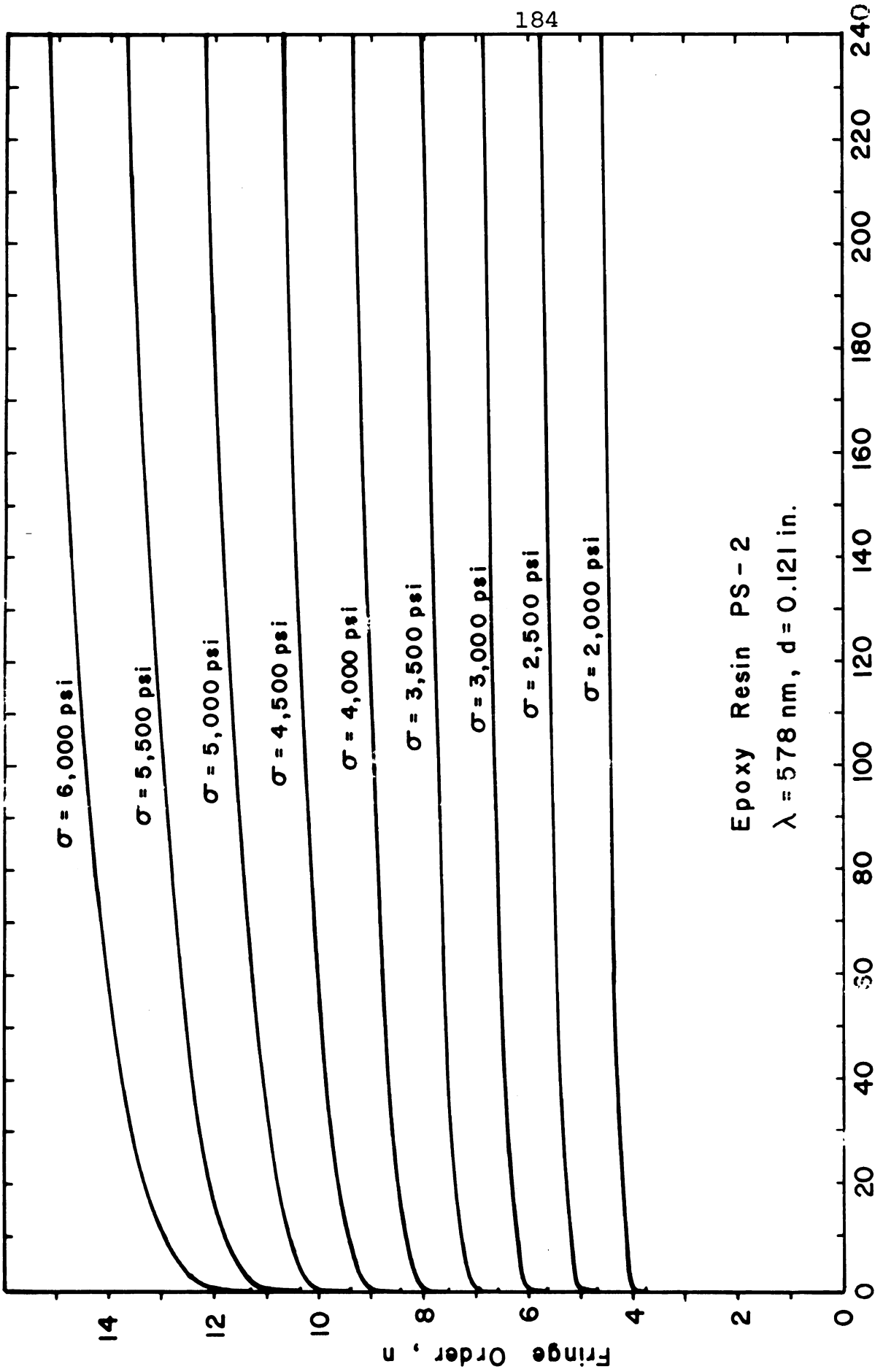

Fig. A3.7--Isochromatic fringe order n vs. time, $\sigma = \sigma_1, \sigma_2, \ldots, \sigma_n$ for PS-2.

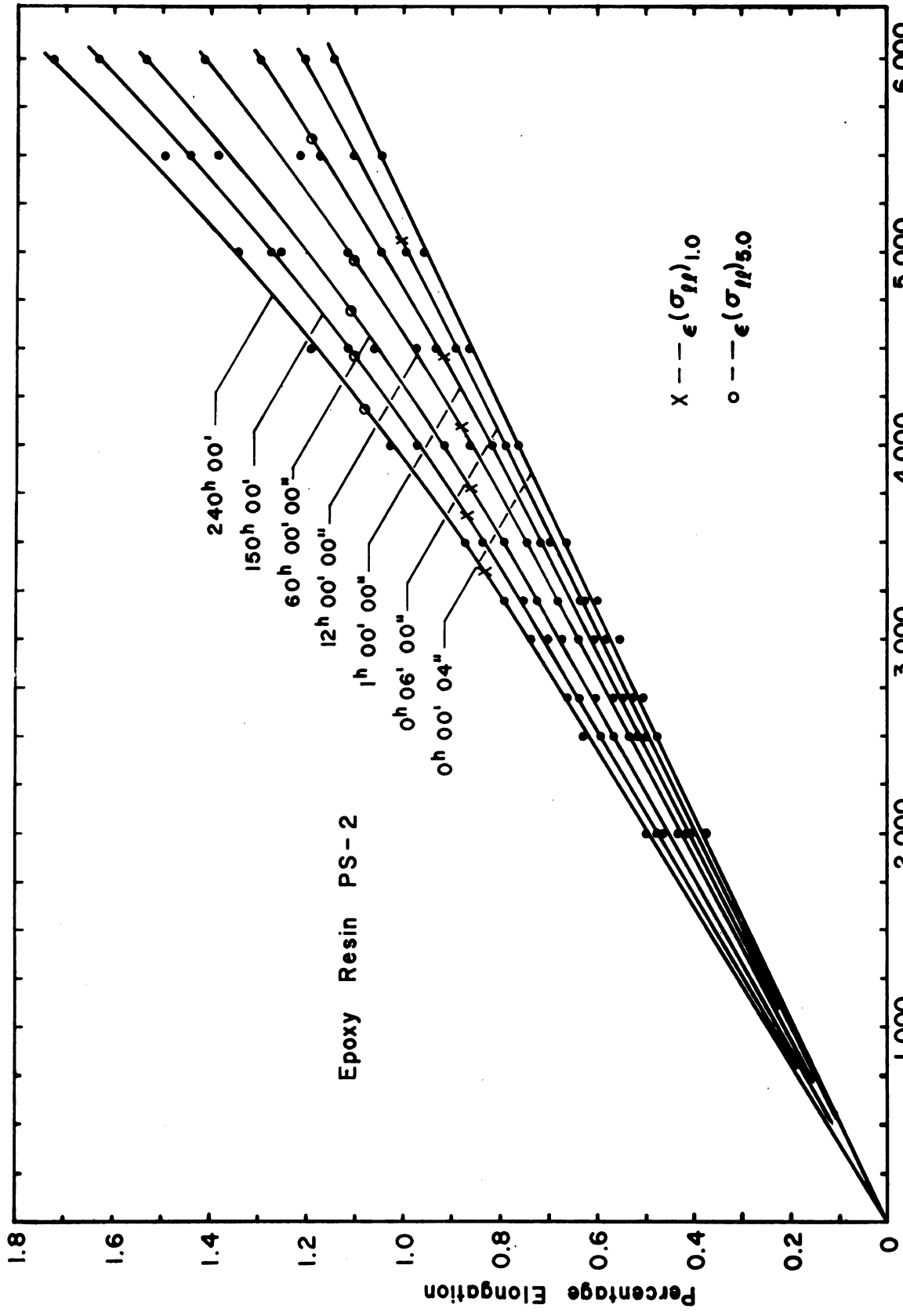

Fig. A3.8--Percentage elongation vs. stress, $t = t_1, t_2, \ldots, t_n$ for PS-2.

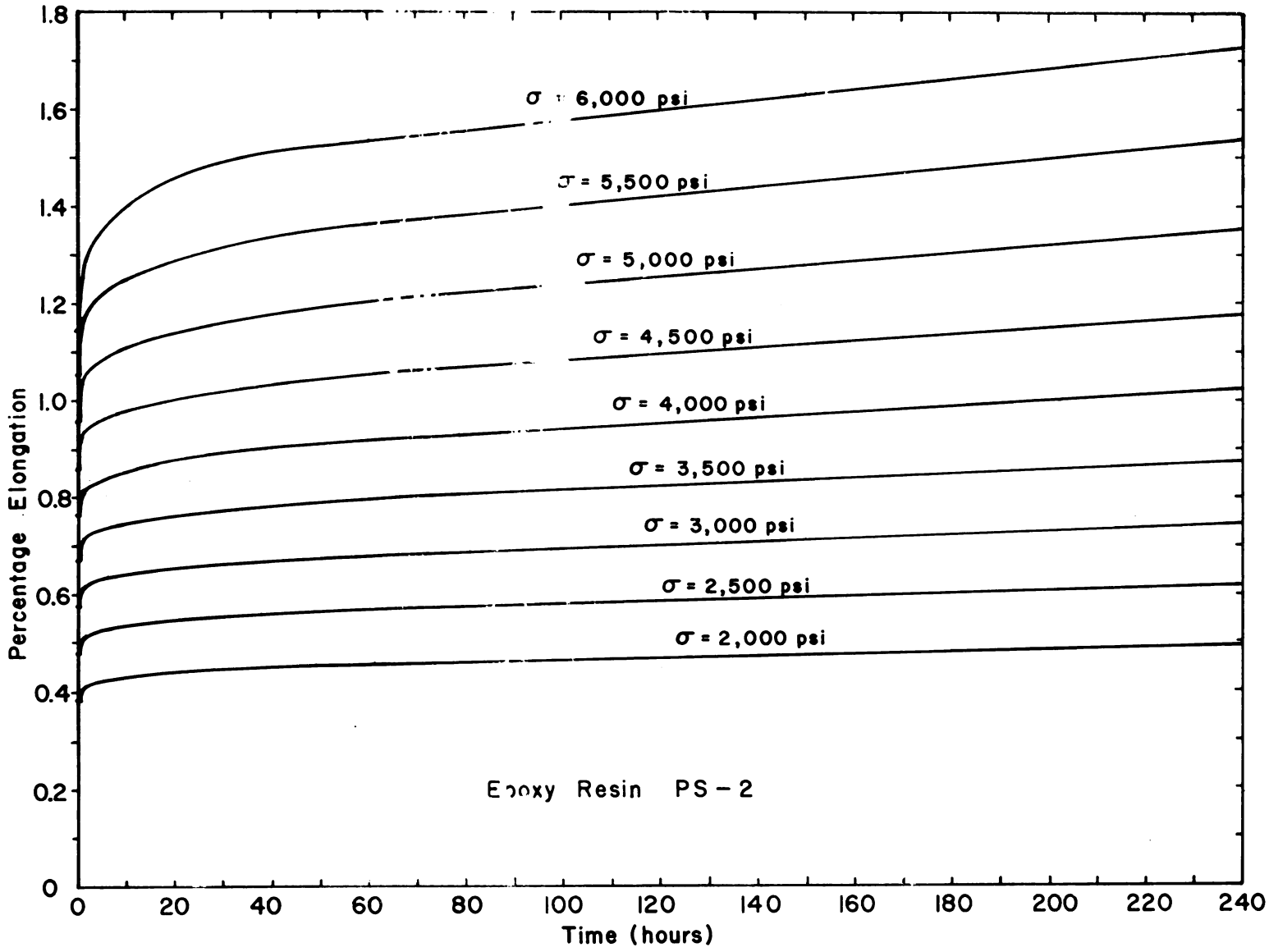

Fig. A3.9--Percentage elongation vs. time, $= \sigma_1, \sigma_2, \ldots, \sigma_n$ for PS-2.

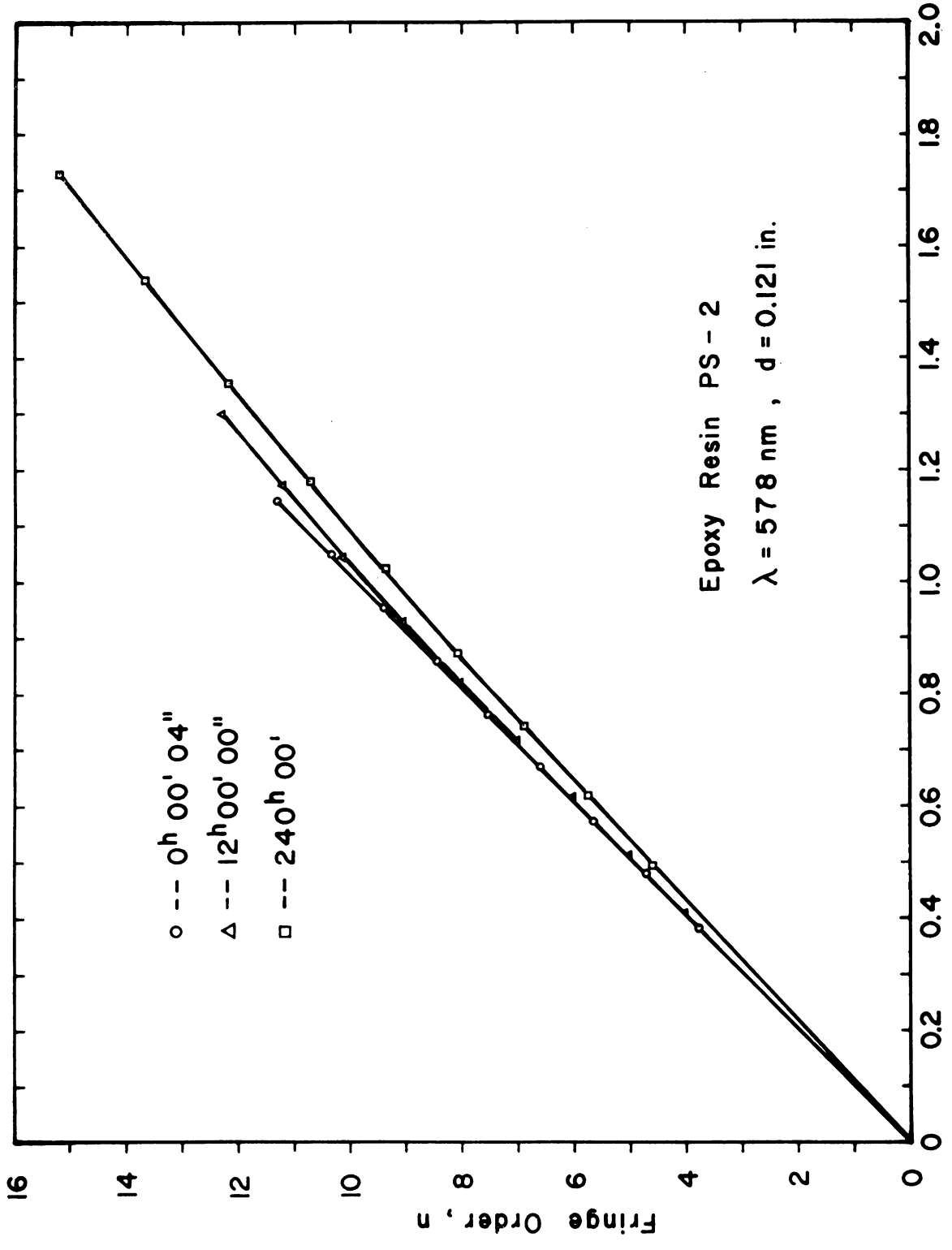

Fig. A3.10--Isochromatic fringe order n vs. percentage elongation, $t = t_1, t_2, \ldots, t_n$ for PS-2.

Polyester Resin Palatal P6-K

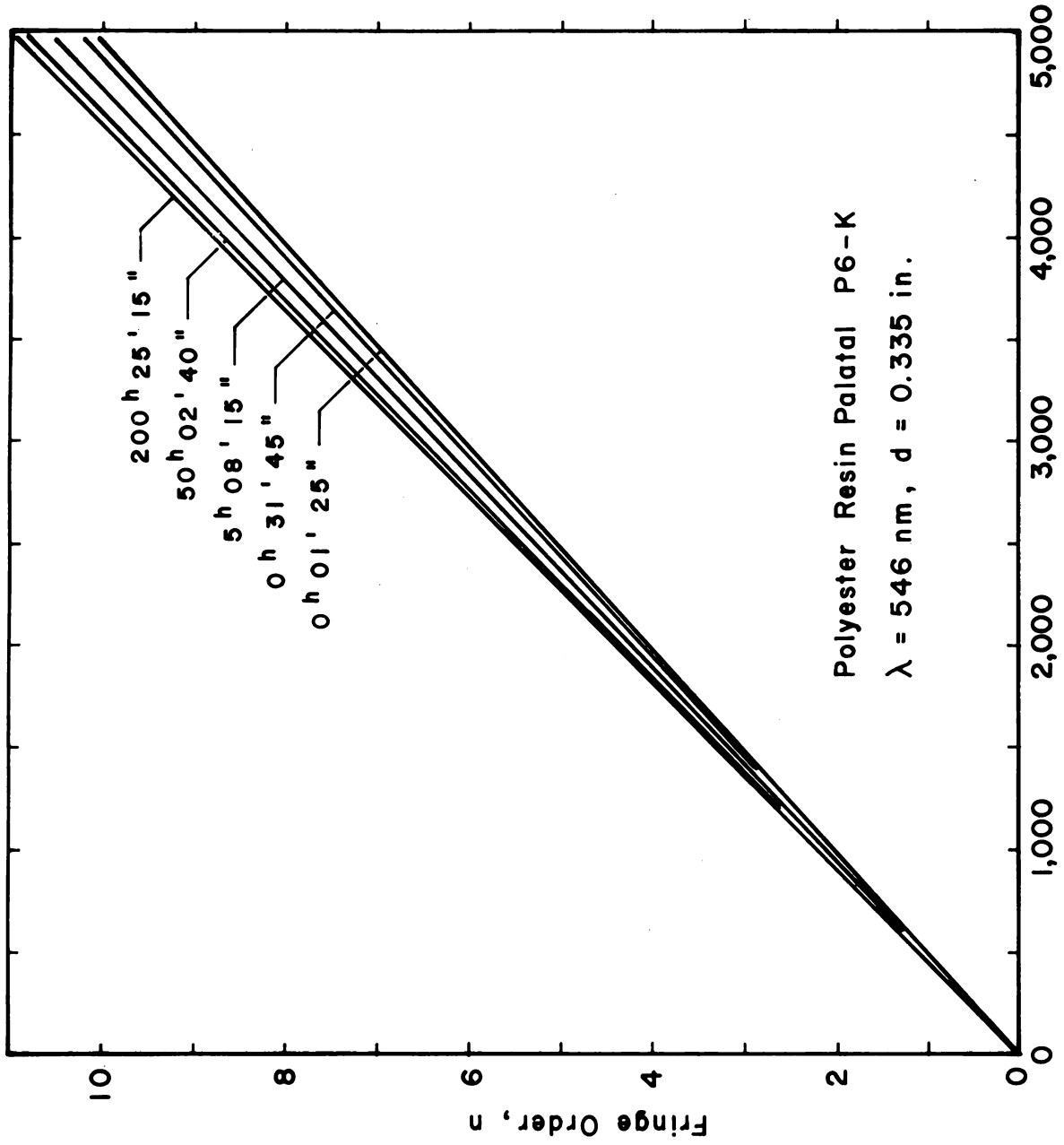

Fig. A3.11--Isochromatic fringe order n vs. stress, $t = t_1, t_2, \ldots, t_n$ for P6-K.

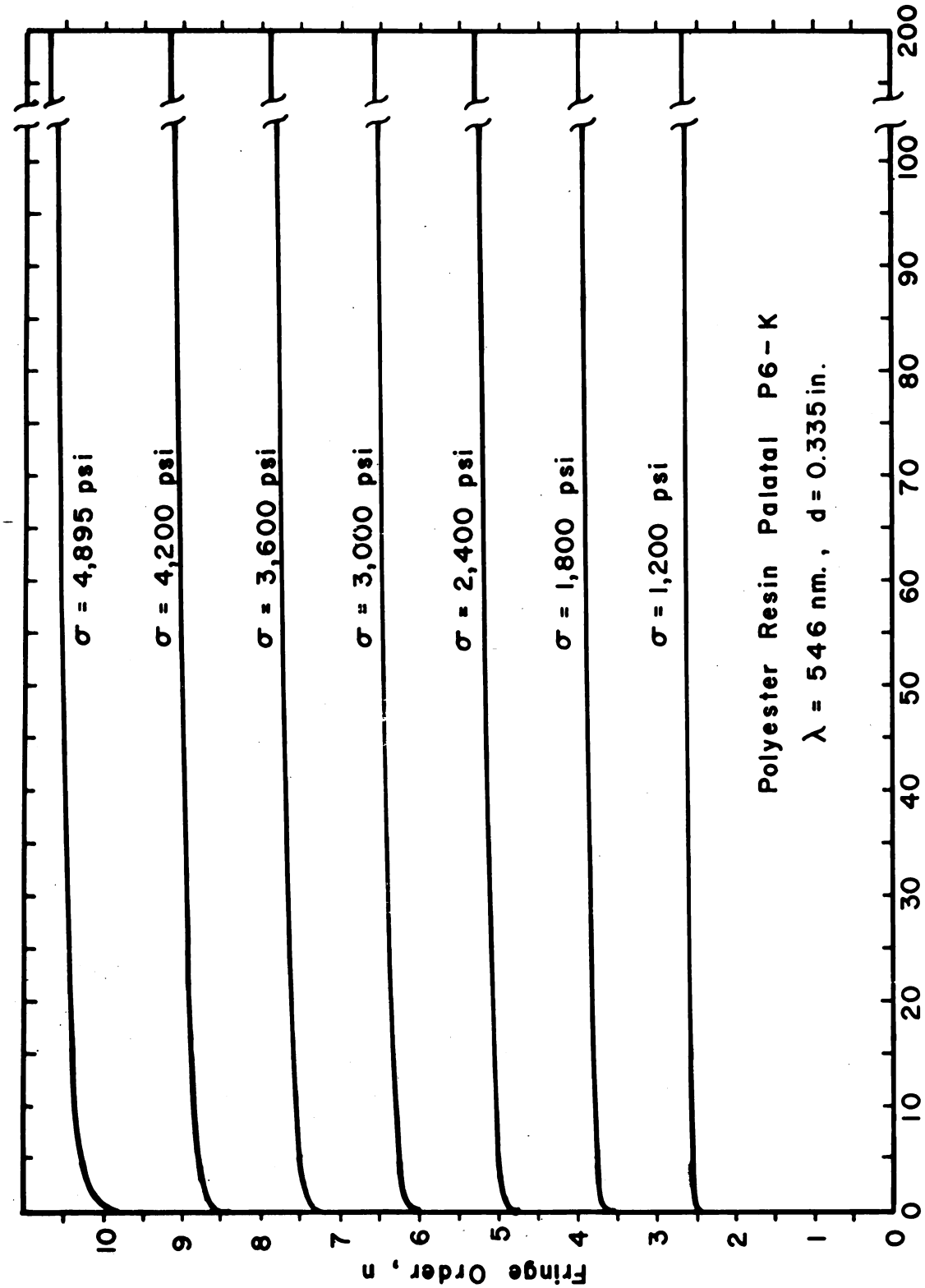

Fig. A3.12--Isochromatic fringe order n vs. time, $\sigma = \sigma_1, \sigma_2, \ldots, \sigma_n$ for P6-K.

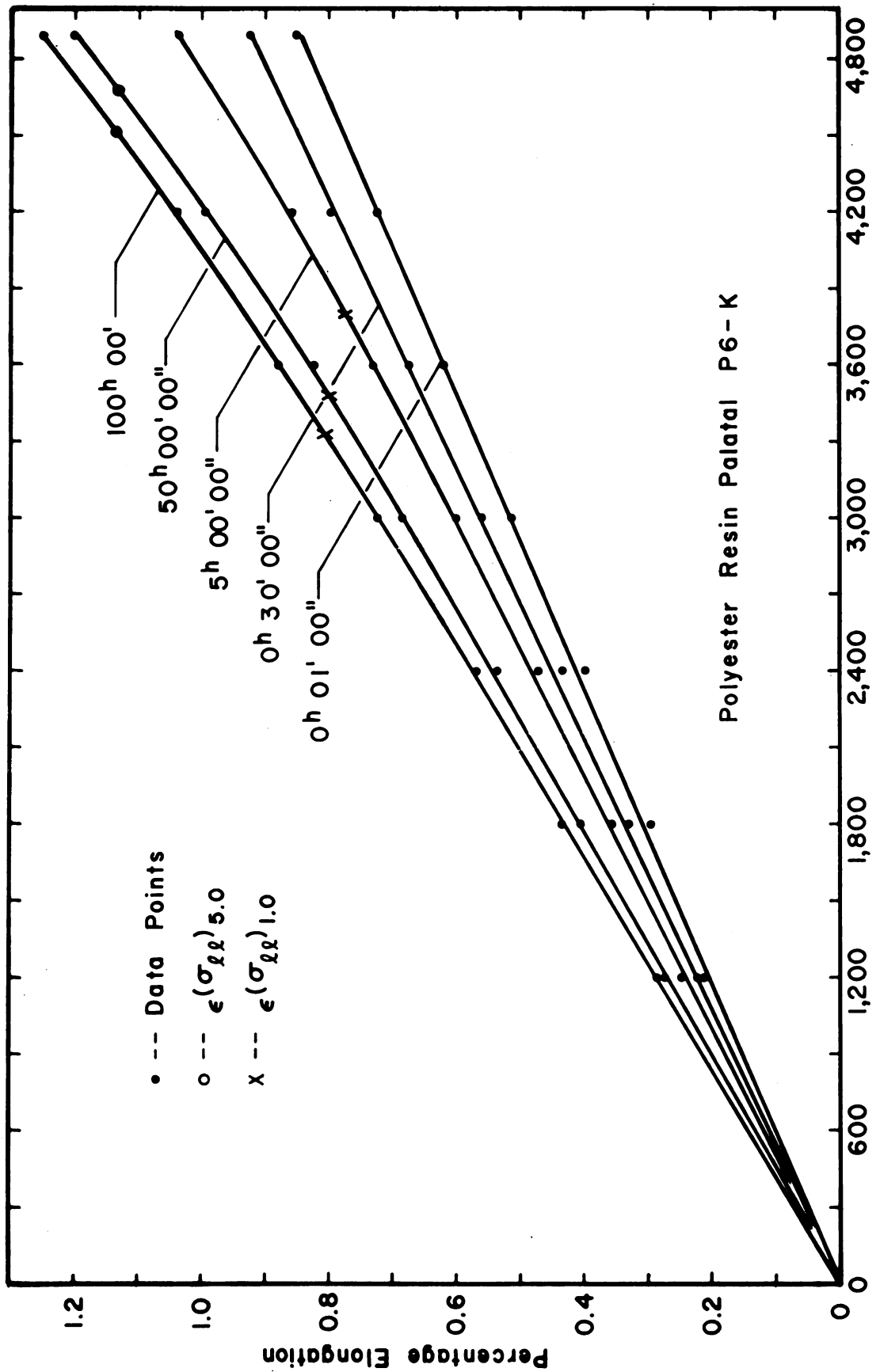

Fig. A3.13--Percentage elongation vs. stress, $t = t_1, t_2, \ldots, t_n$ for P6-K.

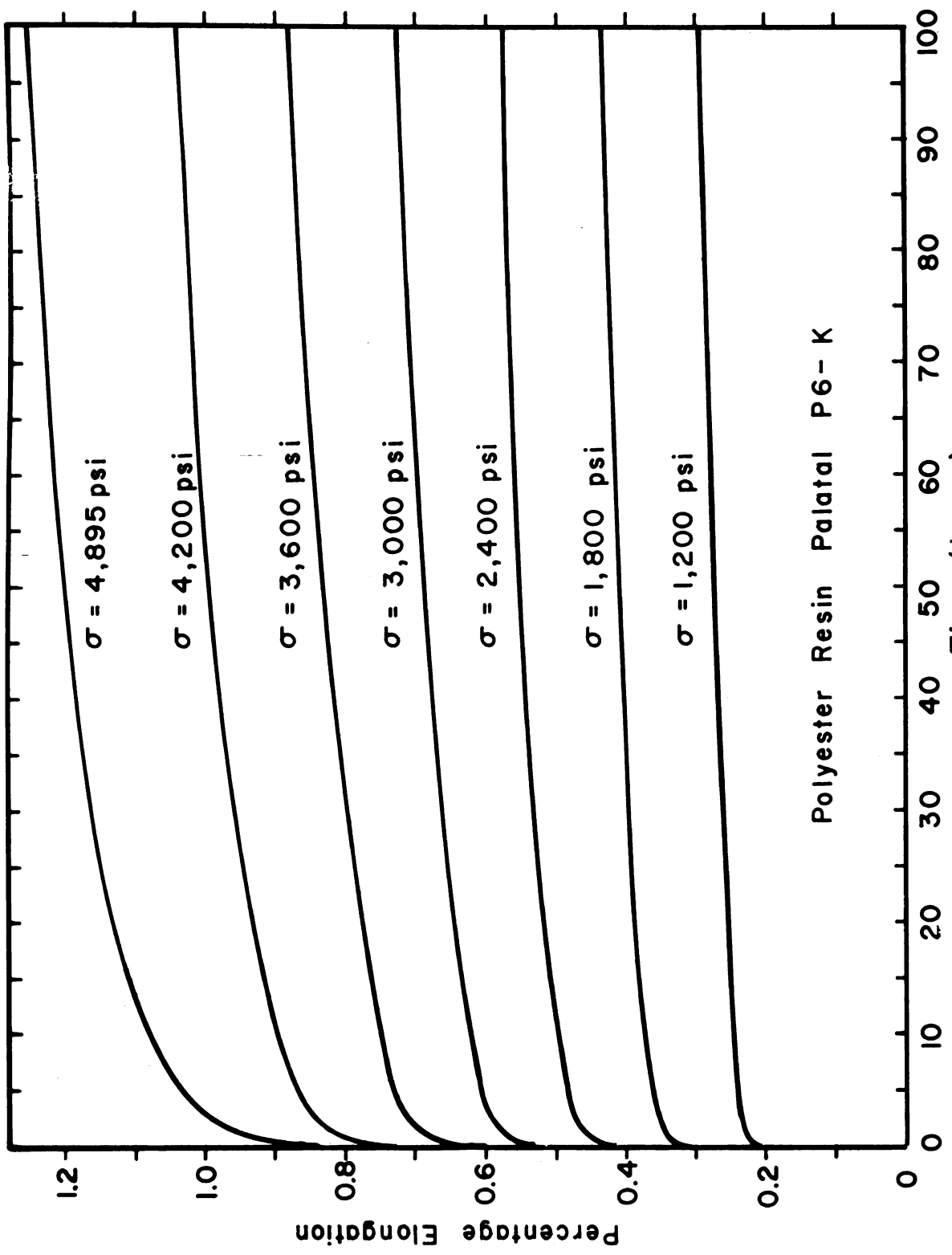

Fig. A3.14--Percentage elongation vs. time, $\sigma = \sigma_1, \sigma_2, \ldots, \sigma_n$ for P6-K.

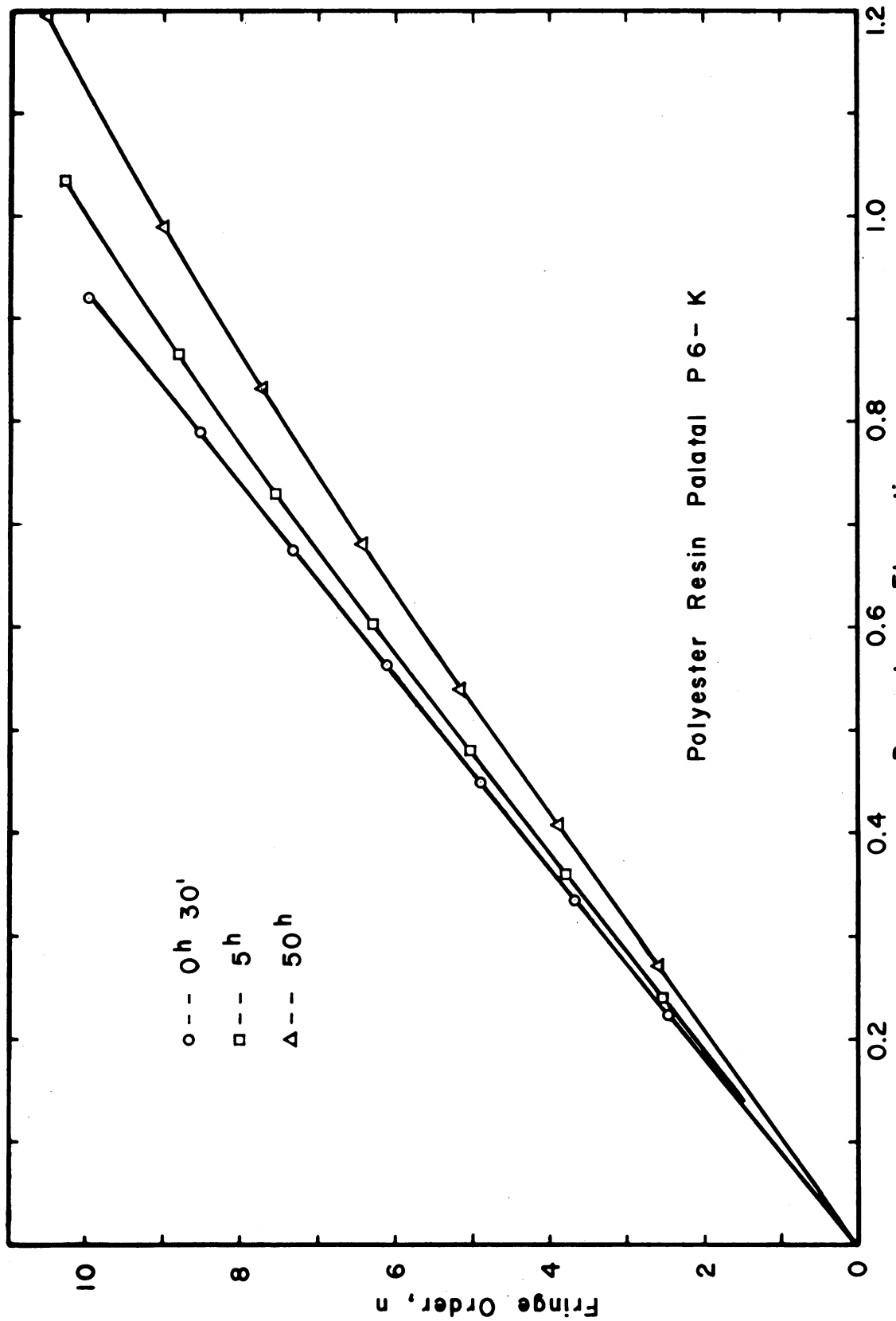

Fig. A3.15--Isochromatic fringe order n vs. percentage elongation, $t = t_1, t_2, \ldots, t_n$ for P6-K.